State Space Modeling of Differential-Algebraic Systems using Singularly Perturbed Sliding Manifolds

by

Brandon W. Gordon

B.A.Sc., Mechanical Engineering
University of Waterloo, 1994

M.S., Mechanical Engineering
Massachusetts Institute of Technology, 1996

Submitted to the Department of Mechanical Engineering
in Partial Fulfillment of the Requirements for the Degree of
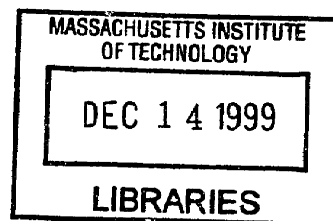
DOCTOR OF PHILOSOPHY

at the

MASSACHUSETTS INSTITUTE OF TECHNOLOGY
August 31, 1999
[September 1999]
© 1999 Massachusetts Institute of Technology
All rights reserved

Signature of Author_____

Department of Mechanical Engineering
August 31, 1999

Certified by_____

Haruhiko H. Asada, Professor of Mechanical Engineering
Thesis Supervisor

Certified by_____

Sheng Liu, Research Scientist of Mechanical Engineering
Thesis Co-supervisor

Accepted by _____

Ain A. Sonin
Chairman, Department Graduate Committee

State Space Modeling of Differential-Algebraic Systems using Singularly Perturbed Sliding Manifolds

by

Brandon W. Gordon

ABSTRACT

This thesis introduces a new approach for modeling and control of algebraically constrained dynamic systems. The formulation of dynamic systems in terms of differential equations and algebraic constraints provides a systematic framework that is well suited for object oriented modeling of thermo-fluid systems. In this approach, differential equations are used to describe the evolution of subsystem states and algebraic equations are used to define the interconnections between the subsystems (boundary conditions). Algebraic constraints also commonly occur as a result of modeling simplifications such as steady state approximation of fast dynamics and rigid body assumptions that result in kinematic constraints. Important examples of algebraically constrained dynamic systems include multi-body problems, chemical processes, and two phase thermo-fluid systems.

Differential-algebraic equation (DAE) systems often referred to as descriptor, implicit, or singular systems present a number of difficult problems in simulation and control. One of the key difficulties is that DAEs are not expressed in an explicit state space form required by many simulation and control design methods. This is particularly true in control of nonlinear DAE systems for which there are few known results. Existing control methods for nonlinear DAEs have so far relied on deriving state space models for limited classes of problems.

A new approach for state space modeling of DAEs is developed by formulating an equivalent nonlinear control problem. The zero dynamics of the control system represent the dynamics of the original DAE. This new connection between DAE model representation and nonlinear control is used to obtain state space representations for a general class of differential-algebraic systems. By relating nonlinear control concepts to DAE structural properties a sliding manifold is constructed that asymptotically satisfies the constraint equations. Sliding control techniques are combined with elements of singular perturbation theory to develop an efficient state space model with properties necessary for controller synthesis. This leads to the singularly perturbed sliding manifold (SPSM) approach for state space realization. The new approach is demonstrated by formulating a state space

model of vapor compression cycles. This allows verification of the method and provides more insight into the problems associated with modeling differential-algebraic systems.

Thesis Supervisor: Haruhiko H. Asada
Title: Professor of Mechanical Engineering

Thesis Co-supervisor: Sheng Liu
Title: Research Scientist of Mechanical Engineering

Acknowledgments

I would like to take this opportunity to express my sincere thanks to my thesis supervisors Haruhiko Asada and Sheng Liu for their guidance and support over the course of my Ph.D. research. I benefited greatly from their constant encouragement, new insights, and feedback on my research progress.

My thesis committee members James Paduano and Kamal Youcef-Toumi have also made valuable contributions and insights over the course of this thesis research.

I express my deep gratitude for my sponsor Daikin Industries Ltd. for its support. To Mr. Itoh for his enthusiasm and Mr. Nakagawa for helping with verification of the vapor compression cycle model. I would especially like to thank Dr. Xiang-Dong for his deep insights and laying the foundation for the modeling of vapor compression cycles. I would like to thank Dr. Torikoshi, Mr. Shimadzu, Mr. Sakamoto, Mr. Yonemoto, Mr. Hori, Mr. Onishi, Mr. Kasahara, and especially Mr. Hiei for their support.

Finally, I would like to thank my friends and colleagues for their help and encouragement over my years at MIT. I have really learned a lot from them. To Dub for teaching me some of the finer points about water. Wes for solving some of my most challenging problems in fluid mechanics. Wayne for showing me the dangers of mixing streams of B and K. To Paolo, Brad, Chris, Dave, and Charles for the many interesting conversations while hanging out at various pubs around Boston. To Bei, Ellie, Bernardo, Joe, Cem, Murali, Shrikant, Danieller, Kerri, Joan, Leslie, Tiina, Brigitte, and all the others I have so absent mindedly forgotten. Farewell.

Table of Contents

List of Figures

1. Introduction

1.1 Motivation

This thesis investigates new methods for modeling and control of algebraically constrained dynamic systems. These problems are often referred to as descriptor, implicit, or differential-algebraic equation (DAE) systems [1]. Recently, a growing interest in DAEs has formed because physical models are often more systematically formulated in terms of differential equations and algebraic constraints. In this approach, differential equations are used to describe the evolution of subsystem states and algebraic equations are used to define the interconnections between the subsystems. This process is known to be an effective method that is well suited for object oriented modeling [7]. For interconnected thermo-fluid systems, such as vapor compression cycles, DAEs provide the key to systematic model representation (see Figure 1). Algebraic constraints also commonly occur as a result of modeling simplifications such as steady state approximation of fast dynamics and rigid body assumptions that result in kinematic constraints. Further motivation for studying DAE systems stems from the fact they represent a more general class of dynamic systems and are capable of behavior that is fundamentally different from conventional ordinary differential equations (ODEs) [14].

Despite the generality of DAEs and their simplification of the modeling process few methods currently exist for control of this class of systems. Often the constraints are nonlinear and cannot be eliminated so the DAE must be studied directly. However, differential-algebraic systems present a number of significant problems in simulation and control [13]. A key difficulty is that DAEs are not expressed in an explicit state space form required by many control methodologies and numerical integration methods. This is particularly true in control of nonlinear DAE systems for which there are few known results. Existing methods for control

of nonlinear DAEs have relied on deriving state space representations for limited classes of problems [16].

The main objective of this thesis is to expand the validity of nonlinear control and simulation methods to a general class of nonlinear DAEs by developing systematic methods for constructing explicit state space representations. This process, often referred to as DAE realization has so far been successful only for restricted classes of problems such as systems that are linear in the constrained states [13] or index one systems [6]. The index property of a differential-algebraic system is defined as the number of times the constraint equations must be differentiated in order to solve for the derivatives of the constrained states. It is a measure of the singularity of the system and can significantly affect the behavior of the solution. Simulation of high index systems is generally more difficult and there are few existing software packages for systems with an index greater than two. However, many important classes of systems are naturally described by high index DAEs. These include multi-body mechanical systems [22], chemical processes [13], and two phase thermo-fluid systems [7]. This clearly suggests the need for a systematic approach for realization of high index DAE problems.
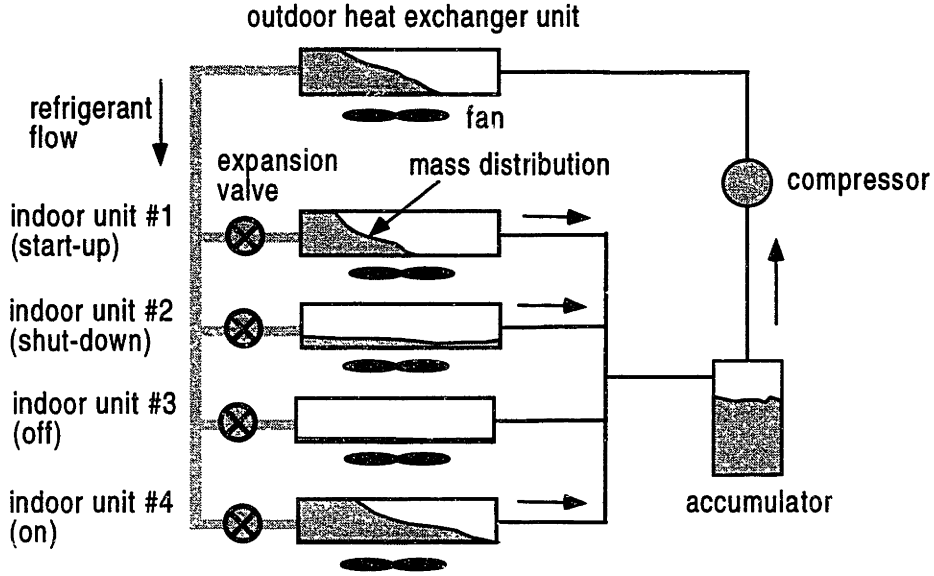
Figure 1. A multiple-zone vapor compression cycle

1.2 Thesis Contribution

In this thesis, a new approach is developed for constructing explicit state space realizations for a general class of high index DAE systems. A differential-algebraic system can be expressed in the general form:

$$\dot{x} = f(t, x, z) \tag{1}$$
$$0 = g(t, x, z)$$

where $x \in \mathfrak{R}^n$, $z \in \mathfrak{R}^m$, $f : \mathfrak{R} \times \mathfrak{R}^n \times \mathfrak{R}^m \to \mathfrak{R}^n$, and $g : \mathfrak{R} \times \mathfrak{R}^n \times \mathfrak{R}^m \to \mathfrak{R}^m$. It is assumed that f and g are sufficiently differentiable with respect to their arguments, and that a well defined solution for x and z exists [1]. In general, the constrained variables z cannot be eliminated because the constraint equations are nonlinear. This presents difficulty in control design since existing nonlinear control methods do not apply to this form of problem. In many cases the constraints no longer

depend on z and they cannot be directly inverted. This is an example of a high index DAE system.

A new approach for realization of high index DAEs is introduced by formulating an equivalent nonlinear control problem (see Figure 2):

$$\dot{x} = f(t, x, z)$$
$$\dot{z} = v \qquad\qquad (2)$$
$$w = g(t, x, z)$$

Where v is some fictitious input that drives z (now assumed to be independent) which is allowed to violate the constraint equations producing an output w. This modeling approach differs significantly from a typical nonlinear control problem since the objective is to have the two dynamic systems (1,2) converge in some appropriate manner.

By relating nonlinear control concepts to the index property a sliding manifold is developed that satisfies the constraints of the DAE. This results in a new type of sliding control problem. However, DAE realization presents a number of new problems for the sliding control method. These issues are related to the convergence of the approximation error in the presence of state variations. These problems are investigated using the methods of feedback linearization and singular perturbation theory. Important issues such as reduction of computational complexity and bounding the approximation error are dealt with in this theoretical framework. Together, these new results lead to the singularly perturbed sliding manifold approach (SPSM) to DAE realization.

Application of new methods to specific problems is an important part of control research because it provides valuable insights into their utility, and helps illuminate new ideas and research avenues. With these objectives the SPSM realization approach is applied to vapor compression cycles (see Figure 1). The dynamic behavior of vapor compression cycles are governed by complex interactions between refrigerant flowing in single phase or two phase states and fin arrays that

thermally communicate with ambient environments. These coupled fluid mechanics and heat transfer processes are inherently distributed in nature. Low order approximation of these processes results in models described by nonlinear high index DAEs. Application of the SPSM to this problem yields a new control theoretic model of vapor compression cycles that is useful for simulation and multivariable control design. This in turn provides valuable new insights into modeling and state space realization of DAE systems.
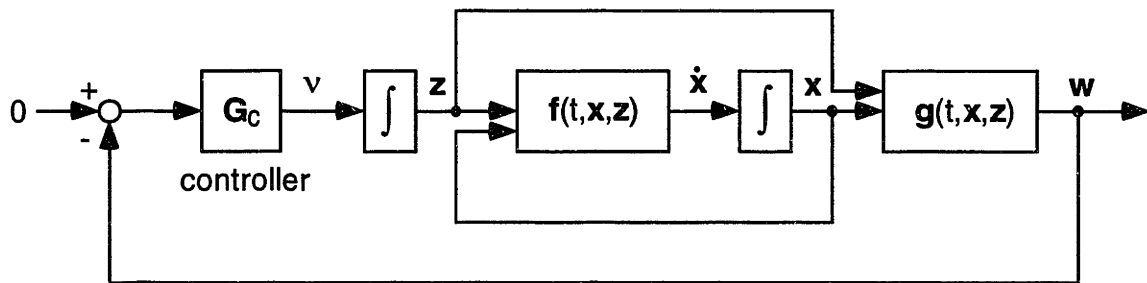
Figure 2. Block diagram of DAE realization approach

1.3 Related Work and Previous Literature

The main areas of relevant works are related to numerical analysis, sliding control, and singular perturbation analysis. The interconnections between these bodies of work are carefully investigated in this thesis to establish new underpinning principles for realization of DAE systems.

The study of DAE systems has attracted substantial attention by the numerical analysis community over the last several years [1,3]. This research is motivated by the many challenging computational problems that result when simulating multibody systems, chemical processes, and trajectory control problems [3]. An important concept that was discovered in this research is the index

property. It is a measure of the singularity of the system and can significantly affect numerical behavior of the solution. Discretization of high index systems often results in ill conditioned equations [1]. To overcome this problem several methods have been proposed with varying degrees of success [3]. However, high index systems remain a challenging numerical analysis problem.

The realization of high index DAE systems involves the satisfaction of a number of algebraic constraints that form an invariant set in the system. It is shown that this can by achieved by using an appropriately defined sliding manifold. Sliding control methods can then be employed to force the constraints to zero. This leads to boundary layer interpolation methods that can be used to bound the approximation error of the realization [19]. However, DAE realization presents a number of new problems for the sliding control method that are related to convergence of the approximation. These issues are addressed using normal form representation from feedback linearization theory [9], and the singular perturbation method.

In general, a high gain controller is necessary in order to force the constraints to small values while the unconstrained state $\mathbf{x}$ is varying (see Figure 2). This results in fast dynamics for the constrained states $\mathbf{z}$ and two-time-scale behavior. Singular perturbation theory has been used with great success in the control community as a means of studying systems with fast dynamics [12,11]. It is demonstrated how this technique can be inverted to guide the synthesis of fast dynamics that converge to index one constraints. The approach is then extended to high index systems approximated by sliding manifolds. Furthermore, properties such as stability, controllability, and observability of singular perturbation approximations are investigated to ensure a DAE realization can be used for control design.

1.4 Organization of Thesis

This thesis is organized into seven chapters. In chapter 2, the realization of index one systems is investigated. It is shown how algebraic constraints can be modeled using fast dynamics. The singular perturbation method of analyzing systems with fast dynamics is then introduced. Using this technique criteria are developed for systematically developing fast dynamics that converge to the constraints until only a small error is involved.

Chapter 3 investigates the realization problem for high index (>1) DAEs. It is shown how the DAE realization process can be formulated as an equivalent nonlinear control problem. From this new connection a key relation between the index property and the relative degree is obtained. This allows the constraints to be combined into a sliding manifold. The sliding manifold is then used to generalize the singular perturbation approach and develop a realization method based on a sliding control analogy. Finally, normal form representation of DAEs is introduced. This technique leads to new insights about DAEs and provides new methods to study the convergence properties of sliding realizations.

In chapter 4, the boundary layer method for approximating sliding controllers is introduced. Combining this approach with the generalized singular perturbation method results in the singularly perturbed sliding manifold approach to realization. The convergence properties of the method are rigorously proven using singular perturbation analysis, normal form representation, and a sliding condition analysis. This provides valuable bounds on the approximation error and some guidance for the selection of important parameters. A simple heat pendulum example is then used to illustrate the SPSM approach. Furthermore, the existence of control properties such as controllability and observability are proven for SPSM realizations. This leads to additional criteria for selecting model parameters. The concluding section presents a technique to guide the selection of parameters based on linearization of the SPSM.

Chapters 5 and 6 involve the application of the SPSM modeling approach to vapor compression cycles. A systematic approach for modeling the dynamics of vapor compression cycles is introduced based on a DAE representation. From this process physical insights are gained about DAE models. The SPSM method is then used for realization of the nonlinear high index DAE problem. This yields an explicit state space model that can be used for simulation and control design.

Finally, the concluding remarks are given in chapter 7.

2. A Singular Perturbation Approach for DAE Realization

2.1 Introduction

In the process of modeling physical systems approximations are frequently made to reduce the dimension and frequency range of the model. Rigid body assumptions and neglecting fast dynamics can often lead to algebraic constraints among state variables and derivatives. Algebraic constraints occur because the dynamics of the constraining interactions are not directly modeled. At more fundamental modeling levels, such as the N-body equation of classical mechanics and the multibody Schrodinger equation, there are no algebraic constraints between variables. This is a reflection of the finite signal propagation rate required by physical laws.

The idea of directly modeling algebraic constraints has been used with some success for realization of DAE systems. This chapter introduces this approach, known as the stiff dynamic element method, and illustrates some of its shortcomings. It is shown how this physically motivated technique can be generalized using singular perturbation theory to yield an improved method for DAE realization. Conditions for convergence and approximation methods are investigated. These new results form an important part of the theoretical foundation needed for the singularly perturbed sliding manifold approach.

2.2 The DAE Realization Problem

The most general DAE problem considered in this thesis is the mixed set of implicit differential and algebraic equations given by

$$\mathbf{F}(t, \mathbf{x}, \dot{\mathbf{x}}) = \mathbf{0} \tag{3}$$

where $x \in \Re^p$, $F:\Re \times \Re^p \times \Re^p \to \Re^p$. For a DAE system $[\partial F / \partial \dot{x}]$ is singular so that some of the state variables are algebraically constrained. Further, it is assumed that a well defined solution for x exists with consistent initial conditions [1]. The system presented is not under or over constrained. To facilitate analysis the DAE system will be written in a semi-explicit form:

$$\dot{x} = f(t, x, z) \qquad (4)$$

$$0 = g(t, x, z) \qquad (5)$$

where $x \in \Re^n$, $z \in \Re^m$, $f:\Re \times \Re^n \times \Re^m \to \Re^n$, and $g:\Re \times \Re^n \times \Re^m \to \Re^m$. Implicit state derivatives and constraints such as equation (3) can be converted to this form as follows:

$$\dot{x} = z \qquad (6)$$

$$0 = F(t, x, z) \qquad (7)$$

In this section it will be assumed that equations (4) and (5) are continuously differentiable with respect to their arguments and that

$$\det\left[\frac{\partial g}{\partial z} \right] \neq 0 \qquad (8)$$

in some neighborhood of the exact solution, which is guaranteed by the implicit function theorem if g can be explicitly solved for z. This situation corresponds to an index one DAE. High index systems (>1) will be investigated in the next chapter.

2.3 Previous Solution Methods

In this section, a brief overview of existing methods for solving DAE problems is presented. This gives some background on the field and the difficulties that may be encountered during DAE realization.

Implicit integration is one of the earliest techniques proposed for solving differential algebraic systems [1]. In this method, the derivatives are replaced by finite difference approximations which results in a set of nonlinear algebraic equations that are solved for x[n] and z[n]. For example, using a first order approximation yields

$$\mathbf{x}[n] = \mathbf{x}[n-1] + \Delta t \cdot \mathbf{f}(t[n], \mathbf{x}[n], \mathbf{z}[n])$$
$$\mathbf{0} = \mathbf{g}(t[n], \mathbf{x}[n], \mathbf{z}[n])$$

(9)

This approach has been successfully applied for simulation of DAEs (see Figure 3). However, it does not result in an explicit state space representation, so its usefulness for control design is quite limited. Furthermore, the method becomes numerically ill conditioned for systems with index greater than two.

A common approach for realization of DAEs is to differentiate the algebraic constraints until derivatives of the constrained states appear. For an index one system only one differentiation is required

$$\frac{d\mathbf{g}}{dt} = \left[\frac{\partial \mathbf{g}}{\partial \mathbf{z}}\right]\dot{\mathbf{z}} + \left[\frac{\partial \mathbf{g}}{\partial \mathbf{x}}\right]\dot{\mathbf{x}} + \left[\frac{\partial \mathbf{g}}{\partial t}\right] = \mathbf{0}$$

(10)

The Jacobian $[\partial \mathbf{g}/\partial \mathbf{z}]$ is invertible so we can solve for $\dot{\mathbf{z}}$. A potential difficulty with this approach is that differentiation operations can result in complicated differential equations and Jacobian terms that are difficult to calculate. This problem is described in later sections. Another problem is that the solution can drift of the constraints because (10) only enforces the constraints at the differential

level. Small numerical errors will accumulate in a direction normal to the constraint surface (see Figure 4). This could potentially result in numerical and controller instability problems.

A popular DAE realization approach is to approximate the algebraic constraints using stiff dynamic elements. This procedure was originally introduced to model the dynamics of two dimensional mechanisms [10]. Recently, the method has been generalized to multibody systems [22]. This approach converts the DAEs to an explicit state space form by directly modeling the constraints in the system using stiff spring and damper elements. Figure 5 shows an example of how the kinematic constraints in a four bar linkage can be approximated. The main difficulty with this approach is that it requires sharp physical intuition or a bond graph based method [17] to determine where to place the additional elements in the system and how stiff to make the elements to obtain an accurate approximation. Furthermore, adding new energy storage elements could potentially induce high frequency interactions between the new elements and the original system. To suppress high frequency oscillations, proper dampers must be added. In many cases, particularly thermo-fluid systems, excess damping could result in substantial error between the realization and the original system behavior. For general systems, new methods are needed for designing well behaved fast dynamics that guarantee convergence to the algebraic constraints. A geometrical interpretation of the method is illustrated in Figure 6. It is evident that the method results in an explicit ODE that converges to a manifold that is a small distance from the DAE without drifting effects. However, a very high stiffness may be necessary for a good approximation which could limit the utility of the approach for simulation and control design.
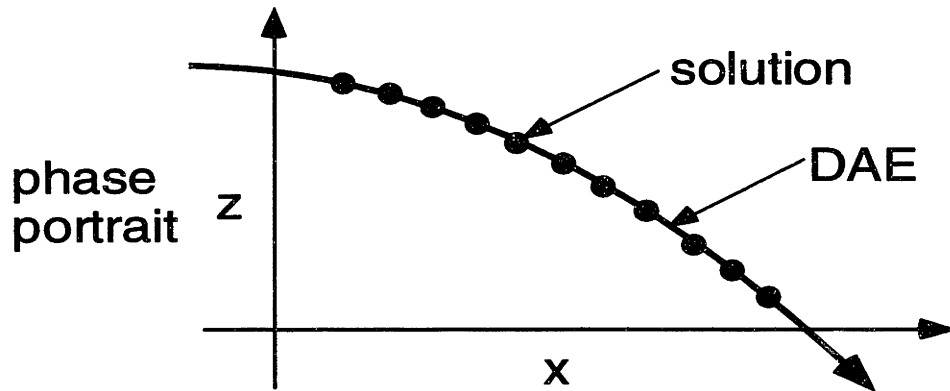
Figure 3. Geometrical interpretation of implicit integration
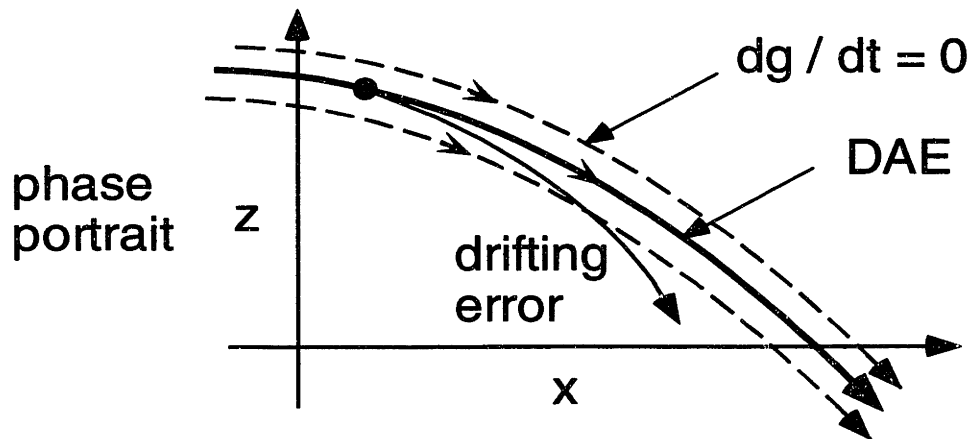
Figure 4. Geometrical interpretation of differentiation based methods
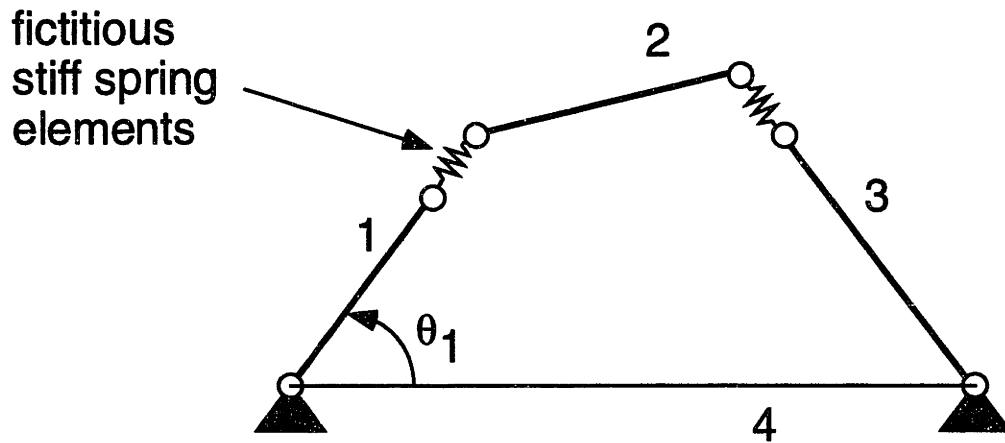
Figure 5. The stiff dynamic element method
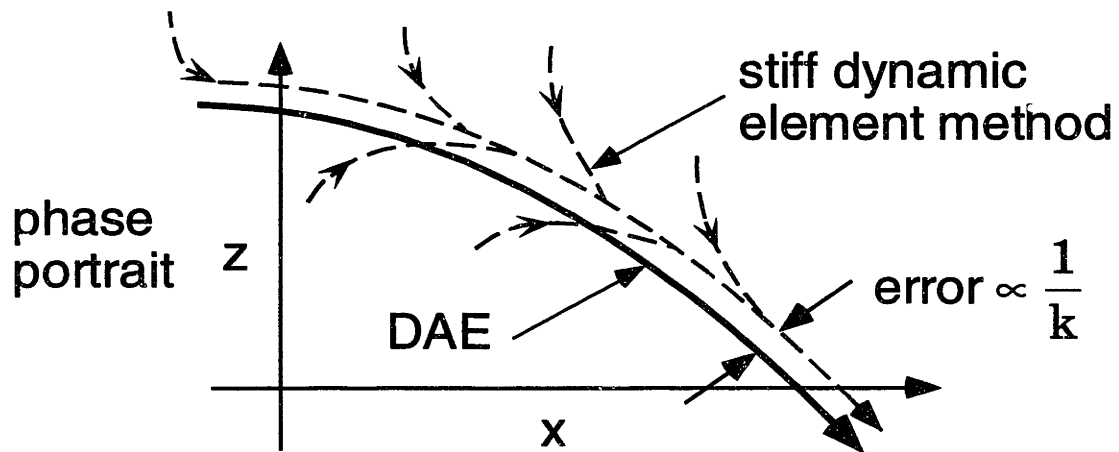
Figure 6. Geometrical interpretation of the stiff dynamic element method

2.4 The Stiff Dynamic Element Method

In this section, an attempt to model a simple DAE system using the stiff dynamic element method and some potential problems are illustrated. A lumped parameter model of a two phase flow heat exchanger represents a simple

illustrative example of a DAE system (see Figure 7). The system is composed of three control volumes representing the fluid inside the heat exchanger (node 1), fluid inside the connecting pipes (node 2), and the thermal capacitance of the heat exchanger wall and fins (node 3). The state equations for this system can be determined by applying conservation of mass and energy together with thermodynamic properties for each control volume in the system. This results in state equations of the form:

$$\dot{x} = f(t, x, z) \tag{11}$$

where

$$x = \begin{bmatrix} P_1 & \rho_1 & P_2 & \rho_2 & T_3 \end{bmatrix}^T \;\; , \;\; z = \dot{m}_1 \tag{12}$$

The constant boundary conditions are given by T_a , $\dot{m}_i$, h_i , and $\dot{m}_2$. A full description of the state equations appear in appendix A.

A common assumption made in modeling heat exchangers is that pressure variations along its length have negligible impact on energy interactions, so that all control volumes are assumed to have the same pressure. This results in the following pressure constraint equation:

$$0 = g(x) = x_1 - x_3 \tag{13}$$

The differential-algebraic equations (11,13) can be converted to an explicit state space form by finding a state equation for the mass flow rate $\dot{m}_1$. The combined system should closely approximate the original DAE system. In analogy to the stiff dynamic element method, an equation for the mass flow rate can be determined from a momentum balance on a negligibly small section of pipe between the components (see Figure 8). A simple approximation is

$$\varepsilon_1 \frac{d\dot{m}_1}{dt} = -\dot{m}_1 + \frac{1}{\varepsilon_2}(P_1 - P_2) \quad , \quad 0 < \varepsilon_1 << 1 \tag{14}$$

Where ε_1 represents the ratio of inertia to frictional damping and ε_2 is the ratio of friction to pipe cross section area.

The response of the system for a typical set of parameters and initial conditions is shown in Figure 9. It is apparent that the addition of the momentum equation results in fast pressure oscillations in the system. If damping is increased, the oscillation decays faster; however, the approximation error becomes higher, as shown in Figure 10. Evidently, the stiff dynamic element method (small inertia method in this case) can lead to high frequency oscillations due to the interactions between the new elements (fast dynamics) and the original system. This is especially true for thermo-fluid systems, where energy exchange between fluid and thermal domains can become substantially complicated when new storage elements are introduced. Connecting new storage components in parallel, closed loop, or other types of configurations in a thermo-fluid system does not guarantee a good approximation, or in many cases even stability [20]. The results of this example suggest the need for a systematic method of adding fast dynamics that guarantees convergence to the original system described by DAEs. The singular perturbation approach presented in the following section provides a systematic generalization of this physically motivated approach.
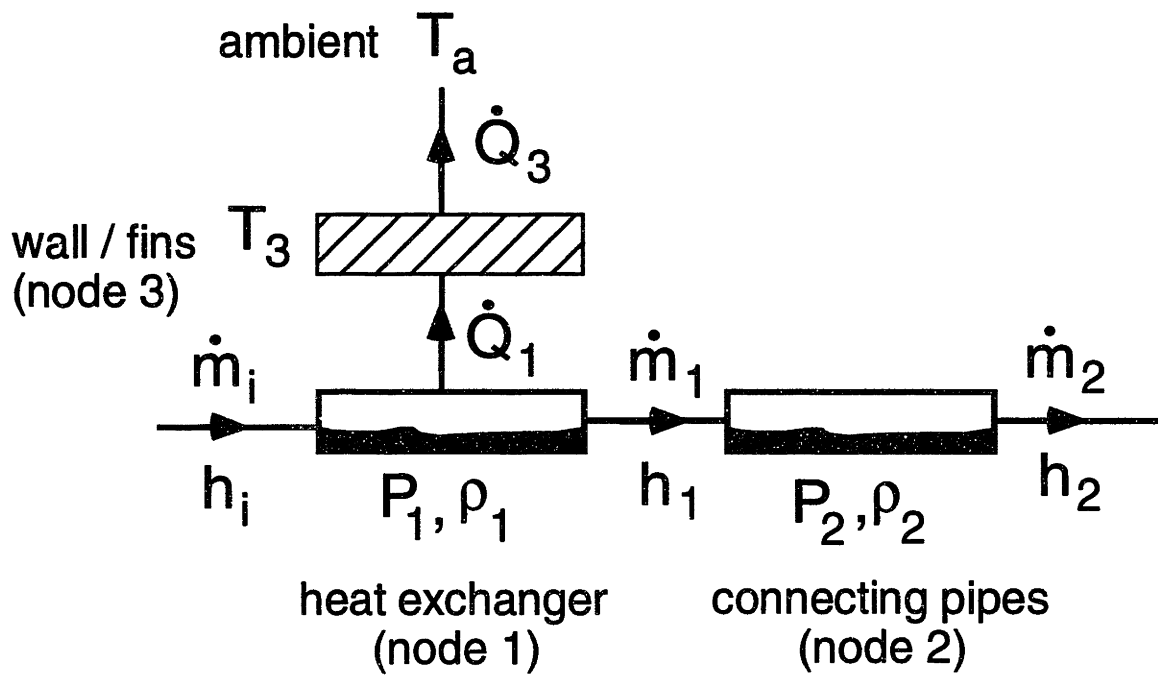
Figure 7. A two phase flow heat exchanger
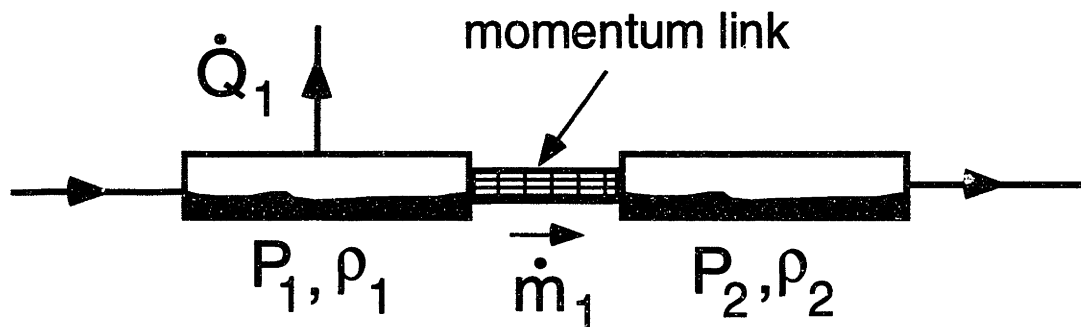
Figure 8. The stiff dynamic element method
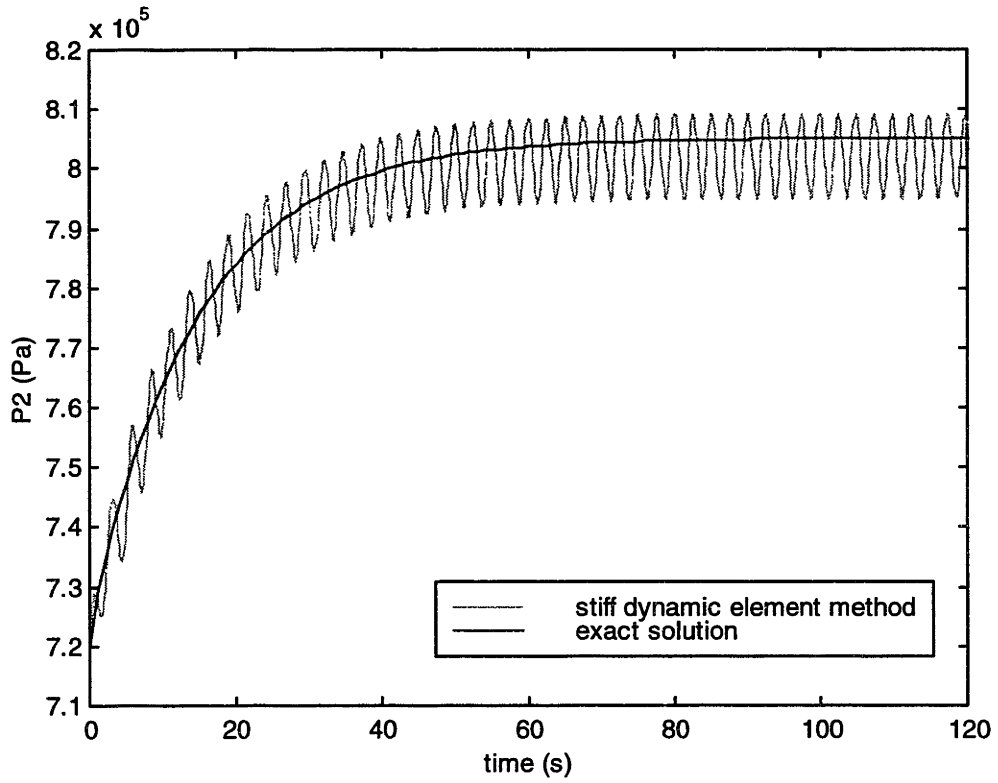
Figure 9. Low damping response
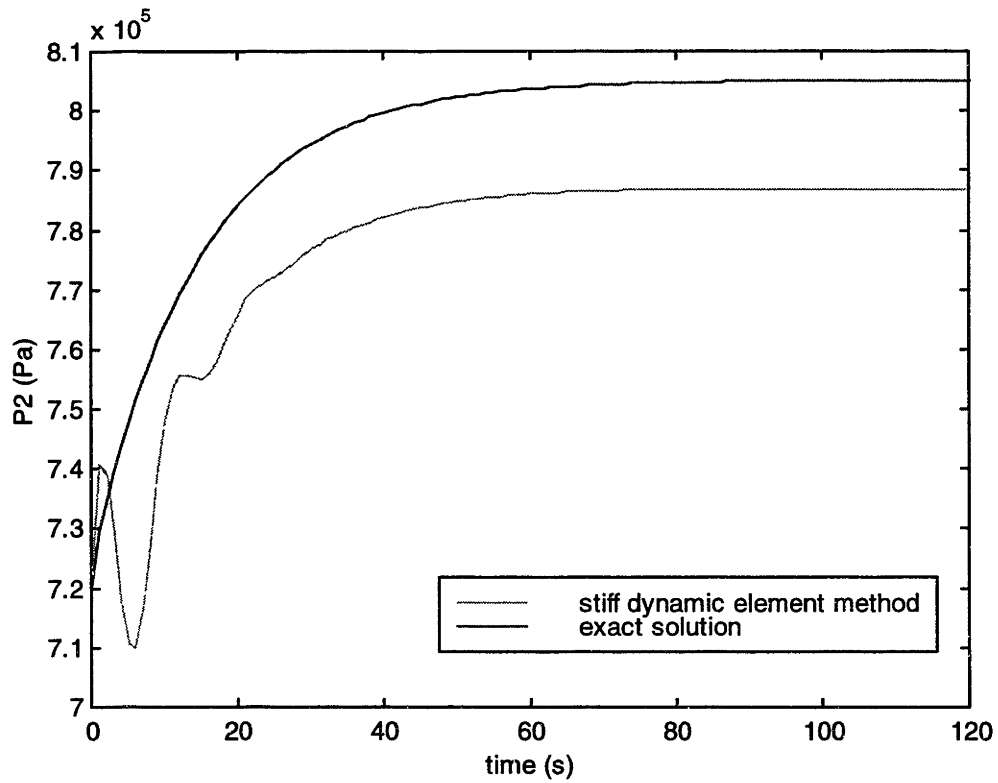
Figure 10. High damping response

2.5 The Singular Perturbation Approach

The standard form of the singular perturbation problem is [11]:

$$\dot{x} = f(t, x, z, \varepsilon), \quad x(t_0) = x_0, \quad x \in \Re^n \tag{15}$$

$$\varepsilon \dot{z} = g(t, x, z, \varepsilon), \quad z(t_0) = z_0, \quad z \in \Re^m \tag{16}$$

When the functions f and g are scaled to have the same order of magnitude, the perturbation parameter ε represents the ratio of time scales associated with x and z. When ε approaches zero the dynamics of z become infinitely faster than x and the system under certain conditions approaches the solution obtained by setting ε to zero

$$\dot{x} = f(t, x, z) \tag{17}$$

$$0 = g(t, x, z) \tag{18}$$

which is in the same form as a set of differential-algebraic equations (equations (4) and (5)). This observation suggests that a set of DAEs can be transformed to an explicit set of ordinary differential equations by adding appropriate singularly perturbed dynamics to the differential-algebraic system. Singular perturbation analysis techniques can be used to analyze the behavior of this class of systems and help guide the synthesis of appropriate fast dynamics. The conditions for asymptotic convergence are derived in the following paragraphs.

The degree of violation of the algebraic constraints by the augmented system (15,16) can be expressed by the function

$$w = g(t, x, z), \quad w \in \Re^m \tag{19}$$

The convergence of the model to the algebraic constraints of the DAE can be examined through the dynamics of w. Ideally, we would like the system to converge to an invariant set [19]:

$$w = 0 \tag{20}$$

The invariance property implies that trajectories are confined to the set for all time after the system converges. Thus, after the constraints are satisfied they will continue to be exactly satisfied. A simple equation that accomplishes this goal is

$$\dot{w} = -\frac{1}{\varepsilon}w = \frac{\partial w}{\partial t} + \frac{\partial w}{\partial x}\dot{x} + \frac{\partial w}{\partial z}\dot{z} \tag{21}$$

where ε is a positive scalar. The DAE system is essentially approximated by a set of ODEs with an attractive manifold given by the constraint equations. To be a physically valid approximation it is important that the manifold be attractive. A common approach for deriving state space formulations is to use the marginally stable manifold formed by differentiating the constraint equations

$$\dot{w} = 0 = \frac{\partial w}{\partial t} + \frac{\partial w}{\partial x}\dot{x} + \frac{\partial w}{\partial z}\dot{z} \tag{22}$$

However, this differentiation based approach will eventually drift off the constraints in the in the presence of small numerical errors.

Equation (21) can be solved for $\dot{z}$ since the Jacobian matrix $[\partial w / \partial z]$ is non-singular. The combined system can thus be written as

$$\dot{x} = f(t, x, z) \tag{23}$$

$$\varepsilon\dot{z} = -\left[\frac{\partial w}{\partial z}\right]^{-1} w - \varepsilon\left[\frac{\partial w}{\partial z}\right]^{-1}\left[\frac{\partial w}{\partial t} \cdots \frac{\partial w}{\partial x}f\right] \qquad (24)$$

This system will asymptotically converge to the invariant set of algebraic constraints in some local neighborhood of the exact solution where the Jacobian is non-singular. From the implicit function theorem it follows that there will be at least some small nonsingular region around the solution. Initial conditions should be chosen sufficiently close to the exact solution to avoid singularities during convergence or convergence to an invalid solution.

2.6 Approximate Dynamics

In practice, the calculation of the Jacobians, $[\partial w/\partial z]$ and $[\partial w/\partial x]$, may introduce substantial computational burden. This is often the case for large scale thermo-fluid networks where computationally intensive thermodynamic property routines must be numerically differentiated. From equation (24), it can be seen that the fast dynamics of z are mainly driven by the first term on the right hand side of the equation since the second term is ε times smaller than the first term. This suggests that the fast dynamics can be approximated by neglecting the second term. Furthermore, to avoid calculation of the inverse of the Jacobian matrix $[\partial w/\partial z]$, it is desired to seek another candidate for the coefficients of w. An approximate form of the fast dynamics is proposed as follows:

$$\varepsilon\dot{z} = R(t,x,z)w \quad , \quad R \in \Re_{mxm} \qquad (25)$$

where R is an approximate gradient that allows small insignificant terms in the dynamics to be neglected to help improve efficiency for simulation and real-time controller implementation. The criteria for convergence of the approximation are given by the following theorem.

Theorem 1. Consider the matrix defined by

$$\mathbf{JR} \tag{26}$$

where

$$\mathbf{J} = \frac{\partial \mathbf{w}}{\partial \mathbf{z}}(t, \mathbf{x}, \mathbf{z}) \tag{27}$$

If the matrix is negative definite and $\mathbf{J}$ is non-singular in a region of state space around the DAE solution then there exists a value of ε such that difference between the exact and approximate solution is given by

$$\mathbf{x}(t, \varepsilon) - \mathbf{x}(t) = \mathbf{O}(\varepsilon) \tag{28}$$

$$\mathbf{z}(t, \varepsilon) - \mathbf{z}(t) = \mathbf{O}(\varepsilon) \tag{29}$$

This result holds uniformly for some time interval $[t_b, t_1]$ after a short period $[t_o, t_b]$.

Proof. Singular perturbation analysis can be used to establish the validity of the approximate two-time-scale system (23,25) [12]. In particular, we need to analyze the stability of a boundary layer defined as the difference between the exact solution and the singularly perturbed system as ε approaches zero. When $\varepsilon \to 0$ the governing equations approach

$$\dot{\mathbf{x}} = \mathbf{f}(t, \mathbf{x}, \mathbf{z}) \tag{30}$$

$$\mathbf{0} = \mathbf{w}(t, \mathbf{x}, \mathbf{z}) \tag{31}$$

under the condition that $\mathbf{R}$ is not singular. It is assumed that equation (31) has an isolated real root so that we may invoke the implicit function theorem

$$z = h(t,x) \tag{32}$$

Then the exact solution to equations (30) and (31) can be obtained by solving the reduced order problem

$$\dot{x} = f(t,x,h(t,x)) \tag{33}$$

The convergence of the two-time-scale system to the exact solution can be established by investigating the dynamics in the fast time scale $t = \varepsilon\tau$. The system in this new time scale is

$$\frac{dx}{d\tau} = \varepsilon f(t_0 + \varepsilon\tau, x, z) \tag{34}$$

$$\frac{dz}{d\tau} = \mathbf{R}(t_0 + \varepsilon\tau, x, z)w(t_0 + \varepsilon\tau, x, z) \tag{35}$$

To show convergence to the true solution we need to investigate the stability of the boundary layer defined by

$$y = z - h(t,x) \tag{36}$$

Substituting this into (35) and taking the limit as $\varepsilon \to 0$ yields

$$\frac{dx}{d\tau} = 0 \tag{37}$$

$$\frac{dy}{d\tau} = \mathbf{R}(t_0, x_0, h(t_0, x_0) + y)w(t_0, x_0, h(t_0, x_0) + y) \tag{38}$$

The first equation implies that **x** is frozen at its initial value. If the boundary layer equation is locally exponentially stable uniformly in the frozen parameters t_0 and x_0, then Tikhonov's theorem [11] guarantees that there exists a value of ε such that the solution uniformly approximates the true solution after a short "boundary layer" interval $[t_0, t_b]$ (see Figure 11). That is,

$$\mathbf{x}(t,\varepsilon) - \mathbf{x}(t) = \mathbf{O}(\varepsilon) \qquad (39)$$

$$\mathbf{z}(t,\varepsilon) - \mathbf{h}(t,\mathbf{x}) = \mathbf{O}(\varepsilon) \qquad (40)$$

holds uniformly for a given time interval $[t_b, t_1]$.

Uniform exponential stability of the boundary layer dynamics can be established by finding a Lyapunov function $V(t_0, x_0, y)$ that satisfies the following conditions [11]:

$$c_1 \|y\|^2 \le V(t_0, x_0, y) \le c_2 \|y\|^2 \quad , \quad \|y\| \le \rho \qquad (41)$$

$$\frac{dV}{d\tau} \le -c_3 \|y\|^2 \qquad (42)$$

$$c_1 > 0 \quad , \quad c_2 > 0 \quad , \quad c_3 > 0 \qquad (43)$$

for all t_0 and x_0 in some region around the origin of the boundary layer ρ. These conditions can be proven using the Lyapunov function $V = w^T w / 2$. Close to the origin w can be expressed using a first order Taylor expansion

$$\mathbf{w} = J_0 \mathbf{y} + \text{higher order terms} \qquad (44)$$

32

where

$$J_o = \frac{\partial \mathbf{w}}{\partial \mathbf{y}}(t_o, \mathbf{x}_o, \mathbf{h}(t_o, \mathbf{x}_o)) \tag{45}$$

Near the origin the first order terms will dominate and the Lyapunov function is given by

$$V = \frac{1}{2}\|J_o \mathbf{y}\|^2 \tag{46}$$

This expression is bounded by

$$\frac{1}{2}\sigma_{min}^2(J_o)\|\mathbf{y}\|^2 \leq V \leq \frac{1}{2}\sigma_{max}^2(J_o)\|\mathbf{y}\|^2 \tag{47}$$

Since J_o is non-singular we have

$$c_1 = \frac{1}{2}\min_{t,x}\sigma_{min}^2(J_o) > 0 \quad , \quad c_2 = \frac{1}{2}\min_{t,x}\sigma_{max}^2(J_o) > 0 \tag{48}$$

The derivative of the Lyapunov function is given by

$$\frac{dV}{d\tau} = \mathbf{w}^T\frac{d\mathbf{w}}{d\tau} = \mathbf{w}^T J\frac{d\mathbf{y}}{d\tau} \tag{49}$$

where

$$J = \frac{\partial \mathbf{w}}{\partial \mathbf{y}}(t_0, \mathbf{x}_0, \mathbf{h}(t_0, \mathbf{x}_0) + \mathbf{y}) \tag{50}$$

Substituting the boundary layer dynamics (38) gives

$$\frac{dV}{d\tau} = \mathbf{w}^T J R \mathbf{w} \tag{51}$$

Since [JR] is negative definite we have [19]

$$\lambda_{min}(\mathbf{M})\|\mathbf{w}\|^2 \leq -\frac{dV}{d\tau} \leq \lambda_{max}(\mathbf{M})\|\mathbf{w}\|^2 \tag{52}$$

Where **M** is the symmetric positive definite part of [-JR]

$$\mathbf{M} = \frac{-JR - (JR)^T}{2} > 0 \tag{53}$$

Since **M** is symmetric positive definite the eigenvalues are always positive and the Lyapunov function is therefore bounded by

$$\frac{dV}{d\tau} \leq -\lambda_{min}(\mathbf{M})\|\mathbf{w}\|^2 \tag{54}$$

Using the Taylor expansion of **w** near the origin (44) it can be shown that this expression is bounded by

$$\frac{dV}{d\tau} \leq -\lambda_{min}(\mathbf{M})\sigma_{min}^2(J_0)\|\mathbf{y}\|^2 \tag{55}$$

The expression for c_3 is thus given by

$$c_3 = \min_{t,x,y} [\lambda_{min}(\mathbf{M})\sigma^2_{min}(\mathbf{J_o})] > 0 \qquad (56)$$

Therefore, it can be concluded that the origin is exponentially stable and that the results from Tikhonov's theorem apply. The criteria for exponential stability of the boundary layer are therefore equivalent to

$$\mathbf{JR} < 0, \quad \mathbf{J} = \frac{\partial \mathbf{w}}{\partial \mathbf{z}}(t_0, x_0, z) \qquad (57)$$

for all t_0 and x_0 in the domain of interest. An exact matrix that accomplishes this goal, while avoiding inversion of the Jacobian is

$$\mathbf{R} = -\mathbf{J}^T \qquad (58)$$

For a uniform approximation on infinite time intervals there is the additional requirement that the DAE system be exponentially stable. The convergence criteria depend on **J** being non-singular around some region of the exact solution. For some value of ε the solution will be sufficiently close to the exact solution to ensure that **J** is not singular. Singularities correspond to a possible transition between different physical configurations and usually should be avoided. The validity of the approximation can be checked by ensuring that det(**J**) does not vanish. This concludes the convergence theorem. ◻

The singular perturbation method is typically used for model reduction [12]. This new realization approach inverts the method to convert DAEs to ODEs. A geometrical interpretation of the approach is shown in Figure 12. It is apparent that the method constructs a set of ODEs that converge to a manifold that is a small

distance from the DAE. From a geometrical perspective the method is similar to the stiff dynamic element method. However, it has a number of significant advantages. The singular perturbation method has only one parameter to adjust (ε) versus two (stiffness and damping) for each dynamic element placed in the model. For large scale thermo-fluid systems the stiff dynamic element method could result in hundreds of parameters that have to be carefully adjusted to achieve a good approximation. Therefore, the new realization approach is far more systematic in this respect. Furthermore, it will be shown in chapter 4 that the stability of the realization is guaranteed for some value of ε. No such guarantee exists using stiff dynamic elements. Certain combinations could conceivably result in unstable interactions. It will later be shown that this new approach is much more accurate for a given stiffness of the dynamics. This is because the dynamics are directly forced by the constraints, whereas in the stiff dynamic element method they are only forced indirectly. Lastly, the singular perturbation method has the important advantage that there exists a large number of control methods that deal with systems in standard singular perturbation form [12]. The stiff dynamic element method (14) cannot easily be written in this form so it is not as well suited for control design.

In this chapter, a new approach based on singular perturbation analysis was introduced for converting a system described by DAEs to an explicit state space representation. This was achieved through the addition of fast dynamics that converge to the algebraic constraints. Since the constraints were assumed to be non-singular the approach is limited to index one problems. However, it will later be shown that this result plays an important role in the realization of high index DAEs.
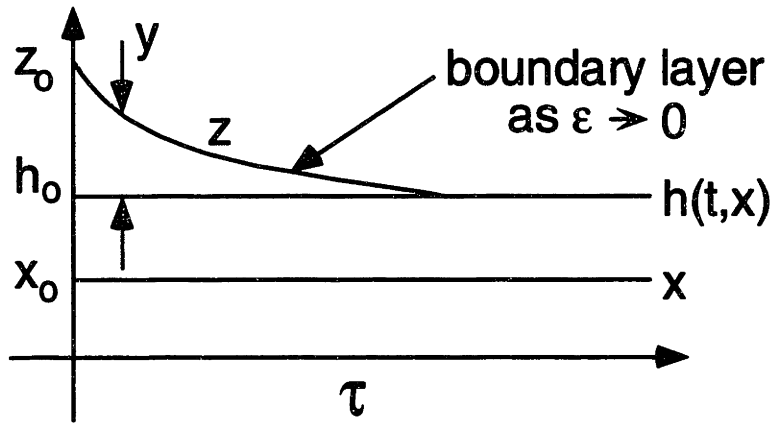
Figure 11. Boundary layer dynamics
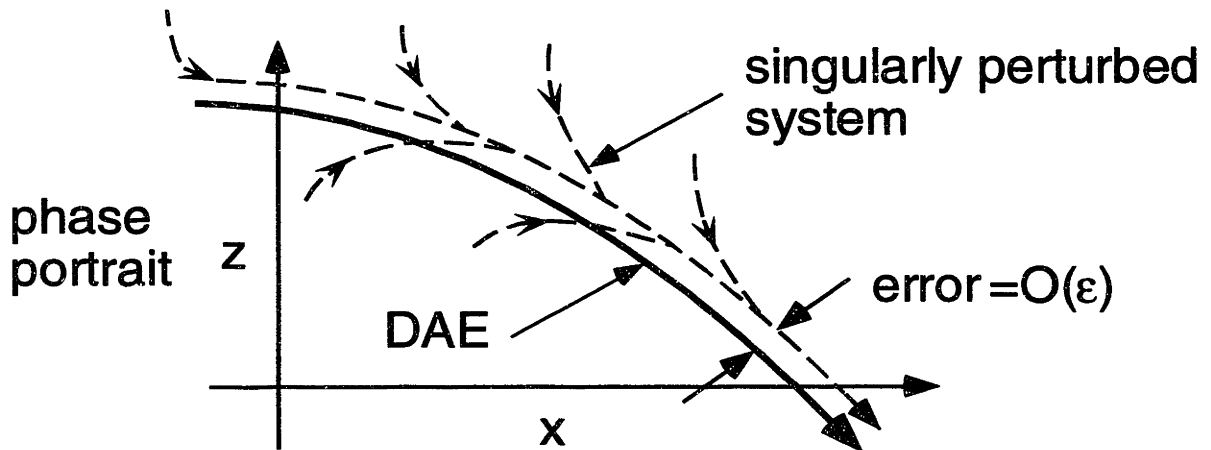
Figure 12. The singular perturbation approach

3. State Space Realization of High Index DAEs

3.1 Introduction

In the singular perturbation approach it was assumed that the constraint equations are nonsingular which corresponds to an index one DAE. High index systems present more difficult problems in simulation and control due to the presence of additional constraints that must be satisfied. In this chapter, new methods are developed to address this more general class of problems. By relating the index property to nonlinear control concepts a new type of control problem is formulated that is equivalent to the realization process for high index systems. This leads to representation of constraints in terms of sliding manifolds and a generalization of the singular perturbation method. Further, a new realization approach is developed based on a sliding control analogy. Together, these results provide the key elements needed for development of the singularly perturbed sliding manifold approach to realization.

3.2 The Index Property of a DAE System

A high index differential-algebraic system can be expressed in the general form

$$\dot{x} = f(t, x, z) \tag{59}$$

$$0 = g(t, x, z) \tag{60}$$

where $x \in \Re^n$, $z \in \Re^m$, $f: \Re \times \Re^n \times \Re^m \to \Re^n$, and $g: \Re \times \Re^n \times \Re^m \to \Re^m$. In the following discussion it is assumed that that f and g are sufficiently differentiable and that a well defined solution for x and z exists with consistent initial conditions.

Under these assumptions an important structural property of a DAE known as the index can be defined [1].

Definition 1. The minimum number of times that all or part of the constraint equations (60) must be differentiated with respect to time in order to solve for $\dot{z}$ as a continuous function of t, **x**, and **z** is the *index* of the DAE (59-60).

Carrying out the differentiation procedure once gives

$$0 = \frac{\partial \mathbf{g}}{\partial t} + \frac{\partial \mathbf{g}}{\partial \mathbf{x}} \mathbf{f} + \frac{\partial \mathbf{g}}{\partial \mathbf{z}} \dot{\mathbf{z}} \tag{61}$$

It is apparent that if the Jacobian $[\partial \mathbf{g}/\partial \mathbf{z}]$ is nonsingular then it is possible to solve for $\dot{z}$ and the system has an index of one. For high index systems (index > 1) the Jacobian is not invertible and the constraint equations are identically singular with respect to **z**. This violates the assumption made in standard singular perturbation theory that the constraints have an isolated root. Therefore, the singular perturbation approach cannot be used for high index systems without further modification. Realization of a high index DAE generally involves differentiating the constraint equations. However, it will be shown later that differentiation by itself is not an acceptable method for generating state space realizations.

High index problems are common in many control applications [3]. A constrained multi-body mechanical system, such as a four bar linkage (see Figure 13), is a common example of a high index DAE system. The Lagrange formulation for the equations of motion can be expressed as

$$\mathbf{M}(\mathbf{x})\dot{\mathbf{v}} = \mathbf{b}(\mathbf{x}, \mathbf{v}) - \mathbf{g}_{\mathbf{x}}^{\mathrm{T}}(\mathbf{x})\mathbf{z} \tag{62}$$
$$\dot{\mathbf{x}} = \mathbf{v}$$
$$0 = \mathbf{g}(\mathbf{x})$$

This is a high index problem since the constraints g do not involve z. From a geometrical point of view, high index DAEs correspond to systems that have additional algebraic constraints that involve the assumed unconstrained states x. For instance, the four bar linkage has only one degree of freedom which implies that the states of the other three links are algebraically coupled. A deeper geometric interpretation of high index behavior will be given in section 3.7 using the normal form representation of a DAE system. Conceivably, the index could vary at different points in state space. However, many types of physical systems have a constant index in a large domain of operation. Therefore, it will be assumed that the index remains constant in some local region of state space around the DAE solution. Changes in index correspond to critical configuration changes such as kinematic singularities so caution should be used in these situations to ensure that the system index remains constant.
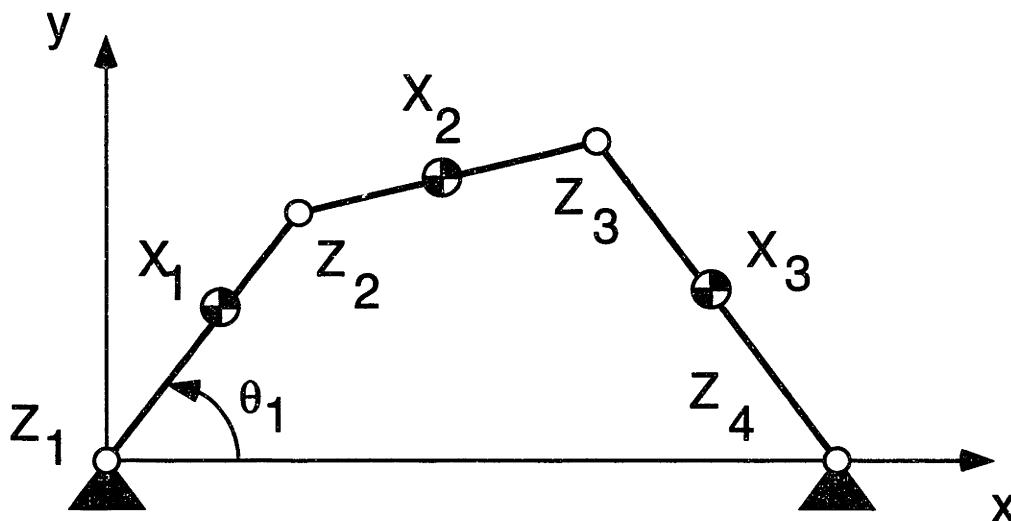
Figure 13. An example of a high index DAE

3.3 A Relation between DAE Realization and Nonlinear Control

In this section, an important connection between DAE systems and nonlinear control theory is made by formulating a control problem that is equivalent to the DAE realization process. This has substantial implications since it allows existing insights from geometrical control theory to be used for analysis and realization of high index DAE systems. This new connection is expressed in the following proposition.

Proposition 1. Consider the SISO nonlinear control problem defined by

$$\dot{\mathbf{x}} = \mathbf{f}(t, \mathbf{x}, \mathbf{z})$$
$$\dot{z} = v \tag{63}$$
$$\mathbf{w} = \mathbf{g}(t, \mathbf{x}, \mathbf{z})$$

where v is some fictitious input that drives z which is now assumed to be independent, and w is an output equal to the violation of the constraint equations. Then the relative degree of this problem is equal to the index of the DAE, and the zero dynamics represent the dynamics of the high index DAE.

Remark 1. The input, by definition, is equal to $\dot{z}$. The relative degree is defined as the number of times the output must be differentiated to explicitly determine the input. By analogy to definition 1 it is evident that the index and relative degree are equal. Furthermore, the zero dynamics are defined as the system dynamics when the input is chosen to force the output to zero. It is evident that integrating this input yields a solution to the high index DAE problem. Since it was assumed that the high index DAE has a unique solution the zero dynamics are therefore equivalent to the DAE system.
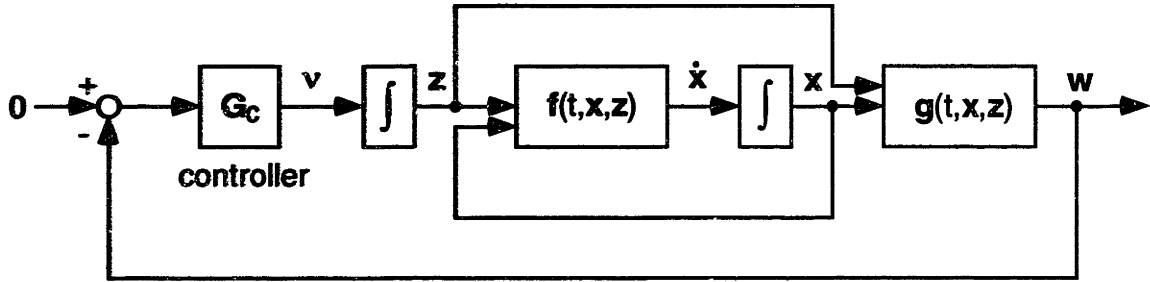
Figure 14. Block diagram of DAE realization approach

These results imply that the realization of an explicit state space model for a high index DAE system can be interpreted as finding a controller that forces the defined output to zero (see Figure 14). Most DAE problems have an equal number constraints, and excess constraint equations can in principle be removed. Therefore, it can be assumed without much loss of generality that the number of outputs are equal to the number of inputs. Problems with this property, known as square systems, simplify the design of output controllers considerably. For SISO systems the analogy between index and relative degree is relatively straightforward. However, for MIMO systems the definition of the index needs to be generalized in the following manner.

Definition 2. The *vector index* of a multiple constraint DAE is defined as

$$r \equiv [r_1 \quad \dots \quad r_m]^T \tag{64}$$

Where r_i is the number of times each constraint w_i must be differentiated for components of $\dot{z}$ to appear. If the required differentiations are constant in some

42

region of state space around the DAE solution and they explicitly determine $\dot{z}$ then the vector index is well defined.

This property is analogous to the vector relative degree used in MIMO control with a specialized form of input and domain [9]. Since the number of constraints are equal to the number of constrained states the control problem is square. Note that the index of the previous definition is the largest component of the vector index. It will be found later that another index measure analogous to the total relative degree is also theoretically important.

Definition 3. The *total index* of a multiple constraint DAE is defined as

$$r_t \equiv \sum_{i=1}^{m} r_i \tag{65}$$

Where r_i are the components of the vector index.

In order for the vector index to be well defined the definition requires that $\dot{z}$ is explicitly determined after performing the required differentiations. The criteria for this property can be determined by differentiating the constraints to obtain a set of algebraic equations that must always be satisfied by an exact solution of the DAE [1]:

$$
\begin{aligned}
0 &= w_i(t, x) \\
0 &= \frac{dw_i}{dt}(t, x) \\
&\quad \dots \\
0 &= \frac{d^{r_i-1}w_i}{dt^{r_i-1}}(t, x, z) \qquad \text{for } 1 \le i \le m
\end{aligned}
\tag{66}
$$

For z to be explicitly determined by the constraints (66) the implicit function theorem requires that the following Jacobian matrix be nonsingular.

$$J_\Omega = \frac{\partial \Omega}{\partial z} \qquad (67)$$

Where

$$\Omega_i = \frac{d^{r_i - 1} w_i}{dt^{r_i - 1}}(t, x, z) \qquad \text{for } 1 \le i \le m \qquad (68)$$

For many types of physical systems it can be shown that the Jacobian is always nonsingular. The non-singularity criteria is equivalent to the assumption made in the vector index that the constraints explicitly determine $\dot{z}$. This can be seen from the following expression for $\dot{\Omega}$ which can in principle be solved for $\dot{z}$

$$0 = \frac{\partial \Omega}{\partial t} + \frac{\partial \Omega}{\partial x} f + \frac{\partial \Omega}{\partial z} \dot{z} \qquad (69)$$

The Jacobian invertibility criteria thus completes the definition of the vector index.

The analogy between nonlinear control and high index DAE systems has substantial implications since it allows existing insights from nonlinear control theory to be used for analysis and realization of high index DAE systems. Nonlinear control methods can thus be used to help systematically construct realizations of DAE systems. However, it should be noted that this problem differs significantly from a typical nonlinear control problem since the objective is to have the two dynamic systems (59-60,63) converge in some approximate manner in the presence of state variations and controller activity. The three main issues that need to be addressed are

1)   How to force high index constraints to zero

2)   How to reduce computational complexity

3)   How to guarantee convergence

The first issue is addressed in section 3.4 by constructing an appropriate sliding manifold. In chapter 4, boundary layer sliding control is combined with the singular perturbation method to address the second problem. Furthermore, singular perturbation analysis and results from feedback linearization theory are used to determine the necessary criteria for convergence.

3.4 Modeling of Algebraic Constraints using Sliding Manifolds

Systematic methods will now be developed for designing control inputs that force the high index constraints to zero. For a valid solution each of the constraint equations (66) must be simultaneously satisfied. This objective can be achieved by constructing a sliding manifold with an attractive invariant set composed of the constraint equations. The criteria for this procedure are outlined in the following theorem

Theorem 2. If a DAE system has a vector index of r then a sliding manifold s can be constructed with components defined as

$$s_i = \left(\mu\frac{d}{dt}+1\right)^{r_i-1} w_i \quad , \quad \mu > 0 \qquad \text{for } 1 \le i \le m \tag{70}$$

so that $s = 0$ has an attractive invariant set composed of the constraint equations. Furthermore, s needs to be differentiated only once to explicitly determine $\dot{z}$ (or v).

Proof. By construction, each equation $s_i = 0$ represents a high order differential equation in w_i with stable poles at $\lambda = -\mu^{-1}$. Therefore, the constraint dynamics are exponentially stable and the constraints are asymptotically satisfied

$$
\begin{aligned}
& w_i(t,x) \to 0 \\
& \frac{dw_i}{dt}(t,x) \to 0 \\
& \quad ... \\
& \frac{d^{r_i-1}w_i}{dt^{r_i-1}}(t,x,z) \to 0 \qquad \text{for } 1 \le i \le m \quad \text{as} \quad t \to \infty
\end{aligned}
\tag{71}
$$

Thus, $s = 0$ has an invariant set composed of the high index constraints equations (66). This implies that after the constraints are satisfied they will continue to be exactly satisfied, which will result in an exact solution of the high index DAE. Further, the derivative of s is given by

$$
\frac{ds}{dt} = \frac{\partial s}{\partial z}\dot{z} + \frac{\partial s}{\partial x}f + \frac{\partial s}{\partial t}
\tag{72}
$$

Expand each component of s noting that lower order derivatives are independent of z

$$
s_i = \left(\mu\frac{d}{dt}+1\right)^{r_i-1} w_i = \beta_i(t,x) + \mu^{r_i-1}\frac{d^{r_i-1}w_i}{dt^{r_i-1}} \qquad \text{for } 1 \le i \le m
\tag{73}
$$

Combining the components and using definition 2 yields

46

$$s = \beta(t,x) + \text{diag}[\mu^{r_i-1}]\, \Omega(t,x,z)$$

(74)

Therefore,

$$\frac{\partial s}{\partial z} = \text{diag}[\mu^{r_i-1}]\frac{\partial \Omega}{\partial z}$$

(75)

From the definition of the vector index it is apparent that $[\partial s/\partial z]$ is non-singular around the DAE solution. This implies that the derivative of s (72) explicitly determines $\dot{z}$ which completes the proof. ◻

The realization problem now becomes how to force s to zero. One simple way this can be accomplished is by designing inputs that enforce exponentially stable dynamics for s:

$$\mu \dot{s} = -s$$

(76)

This expression can be solved for v by expanding the derivative term

$$\mu \frac{\partial s}{\partial z} v = -s - \mu\left[\frac{\partial s}{\partial x}f + \frac{\partial s}{\partial t}\right]$$

(77)

Since $[\partial s/\partial z]$ is non-singular we can solve for v, which yields an explicit ODE with an invariant set composed of the algebraic constraints

$$\dot{x} = f(t,x,z)$$
$$\dot{z} = v$$

(78)

This system will asymptotically converge to the invariant set of algebraic constraints in some local neighborhood of the exact solution where the Jacobian multiplying v is nonsingular. Initial conditions should be chosen sufficiently close to the exact solution to avoid singularities during convergence or convergence to an invalid solution. It is evident that an asymptotically exact representation of a high index DAE can easily be obtained using sliding manifolds. However, this may be at the expense of calculating potentially computationally expensive Jacobian terms. The following example illustrates this problem.

Example: A general index two DAE

The asymptotic control method (77) was applied to a general DAE with a vector index of $r_i = 2$ in order to illustrate the technique and gain more insight into the requirements of the method. Start with the definition of a sliding surface for an index two problem

$$s = \mu \frac{dw}{dt} + w \qquad (79)$$

$$\dot{s} = \mu \left[\frac{\partial}{\partial t}\left(\frac{dw}{dt}\right) + \frac{\partial}{\partial x}\left(\frac{dw}{dt}\right) \cdot f + \frac{\partial}{\partial z}\left(\frac{dw}{dt}\right) \cdot v \right] + \frac{dw}{dt} \qquad (80)$$

where

$$\frac{dw}{dt} = \frac{\partial w}{\partial t} + \frac{\partial w}{\partial x} f \qquad (81)$$

Substituting these expressions into the sliding dynamics (76) and solving for v gives

$$\mu^2 \frac{\partial}{\partial z}\left(\frac{dw}{dt}\right) \cdot v = -w - 2\mu\left(\frac{dw}{dt}\right) - \mu^2\left[\frac{\partial}{\partial t}\left(\frac{dw}{dt}\right) + \frac{\partial}{\partial x}\left(\frac{dw}{dt}\right) \cdot f\right] \tag{82}$$

This controller will asymptotically converge to the invariant set of algebraic constraints in some local neighborhood of the exact solution. However, this may be achieved at the expense of calculating computationally expensive Jacobians of terms which are in turn composed of other Jacobians. The recursive complexity associated with calculating Jacobians could limit the usefulness of the sliding manifold approach. This warrants the investigation of model reduction techniques for more efficient computation.

3.5 Generalization of the Singular Perturbation Approach

Using the results of the previous sections the singular perturbation approach for index one DAE systems can be extended to high index problems. The singular perturbation realization method has the form

$$\dot{x} = f(t,x,z)$$
$$\varepsilon\dot{z} = R(t,x,z)w(t,x,z) \quad , \quad 0 < \varepsilon \ll 1 \tag{83}$$

The critical assumption made in developing this result is that the constraint equation must be explicitly solvable for z , which corresponds to an index one system. High index systems are identically singular so the method cannot be directly applied.

The singular perturbation approach can be generalized by using the previously defined sliding manifold. This extension is based on the observation that the sliding surface represents an algebraic relation that can be explicitly solved for z . If z is chosen to satisfy s = 0 then the constraints will be asymptotically

satisfied. Therefore, an index one DAE can be constructed that asymptotically converges to the high index DAE

$$\dot{x} = f(t, x, z) \tag{84}$$
$$0 = s(t, x, z)$$

The singular perturbation approach can now be applied as before. This leads to the generalized singular perturbation approach

$$\dot{x} = f(t, x, z) \tag{85}$$
$$\varepsilon\dot{z} = \varepsilon\nu = R(t, x, z)s(t, x, z)$$

where

$$J_s R < 0 \quad , \quad J_s = \frac{\partial s}{\partial z}(t, x, z) \tag{86}$$

The convergence criteria depend, in a similar manner to index one systems, on the Jacobian being non-singular around some region of the exact solution. This follows from theorem 2 if the vector index is well defined. Then for some value of ε the approximation will be sufficiently close to the exact solution to guarantee that the Jacobian is nonsingular. The validity of the solution should be checked by ensuring the determinant of the Jacobian doesn't vanish. Furthermore, it should be noted that the purpose of this section is to motivate a generalization of the singular perturbation approach. By itself, it doesn't constitute a rigorous proof of the method for high index systems. A rigorous proof of these results will be presented in the next chapter after the necessary mathematical results are developed.

Example: A general index 2 DAE

The generalized singular perturbation approach for a DAE with a vector index of $r_i = 2$ was derived to illustrate the technique and to compare it to the other approaches. Applying the method yields

$$\varepsilon v = \mathbf{R}\left[\mu\frac{d\mathbf{w}}{dt} + \mathbf{w}\right]$$

(87)

Where one possible choice for $\mathbf{R}$ is

$$\mathbf{R} = -\left[\mu\frac{\partial}{\partial \mathbf{z}}\left(\frac{d\mathbf{w}}{dt}\right)\right]^{\mathbf{T}}$$

(88)

Comparing this expression to the asymptotic sliding dynamics (82) it can be seen that the Jacobian calculation requirements are substantially reduced. However, there is a tradeoff since a small perturbation parameter may be needed for a good approximation, which could incur additional computational effort. For many applications, including thermo-fluid systems, Jacobian calculations often far outweigh the added expense of the fast dynamics [6].

3.6 Sliding Control Method

An alternative approach that would allow the removal of computationally expensive Jacobian terms is to use a sliding control method to drive s to zero. A sliding condition analysis can be used to determined the necessary criteria for convergence [19]. Start with a quadratic Lyapunov function

51

$$V = \frac{1}{2}s^Ts > 0$$

<div align="right">(89)</div>

Therefore

$$\frac{dV}{dt} = s^T\dot{s} = s^T(\alpha + J_s\nu)$$

<div align="right">(90)</div>

where

$$J_s = \frac{\partial s}{\partial z} \quad , \quad \alpha = \frac{\partial s}{\partial t} + \frac{\partial s}{\partial x}f$$

<div align="right">(91)</div>

Now select the control inputs

$$J_s \cdot \nu = -\hat{\alpha} - \text{diag}(k)\,\text{sgn}(s)$$

<div align="right">(92)</div>

Where $\hat{\alpha}$ is a more computationally efficient approximation of the Jacobian terms α and sgn() is a component-wise sign function. From theorem 2, the coefficients of ν are locally nonsingular. Thus, we can explicitly solve for the required input. This yields

$$\frac{dV}{dt} = s^T(\alpha - \hat{\alpha}) - \sum_{i=1}^{m}k_i|s_i|$$

<div align="right">(93)</div>

Now choose the components of the gain vector k so that

$$k_i \geq |\alpha_i - \hat{\alpha}_i| + \eta_i \quad , \quad \eta_i > 0 \quad \text{for } 1 \leq i \leq m$$

<div align="right">(94)</div>

The sliding condition then follows,

$$\frac{dV}{dt} = \frac{1}{2}\frac{d}{dt}s^Ts \le -\sum_{i=1}^{m}\eta_i|s_i|$$

(95)

Which implies that $s \to 0$ and that the constraints will be asymptotically satisfied. Further, $s = 0$ is an invariant set in the system and the constraints form an invariant set within $s = 0$. Therefore, if $s = 0$ and the other constraints are initially satisfied then they will always be satisfied. Under these conditions the sliding control method produces an exact representation of the DAE.

Example: A general index 2 DAE

Applying the sliding control method to the previous example gives

$$\mu \frac{\partial}{\partial z}\left(\frac{dw}{dt}\right) \cdot v = -\hat{r} - \text{diag}(k)\,\text{sgn}\left[\mu\frac{dw}{dt} + w\right]$$

(96)

where

$$k_i \ge |\alpha_i - \hat{\alpha}_i| + \eta_i \quad , \quad \eta_i > 0 \quad \text{for } 1 \le i \le m$$

(97)

$$\alpha = \mu\left[\frac{\partial}{\partial t}\left(\frac{dw}{dt}\right) + \frac{\partial}{\partial x}\left(\frac{dw}{dt}\right) \cdot f\right] + \frac{dw}{dt}$$

(98)

$$\frac{dw}{dt} = \frac{\partial w}{\partial t} + \frac{\partial w}{\partial x}f$$

(99)

From these equations it is apparent that the sliding control method allows precise control over the tradeoff between Jacobian calculation and the control gain required

for a good approximation. Therefore, large computationally inexpensive terms can be included in $\hat{a}$ to effectively reduce the bandwidth of the controller. The main drawback is the discontinuous control input. This is very undesirable because it can result in chattering behavior that could enter the actual control input and excite unmodeled dynamics. Furthermore, a very small time step is necessary to satisfactorily discretize the method for simulation and implementation. Effective methods to smooth out the discontinuities are investigated in the following chapter.

3.7 Normal Form Representation of DAEs

The normal form representation used in geometrical control theory plays an important role in understanding the zero dynamics and behavior of systems with controlled outputs [9]. By applying the connection between DAE realization and nonlinear control it is possible to use normal form analysis to gain new insights about DAE systems. In addition, this approach provides a means of understanding the convergence properties of the proposed realization methods. In the next chapter this theory will be used to prove various results concerning DAE realizations.

Consider a SISO control system that represents an autonomous DAE system with a single constraint equation

$$
\begin{aligned}
\dot{x} &= f(x,z) \\
\dot{z} &= v \\
w &= g(x,z)
\end{aligned}
\tag{100}
$$

This system can be expressed in the more generic form

$$
\begin{aligned}
\dot{\zeta} &= \gamma(\zeta) + \beta(\zeta)v \\
w &= g(\zeta)
\end{aligned}
\tag{101}
$$

where

$$\zeta = \begin{bmatrix} \mathbf{x} \\ \mathbf{z} \end{bmatrix} \quad , \quad \gamma = \begin{bmatrix} \mathbf{f} \\ 0 \end{bmatrix} \quad , \quad \beta = \begin{bmatrix} \mathbf{0}_{nx1} \\ 1 \end{bmatrix}$$

(102)

If the DAE system has a constant index in a region of state space around some point ζ_0 then it can be proven [9] that locally there exists a smooth invertible nonlinear coordinate transformation

$$\Phi(\zeta) = [p_1 \quad \cdots \quad p_r \quad q_1 \quad \cdots \quad q_{n+1-r}]^T \quad , \quad \Phi : \mathfrak{R}^{n+1} \to \mathfrak{R}^{n+1}$$

(103)

such that the dynamics can be expressed in normal form

$$\dot{\mathbf{p}} = \begin{bmatrix} p_2 \\ \cdots \\ \cdots \\ p_r \\ a(\mathbf{p},\mathbf{q}) + b(\mathbf{p},\mathbf{q})v \end{bmatrix}$$

$$\dot{\mathbf{q}} = c(\mathbf{p},\mathbf{q})$$

(104)

where

$$\mathbf{p} = [w \quad \dot{w} \quad \cdots \quad w^{(r-1)}]^T$$

(105)

The output can be written as

$$w = p_1 \qquad\qquad (106)$$

It is apparent that the first states p in the normal form can be interpreted as constrained states that are zero when the output is zero. The remaining states q represent unconstrained coordinates that, in general, can vary even when the output is zero. In normal form the zero dynamics are given by

$$\dot{p} = 0 \qquad\qquad p(t_o) = 0 \qquad\qquad (107)$$
$$\dot{q} = c(0,q)$$

This representation effectively gives the dynamics of the associated DAE system in an independent generalized coordinate frame. It is evident from the dimension of q that the actual dimension of the DAE dynamics is given by $\Delta = n + 1 - r$. Thus, for an index one system the dimension is equal to the dimension of x. As the index of the system increases the dimension of the DAE decreases. For a system with an index of $(n+1)$ there are no dynamics and the DAE actually represents an algebraic relationship. From a geometrical interpretation of these results it is apparent that the number of independent states is given by Δ. Furthermore, it is possible to define a coordinate transformation such that the system has $n - \Delta$ dependant states. Thus, an index one system has no dependant elements in x whereas a high index DAE will always have dependant states.

The normal form can also be used to study the behavior of systems with controlled outputs. From the definition of the index it follows that $b(p,q)$ is invertible. Therefore, it is always possible to find a nonlinear controller that linearizes the input-output dynamics using the following input transformation

$$v = b(p,q)^{-1}(V - a(p,q)) \qquad\qquad (108)$$

Where V is a redefined input. This leads to linear dynamics for the constrained states

$$\dot{p} = \begin{bmatrix} p_2 \\ \cdots \\ \cdots \\ p_r \\ V \end{bmatrix} \tag{109}$$

It can easily be shown that this form is always controllable and that by using state feedback of the constrained states the pole locations can be arbitrarily specified

$$V = -Fp \quad \Rightarrow \quad \dot{p} = Ap \quad , \quad \lambda(A) \in \Re_r \tag{110}$$

The DAE realization methods proposed in this thesis to some extent use this idea which results in stable output dynamics. However, this procedure is not guaranteed to converge to the DAE if the initial conditions of p are not zero. The stability of a realization method depends on the behavior of the second equation in (104) known as the internal dynamics of the system. Its behavior depends on p so the stability of the internal dynamics depends on the form of the output dynamics. It will be shown in the next chapter, however, that stability of the DAE implies local stability of the realization. Note that p and the terms a(ζ) and b(ζ) in the first equation of (104) can easily be calculated since they only involve derivatives of the constraints. However, selection of the remaining coordinates and the nonlinear transformation generally involves solving a difficult set of partial differential equations (PDEs). The main utility of the normal form representation is as a theoretical tool, and the internal dynamics usually must be studied using another set of co-ordinates.

The normal form representation can be generalized to MIMO systems which occur for autonomous DAE systems with multiple constraints. For the class of DAE systems under consideration the MIMO system is square with the number of inputs equal to the number of outputs. The system can be written in the form

$$
\begin{aligned}
\dot{\mathbf{x}} &= \mathbf{f}(\mathbf{x}, \mathbf{z}) \\
\dot{\mathbf{z}} &= \mathbf{v} \\
\mathbf{w} &= \mathbf{g}(\mathbf{x}, \mathbf{z})
\end{aligned}
\tag{111}
$$

This can be expressed as

$$
\begin{aligned}
\dot{\zeta} &= \gamma(\zeta) + \beta(\zeta)\mathbf{v} \\
\mathbf{w} &= \mathbf{g}(\zeta)
\end{aligned}
\tag{112}
$$

where

$$
\zeta = \begin{bmatrix} \mathbf{x} \\ \mathbf{z} \end{bmatrix} \quad , \quad \gamma = \begin{bmatrix} \mathbf{f} \\ \mathbf{0}_{m \times 1} \end{bmatrix} \quad , \quad \beta = \begin{bmatrix} \mathbf{0}_{n \times m} \\ \mathbf{I}_{m \times m} \end{bmatrix}
\tag{113}
$$

If the system has a constant vector index in a region of state space around some point ζ_0 then it can be proven that locally there exists a smooth invertible nonlinear coordinate transformation of the form

$$
\Phi(\zeta) = \begin{bmatrix} \mathbf{p}^1 \\ \cdots \\ \mathbf{p}^m \\ \mathbf{q}_1 \\ \cdots \\ \mathbf{q}_{n+m-r_t} \end{bmatrix} \quad , \quad \Phi : \mathfrak{R}^{n+m} \to \mathfrak{R}^{n+m}
\tag{114}
$$

The columns of β are always constant and thus have the special property that they form an involutive distribution [9]. This implies that the states q can be chosen such that their dynamics are independent of v. It then follows that the system can be expressed in the normal form representation

$$\dot{p}^i = \begin{bmatrix} p_2^i \\ \cdots \\ \cdots \\ p_{r_i}^i \\ a_i(p,q) + \sum_{j=1}^{m} b_{ij}(p,q)v_j \end{bmatrix} \qquad \text{for } 1 \leq i \leq m \qquad (115)$$

$$\dot{q} = c(p,q)$$

where

$$p^i = [w_i \quad \dot{w}_i \quad \cdots \quad w_i^{(r_i-1)}]^T \qquad (116)$$

$$p = \begin{bmatrix} p^1 \\ \cdots \\ p^m \end{bmatrix} \qquad (117)$$

The outputs can be written as

$$w_i = p_1^i \qquad (118)$$

Note that the elements of matrix b are equal to the Jacobian J_Ω which is nonsingular. The input-output dynamics can be expressed as

$$
\begin{bmatrix} \dot{p}_{r_1}^1 \\ ... \\ \dot{p}_{r_m}^m \end{bmatrix} = \mathbf{a}(\zeta) + \mathbf{b}(\zeta)\mathbf{v} \tag{119}
$$

Therefore, the output dynamics can always be transformed into a linear input-output relationship using the following transformation

$$
\mathbf{v} = \mathbf{b}(\mathbf{p},\mathbf{q})^{-1}(\mathbf{V} - \mathbf{a}(\mathbf{p},\mathbf{q})) \tag{120}
$$

Where $\mathbf{V}$ is a redefined input. This leads to decoupled linear dynamics for the constrained states

$$
\dot{\mathbf{p}}^i = \begin{bmatrix} p_2^i \\ ... \\ ... \\ p_{r_i}^i \\ V_i \end{bmatrix} \qquad \text{for } 1 \le i \le m \tag{121}
$$

It can easily be shown that this form is always controllable and using feedback of the constrained states the pole locations can be arbitrarily specified

$$
V_i = -\mathbf{F}_i \mathbf{p}^i \quad \Rightarrow \quad \dot{\mathbf{p}}^i = \mathbf{A}_i \mathbf{p}^i \quad , \quad \lambda_i(\mathbf{A}_i) \in \Re_{r_i} \tag{122}
$$

Just as before, the physical interpretation of the MIMO normal form can be found by examining the zero dynamics

$$\dot{p} = 0 \qquad\qquad p(t_o) = 0 \qquad\qquad (123)$$
$$\dot{q} = c(0, q)$$

In this case the dimension of the DAE dynamics is given by $\Delta = n + m - r_t$. Therefore, a system with a vector index of $r_i = 1$ has a dimension of n with no dependant states. When the total index is increased further the dimension decreases. The number of dependant states increases with the total index and is given by $n - \Delta$. Since the MIMO normal form has the same structure as the SISO case the same results hold for the relation between the internal dynamics and convergence of DAE realizations. Therefore, MIMO normal forms can be used to study the convergence of realization methods for multiple constraint high index DAEs.

4. The Singularly Perturbed Sliding Manifold Approach

4.1 Introduction

In this chapter the sliding control method and generalized singular perturbation approach are combined to create a new method for DAE realization. This approach has the advantages that it gives explicit error bounds and it allows a precise tradeoff between Jacobian calculation and control bandwidth. The following sections prove the convergence of the SPSM method which leads to significant insights into the nature of the approach. A simple pendulum example is then used to illustrate the method. Furthermore, important control properties of the SPSM such as stability, controllability, and observability are investigated. Finally, guidelines for the selection of parameters are presented based on a root locus analysis technique.

4.2 The Singularly Perturbed Sliding Manifold Approach

The sliding control approach to realization has a number of advantages such as the elimination of the approximation error after convergence. However, the price of this performance is that the sign function introduces discontinuous control activity. This is very undesirable because it can result in chattering behavior that could enter the actual control input and excite unmodeled dynamics. Furthermore, a very small time step is necessary to satisfactorily discretize the method during implementation. To overcome the discontinuity problems a boundary layer interpolation technique is employed [19]. This is achieved by replacing the sign function with a saturation function to smooth the input in a thin boundary layer region around the sliding surface. To achieve a good approximation the boundary layer must be very thin. As a result, the dynamics become singularly perturbed and the sliding control method needs to be combined with the singular perturbation

approach introduced in section 2.5. This results in the singularly perturbed sliding manifold approach (SPSM) to DAE realization:

$$\dot{x} = f(t,x,z)$$
$$\dot{z} = v$$
$$w = g(t,x,z)$$
$$\hat{J}_s v = -\hat{\alpha} - K \operatorname{sat}(\psi) \quad , \quad \psi = \varepsilon^{-1} \operatorname{diag}(\rho) s \quad , \quad 0 < \varepsilon \ll 1 \tag{124}$$
$$s_i = \left(\mu \frac{d}{dt} + 1\right)^{r_i - 1} w_i \quad , \quad \mu > 0 \quad \text{for } 1 \le i \le m$$

where $\hat{J}_s$ is a more computationally efficient approximation of J_s and $\operatorname{sat}(\psi)$ is the vector of components $\operatorname{sat}(\psi_i)$. The relative importance of the sliding surface components are specified by the weighting vector ρ. Further, the assumption that the gain matrix K is diagonal has been removed for the sake of generality. The criteria for the SPSM realization to be a good approximation to the high index DAE are derived in the next section.

4.3 Conditions for Convergence

Figure 15 shows the path that the trajectories of the SPSM realization (124) follow in order to illustrate the conditions required for convergence of the method. These are given as follows

1)   The DAE must have a vector index (definition 2).

2)   A sliding condition given by theorem 3 must be satisfied. This ensures that the trajectories will point into the boundary layer surface and remain inside.

3) Once the trajectory is inside the boundary layer the realization must satisfy a singular perturbation stability criteria (theorem 4). This is important because it ensures that the solution converges in a stable manner to a manifold [11] that is a small distance $O(\varepsilon)$ from the sliding surface which avoids the potential problem of chattering inside the boundary layer. A further consequence is that as ε approaches zero the realization approaches an index one DAE given by

$$\dot{x} = f(t,x,z)$$
$$0 = s(t,x,z)$$
(125)

Finally, a normal form representation is required to show that this equation converges to the high index DAE.
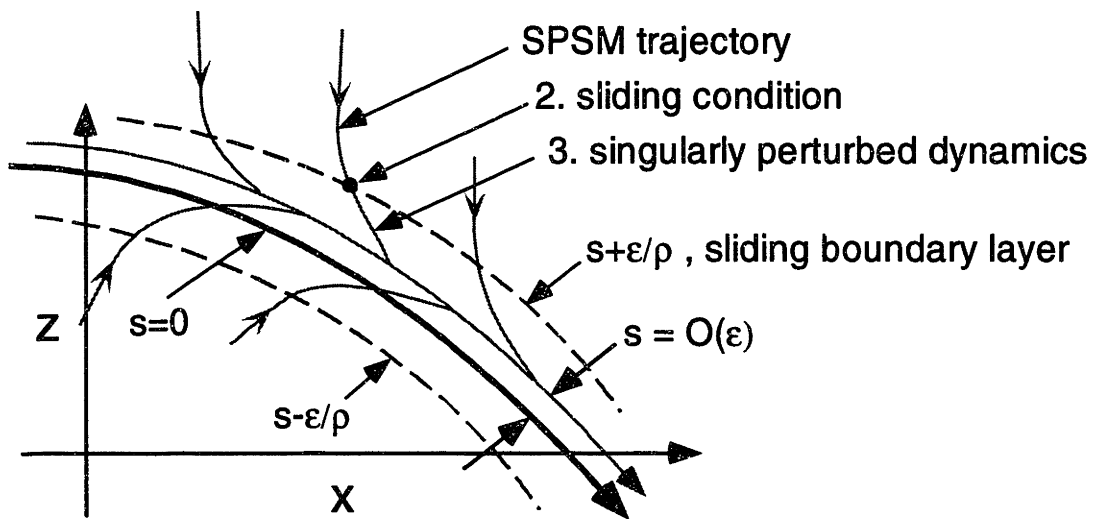

Figure 15. The SPSM realization method

The sliding condition is derived in the following theorem.

Theorem 3. The SPSM realization given by

$$\dot{\mathbf{x}} = \mathbf{f}(t, \mathbf{x}, \mathbf{z})$$
$$\dot{\mathbf{z}} = \mathbf{v}$$
$$\mathbf{w} = \mathbf{g}(t, \mathbf{x}, \mathbf{z})$$
$$\hat{\mathbf{J}}_s \mathbf{v} = -\hat{\alpha} - \mathbf{K} \operatorname{sat}(\psi) \quad , \quad \psi = \varepsilon^{-1} \operatorname{diag}(\rho) \mathbf{s} \quad , \quad 0 < \varepsilon \ll 1$$
$$s_i = \left(\mu \frac{d}{dt} + 1 \right)^{r_i - 1} w_i \quad , \quad \mu > 0 \quad \text{for } 1 \le i \le m$$

$$(124)$$

satisfies a sliding condition, if the DAE has a vector index $\mathbf{r}$ and

$$\mathbf{J}_s \hat{\mathbf{J}}_s^{-1} \mathbf{K} - \mathbf{\Gamma} \quad \text{is positive diagonally dominant} \tag{126}$$

where $\mathbf{\Gamma} = \left| \operatorname{diag}[\alpha - \mathbf{J}_s \hat{\mathbf{J}}_s^{-1} \hat{\alpha}] \right|$ is the uncertainty associated with approximating α. Furthermore, the errors of the constraints and their derivatives as well as the sliding manifold are explicitly bounded by

$$|s_i| \le \frac{\varepsilon}{\rho_i} \quad \text{for } 0 \le i \le m \tag{127}$$

$$\left| \frac{d^j w_i}{dt^j} \right| \le \frac{2^j \varepsilon}{\rho_i \mu^j} \quad \text{for } 0 \le j \le r_i - 1 \quad \text{for } 0 \le i \le m \tag{128}$$

Proof. A component-wise sliding condition can be used to guarantee that the sliding boundary layer is always attractive. This criteria can be expressed as

$$\dot{s}_i < 0 \quad , \quad s_i \geq \frac{\varepsilon}{\rho_i} \quad , \quad \text{for } 0 \leq i \leq m \tag{129}$$

$$\dot{s}_i > 0 \quad , \quad s_i \leq \frac{\varepsilon}{\rho_i} \quad , \quad \text{for } 0 \leq i \leq m \tag{130}$$

The derivative of the sliding manifold is given by

$$\dot{s} = J_s \nu + \alpha \tag{131}$$

Applying the SPSM input (124) gives

$$\dot{s} = \alpha - J_s \hat{J}_s^{-1} \hat{\alpha} - J_s \hat{J}_s^{-1} K \, \text{sat}(\varepsilon^{-1} \text{diag}(\rho) s) \tag{132}$$

Expanding this relationship for a particular component yields

$$\dot{s}_i = \gamma_i - D_{i1} \text{sat}\left[\frac{s_1 \rho_1}{\varepsilon}\right] - \dots - D_{ii} \text{sat}\left[\frac{s_i \rho_i}{\varepsilon}\right] - \dots - D_{im} \text{sat}\left[\frac{s_m \rho_m}{\varepsilon}\right] \tag{133}$$

where

$$\gamma = \alpha - J_s \hat{J}_s^{-1} \hat{\alpha} \quad , \quad D = J_s \hat{J}_s^{-1} K \tag{134}$$

If $s_i \geq \varepsilon / \rho_i$ then

$$\dot{s}_i = \gamma_i - D_{i1} \text{sat}\left[\frac{s_1 \rho_1}{\varepsilon}\right] - \dots - D_{ii} - \dots - D_{im} \text{sat}\left[\frac{s_m \rho_m}{\varepsilon}\right] \tag{135}$$

The sliding condition (129) can be enforced if

$$D_{ii} > \left| \gamma_i - D_{i1}\text{sat}\left[\frac{s_1\rho_1}{\varepsilon}\right] - ... - D_{im}\text{sat}\left[\frac{s_m\rho_m}{\varepsilon}\right] \right| \quad \Rightarrow \quad \dot{s}_i < 0 \qquad (136)$$

Which can be satisfied independently of the other sliding co-ordinates if

$$D_{ii} > |\gamma_i| + |D_{i1}| + ... + |D_{im}| \qquad (137)$$

This is equivalent to the matrix $\mathbf{D} - |\text{diag}(\gamma)|$ being positive diagonally dominant. Substituting the defined expressions (134) gives that $\mathbf{J}_s\hat{\mathbf{J}}_s^{-1}\mathbf{K} - \Gamma$ must be positive diagonally dominant. Following a similar procedure it can be shown that the sliding condition is the same for the other side of the boundary layer.

The sliding condition ensures that the boundary layer is an attractive invariant set. Therefore, once the solution enters the boundary layer it will remain there for all time. From this the error bounds on s follow

$$|s_i| \le \frac{\varepsilon}{\rho_i} \quad \text{for } 0 \le i \le m \qquad (138)$$

Following [19], the sliding manifold can be expressed as a sequence of first order linear filters which leads to bounds on the constraint errors

$$\left| \frac{d^j w_i}{dt^j} \right| \le \frac{2^j \varepsilon}{\rho_i \mu^j} \quad \text{for } 0 \le j \le r_i\text{-}1 \quad \text{for } 0 \le i \le m \qquad (139)$$

□

Remark 2. This result is an important addition to the singular perturbation approach because it can be used to help guide selection of ε. If the time constant μ of the sliding manifold is specified then ε can be adjusted to meet some desired constraint tolerances. The sliding condition can also be used to help guide the trade-off between control bandwidth and Jacobian computation. It is apparent from (126) that as $\hat{a}$ approaches a then less control gain **K** is needed to ensure that the test matrix is positive diagonally dominant. Furthermore, the error bounds can be used to ensure the realization will always be within a certain region of the DAE solution so the Jacobian $\mathbf{J}_s$ is nonsingular. □

In order to study the approximation error between the SPSM realization and the high index DAE system it is necessary to express the system in a special type of normal form representation. This transformation is expressed in the following lemma.

Lemma 1. If the DAE system has a vector index then the SPSM realization

$$
\begin{aligned}
&\dot{\mathbf{x}} = \mathbf{f}(t,\mathbf{x},\mathbf{z}) \\
&\dot{\mathbf{z}} = \mathbf{v} \\
&\mathbf{w} = \mathbf{g}(t,\mathbf{x},\mathbf{z}) \\
&\hat{\mathbf{J}}_s \mathbf{v} = -\hat{\mathbf{a}} - \mathbf{K}\,\mathrm{sat}(\boldsymbol{\psi}) \quad,\quad \boldsymbol{\psi} = \varepsilon^{-1}\mathrm{diag}(\boldsymbol{\rho})\mathbf{s} \quad,\quad 0 < \varepsilon \ll 1 \\
&s_i = \left(\mu\frac{d}{dt}+1\right)^{r_i-1} w_i \quad,\quad \mu > 0 \quad \text{for } 1 \le i \le m
\end{aligned}
\tag{124}
$$

inside the sliding boundary layer can be expressed in a sliding normal form coordinate system

$$\begin{bmatrix} \dot{p}_1^i \\ \cdots \\ \dot{p}_{r_i-2}^i \\ \dot{p}_{r_i-1}^i \end{bmatrix} = \begin{bmatrix} p_2^i \\ \cdots \\ p_{r_i-1}^i \\ (s_i - (r_i-1)\mu^{r_i-2}p_{r_i-1}^{i-1} - \cdots - (r_i-1)\mu p_2^i - p_1^i)/\mu^{r_i-1} \end{bmatrix} \qquad \text{for } 1 \le i \le m \tag{140}$$

$$\varepsilon\dot{s} = \varepsilon(\alpha - J_s\hat{J}_s^{-1}\hat{\alpha}) - J_s\hat{J}_s^{-1}K \,\mathrm{diag}(\rho)\,s$$

$$\dot{q} = c(q,s,\sigma)$$

where $q \in \Re^{n+m-\Sigma r_i}$ represents the internal states of the system, and the output states are given by

$$p^i = [w_i \quad \dot{w}_i \quad \cdots \quad w_i^{(r_i-1)}]^T \qquad \text{for } 1 \le i \le m$$

$$\sigma = \begin{bmatrix} [p_1^1 \quad p_2^1 \quad \cdots \quad p_{r_1-1}^1]^T \\ [p_1^2 \quad p_2^2 \quad \cdots \quad p_{r_2-1}^2]^T \\ \vdots \\ [p_1^m \quad p_2^m \quad \cdots \quad p_{r_m-1}^m]^T \end{bmatrix} \tag{141}$$

Proof. From proposition 1 and definition 2 it follows that if the DAE system has a vector index then the vector relative degree of the associated control problem (124) is well defined. Then from the normal form theory in section 3.7 it can be concluded that locally there exists a smooth invertible nonlinear state transformation

$$\Phi(\zeta) = \begin{bmatrix} p \\ q \end{bmatrix} \quad , \quad \Phi : \Re^{n+m} \to \Re^{n+m} \quad , \quad \zeta = \begin{bmatrix} x \\ z \end{bmatrix} \tag{142}$$

that transforms (124) into normal form co-ordinates

$$\dot{\mathbf{p}}^i = \begin{bmatrix} p_2^i \\ \cdots \\ \cdots \\ p_{r_i}^i \\ a_i(\mathbf{p},\mathbf{q}) + \sum_{j=1}^{m} b_{ij}(\mathbf{p},\mathbf{q})v_j \end{bmatrix} \qquad \text{for } 1 \le i \le m \tag{143}$$

$$\dot{\mathbf{q}} = \hat{\mathbf{c}}(\mathbf{p},\mathbf{q})$$

where **q** represents the internal states of the system and the output states **p** are given by

$$\mathbf{p}^i = [\, w_i \quad \dot{w}_i \quad \cdots \quad w_i^{(r_i-1)} \,]^T \qquad \text{for } 1 \le i \le m \tag{144}$$

This result assumes that the DAE is autonomous. If this is not the case then it is necessary to replace time with an autonomous state equation of the form $\dot{t} = 1$. The nonlinear state transformation of the augmented system is guaranteed to exist in some local region of state space. Therefore, the results will be valid in some time interval.

The normal form (143) can be expressed in terms of sliding co-ordinates using a simple linear transformation between s_i and $p_{r_i}^i$ since the sliding co-ordinates are defined by

$$s_i = \left[\mu\frac{d}{dt}+1\right]^{r_i-1} w_i = \mu^{r_i-1}p_{r_i}^i + (r_i-1)\mu^{r_i-2}p_{r_i-1}^i + \ldots + (r_i-1)\mu p_2^i + p_1^i \tag{145}$$

Therefore, there also exists a smooth invertible transformation of the form

$$\Phi_s(\zeta) = \begin{bmatrix} \sigma \\ s \\ q \end{bmatrix} \quad , \quad \Phi_s : \Re^{n+m} \to \Re^{n+m} \quad , \quad \zeta = \begin{bmatrix} x \\ z \end{bmatrix} \tag{146}$$

where $p_{r_i}^i$ is essentially replaced by s_i. An equation for $\dot{s}$ can be determined from

$$\dot{s} = J_s v + \alpha \tag{147}$$

The SPSM input (124) inside the sliding boundary layer is given by

$$\hat{J}_s v = -\hat{\alpha} - \varepsilon^{-1} K \, \text{diag}(\rho) \, s \tag{148}$$

Substituting this into the previous expression yields a state equation for s

$$\varepsilon \dot{s} = \varepsilon(\alpha - J_s \hat{J}_s^{-1} \hat{\alpha}) - J_s \hat{J}_s^{-1} K \, \text{diag}(\rho) \, s \tag{149}$$

The equation for $\dot{p}_{r_i-1}^i$ can be determined from equation (143)

$$\dot{p}_{r_i-1}^i = p_{r_i}^i \tag{150}$$

which can be expressed in terms of the sliding manifold (145)

$$\mu^{r_i-1} \dot{p}_{r_i-1}^i = s_i - (r_i-1)\mu^{r_i-2} p_{r_i-1}^i - \ldots - (r_i-1)\mu p_2^i - p_1^i \tag{151}$$

By combining the previous results equation (143) can now be expressed in a sliding normal form

$$\begin{bmatrix} \dot{p}_1^i \\ \cdots \\ \dot{p}_{r_i-2}^i \\ \dot{p}_{r_i-1}^i \end{bmatrix} = \begin{bmatrix} p_2^i \\ \cdots \\ p_{r_i-1}^i \\ (s_i - (r_i-1)\mu^{r_i-2}p_{r_i-1}^{i-1} - \cdots - (r_i-1)\mu p_2^i - p_1^i)/\mu^{r_i-1} \end{bmatrix} \qquad \text{for } 1 \le i \le m \tag{152}$$

$$\varepsilon \dot{s} = \varepsilon(\alpha - J_s \hat{J}_s^{-1}\hat{\alpha}) - J_s \hat{J}_s^{-1} K \, \text{diag}(\rho)\, s$$
$$\dot{q} = c(q,s,\sigma)$$

□

Remark 3. This result is important because it separates the internal dynamics from the dynamics of the output. The zero dynamics of the SPSM (124) can then be expressed as

$$\sigma = 0 \tag{153}$$
$$s = 0$$
$$\dot{q} = c(q,0,0)$$

From proposition 1 this is equivalent to the dynamics of the high index DAE. Therefore, this representation can be used to help study convergence to the high index DAE system. Furthermore, it will be found that the effect of ε can be systematically determined from the sliding normal form. □

Using lemma 1 it can be proven that the approximation error of the SPSM realization will be small for sufficiently small values of ε. This result is presented in the following theorem.

Theorem 4. Consider the SPSM realization given by

$$
\begin{aligned}
&\dot{\mathbf{x}} = \mathbf{f}(t, \mathbf{x}, \mathbf{z}) \\
&\dot{\mathbf{z}} = \mathbf{v} \\
&\mathbf{w} = \mathbf{g}(t, \mathbf{x}, \mathbf{z}) \\
&\hat{\mathbf{J}}_s \mathbf{v} = -\hat{\boldsymbol{\alpha}} - \mathbf{K}\, \mathrm{sat}(\boldsymbol{\psi}) \quad , \quad \boldsymbol{\psi} = \varepsilon^{-1} \mathrm{diag}(\boldsymbol{\rho})\, \mathbf{s} \quad , \quad 0 < \varepsilon \ll 1 \\
&s_i = \left(\mu \frac{d}{dt} + 1 \right)^{r_i - 1} w_i \quad , \quad \mu > 0 \quad \text{for } 1 \le i \le m
\end{aligned}
\tag{124}
$$

If the DAE has a vector index and the matrix $[-\mathbf{J}_s \hat{\mathbf{J}}_s^{-1} \mathbf{K}\, \mathrm{diag}(\boldsymbol{\rho})]$ is negative definite in a region around the DAE solution then there exists a value of ε such that the approximation error between the realization and the high index DAE is given by

$$
\mathbf{x}(t, \varepsilon) - \mathbf{x}(t) = \mathbf{O}(\varepsilon)
\tag{154}
$$

$$
\mathbf{z}(t, \varepsilon) - \mathbf{z}(t) = \mathbf{O}(\varepsilon)
\tag{155}
$$

$$
\mathbf{s}(t, \varepsilon) = \mathbf{O}(\varepsilon)
\tag{156}
$$

This result holds uniformly on a given time interval $[t_b, t_1]$ after a short boundary layer interval $[t_0, t_b]$ given consistent initial conditions.

Proof. After the trajectory of the SPSM enters the sliding boundary layer the realization has the form

$$
\begin{aligned}
&\dot{\mathbf{x}} = \mathbf{f}(t, \mathbf{x}, \mathbf{z}) \\
&\dot{\mathbf{z}} = \mathbf{v} \\
&\mathbf{w} = \mathbf{g}(t, \mathbf{x}, \mathbf{z}) \\
&\hat{\mathbf{J}}_s \mathbf{v} = -\hat{\boldsymbol{\alpha}} - \varepsilon^{-1} \mathbf{K}\, \mathrm{diag}(\boldsymbol{\rho})\, \mathbf{s}
\end{aligned}
\tag{157}
$$

Using lemma 1 this system can be expressed in a sliding normal form

$$
\begin{bmatrix} \dot{p}_1^i \\ \cdots \\ \dot{p}_{r_i-2}^i \\ \dot{p}_{r_i-1}^i \end{bmatrix} = \begin{bmatrix} p_2^i \\ \cdots \\ p_{r_i-1}^i \\ (s_i - (r_i-1)\mu^{r_i-2}p_{r_i-1}^{i-1} - \cdots - (r_i-1)\mu p_2^i - p_1^i)/\mu^{r_i-1} \end{bmatrix} \qquad \text{for } 1 \le i \le m
$$
(158)

$$\varepsilon \dot{s} = \varepsilon(\alpha - J_s \hat{J}_s^{-1}\hat{\alpha}) - J_s \hat{J}_s^{-1} K \, \text{diag}(\rho)\, s$$
$$\dot{q} = c(q,s,\sigma)$$

since the DAE has a vector index. This representation is in standard singular perturbation form with respect to ε. It is evident that this system has a form that is similar to the singular perturbation approach (25) described in section 2.6. The extra term $\varepsilon(\alpha - J_s \hat{J}_s^{-1}\hat{\alpha})$ does not change theorem 1 so it may be ignored. As ε approaches zero the system approaches a DAE expressed in terms of the sliding manifold

$$
\begin{bmatrix} \dot{p}_1^i \\ \cdots \\ \dot{p}_{r_i-2}^i \\ \dot{p}_{r_i-1}^i \end{bmatrix} = \begin{bmatrix} p_2^i \\ \cdots \\ p_{r_i-1}^i \\ (-(r_i-1)\mu^{r_i-2}p_{r_i-1}^{i-1} - \cdots - (r_i-1)\mu p_2^i - p_1^i)/\mu^{r_i-1} \end{bmatrix} \qquad \text{for } 1 \le i \le m
$$
(159)

$$0 = s$$
$$\dot{q} = c(q,0,\sigma)$$

where it follows that $[-J_s \hat{J}_s^{-1} K \, \text{diag}(\rho)]$ is invertible since it is negative definite. The algebraic constraints for the constrained states s are trivially invertible so the system is an index one DAE. Therefore, we can directly apply theorem 1 to deduce the criteria necessary for convergence of (158) to (159). The analogous terms are

74

$$\mathbf{R} = -\mathbf{J}_s\hat{\mathbf{J}}_s^{-1}\mathbf{K} \, \text{diag}(\boldsymbol{\rho}) \quad , \quad \frac{\partial \mathbf{g}}{\partial \mathbf{z}} = \mathbf{I}_{mxm} \tag{160}$$

Therefore, the convergence criteria are given by

$$-\mathbf{J}_s\hat{\mathbf{J}}_s^{-1}\mathbf{K} \, \text{diag}(\boldsymbol{\rho}) < 0 \quad , \quad \mathbf{J}_s = \frac{\partial \mathbf{s}}{\partial \mathbf{z}}(t,\mathbf{x},\mathbf{z}) \tag{161}$$

in some region around the DAE solution. From theorem 1 it can be concluded that there exists a value of ε such that the approximation error between the SPSM in sliding norm form (158) and the index one DAE (159) is given by

$$\mathbf{q}(t,\varepsilon) - \mathbf{q}(t) = \mathbf{O}(\varepsilon) \tag{162}$$

$$\mathbf{s}(t,\varepsilon) - \mathbf{s}(t) = \mathbf{O}(\varepsilon) \tag{163}$$

$$\boldsymbol{\sigma}(t,\varepsilon) - \boldsymbol{\sigma}(t) = \mathbf{O}(\varepsilon) \tag{164}$$

This result holds uniformly on a given time interval $[t_b, t_1]$ after a short boundary layer interval $[t_o, t_b]$.

The dynamics of the high index DAE are given by equation (159) when the initial conditions are consistent. That is,

$$\boldsymbol{\sigma}(0) = \mathbf{0} \tag{165}$$

This yields the solution of the high index DAE

$$\begin{aligned} \dot{\boldsymbol{\sigma}} &= \mathbf{0} \quad , \quad \boldsymbol{\sigma}(0) = \mathbf{0} \\ \mathbf{0} &= \mathbf{s} \\ \dot{\mathbf{q}} &= \mathbf{c}(\mathbf{q},\mathbf{0},\mathbf{0}) \end{aligned} \tag{166}$$

Thus, for a given set of consistent initial conditions the approximation error between the SPSM and the high index DAE is given by (162-164). Since the co-ordinate transformation used in lemma 1 is smooth and invertible the mean value theorem can be applied

$$\zeta_j(t,\varepsilon) - \zeta_j(t) = \frac{\partial[\Phi_s^{-1}(\gamma)]_j}{\partial\gamma}\bigg|_{\bar{\gamma}} (\gamma(t,\varepsilon) - \gamma(t)) \quad \text{for } 1 \leq j \leq (n+m) \tag{167}$$

$$\Phi_s(\zeta) = \gamma \quad , \quad \gamma = \begin{bmatrix} \sigma \\ s \\ q \end{bmatrix} \quad , \quad \zeta = \begin{bmatrix} x \\ z \end{bmatrix} \tag{168}$$

where $\bar{\gamma}$ is a mean value evaluated in some region around the high index DAE solution γ. Combining equations (162-164) and (167) gives the approximation error in terms of x and z

$$x(t,\varepsilon) - x(t) = O(\varepsilon) \tag{169}$$

$$z(t,\varepsilon) - z(t) = O(\varepsilon) \tag{170}$$

This completes the proof of the convergence theorem. ☐

4.4 Numerical Example

This section illustrates the SPSM realization approach using a simple pendulum example (see Figure 16). The equations of motion for this system in Cartesian co-ordinates form a high index DAE problem:

$$\dot{v}_x = zx \tag{171}$$

$$\dot{v}_y = zy - g \tag{172}$$

$$\dot{x} = v_x \tag{173}$$

$$\dot{y} = v_y \tag{174}$$

$$x^2 + y^2 - 1 = 0 \tag{175}$$

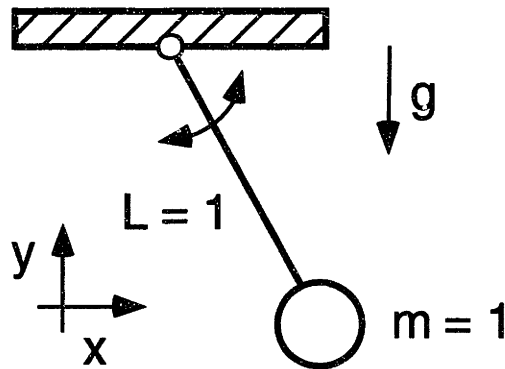Where (x,y) is the position of the pendulum, and z is the compressive force in the rigid link.

Figure 16. A simple pendulum example

The index of this system can be determined by repeated differentiation of the constraint equation (175).

$$\dot{w} = 2xv_x + 2yv_y \tag{176}$$

$$\ddot{w} = 2v_x^2 + 2v_y^2 + 2z(x^2 + y^2) - 2gy \tag{177}$$

$$\dddot{w} = 8z(xv_x + yv_y) + 2\dot{z}(x^2 + y^2) - 2gv_y \tag{178}$$

Since the coefficient of $\dot{z}$ in (178) is nonsingular the system has an index of three. Therefore, the appropriate sliding manifold is given by

$$s = \left(\mu\frac{d}{dt} + 1\right)^{3-1} w = \mu^2\ddot{w} + 2\mu\dot{w} + w \tag{179}$$

$$s = 2\mu^2(v_x^2 + v_y^2 + z(x^2 + y^2) - gy) + 2\mu(2xv_x + 2yv_y) + x^2 + y^2 - 1 \tag{180}$$

The derivative of the sliding surface is thus given by

$$\dot{s} = \mu^2\dddot{w} + 2\mu\ddot{w} + \dot{w} = \alpha + J_s v \tag{181}$$

Substituting the expressions (176-178) into equation (181) results in the following expressions for J_s and α

$$J_s = 2\mu^2(x^2 + y^2) \tag{182}$$

$$\alpha = \mu^2(8z(xv_x + yv_y) - 2gv_y) + 4\mu(v_x^2 + v_y^2 + z(x^2 + y^2) - gy) + 2xv_x + 2yv_y \tag{183}$$

Substituting the previous equations into (124) and using $\hat{J}_s = J_s$ and $\hat{\alpha} = 0$ yields a SPSM realization of the DAE system

78

$$2\mu^2(x^2+y^2)\,v = \tag{184}$$
$$-k\,sat\left[\rho\varepsilon^{-1}[\ 2\mu^2(\,v_x^2+v_y^2+z(x^2+y^2)-gy)+2\mu(2xv_x+2yv_y)+x^2+y^2-1\ ]\right]$$

Theorems 3 and 4 guarantee that there exist values of k, μ, and ε such that the SPSM is a good approximation of the DAE with guaranteed error bounds on the constraints. The following procedure can be used to determine a suitable set of parameters.

1)   Select a value of μ so that the dynamics on the sliding manifold are sufficiently fast.

2)   Select the control gain to satisfy the sliding condition (126).

3)   Choose ε to satisfy some desired error bounds on the constraints (139).

This sequence will result in a realization that satisfies a given set of error bounds. This is a significant improvement over the singular perturbation method since it gives an explicit criteria for selecting ε based on a desired error. Further, it ensures that the realization stays a small distance from the DAE solution so that singularities are not encountered. Simulations can be used to verify the transient properties of the solution, and if they are not optimal then μ can be adjusted and steps 2 and 3 repeated.

For this problem a time constant of $\mu=0.02$ was selected for the sliding manifold. The sliding condition of this problem (126) reduces to

$$k-|\alpha|>0 \tag{185}$$

This relation can be satisfied if

$$k > \max\,[\mu^2(8z(xv_x + yv_y) - 2gv_y) + 4\mu(v_x^2 + v_y^2 + z(x^2 + y^2) - gy) + 2xv_x + 2yv_y] \quad (186)$$

A conservative bound for this expression can be obtained from

$$k > \mu^2(8|z|(|x||v_x| + |y||v_y|) + 2g|v_y|) + 4\mu(|v_x|^2 + |v_y|^2 + |z|(|x|^2 + |y|^2) + g|y|)$$
$$+ 2|x||v_x| + 2|y||v_y| \qquad \qquad \qquad (187)$$

From physical considerations it can be shown that the following bounds are satisfied near the solution

$$|x| \leq 1$$
$$|y| \leq 1$$
$$|v_x| \leq \sqrt{2g}$$
$$|v_y| \leq \sqrt{2g} \qquad (188)$$
$$|z| \leq 3g$$

Substituting these relations gives a numerical value for k

$$k > \alpha_{max} \geq \alpha \qquad (189)$$

Finally, the parameter ε can be selected to achieve some desired error bounds. For example, the position error is bounded by

$$|w| \leq \varepsilon \qquad (190)$$

Where ρ is set equal to one, since there is only one sliding component. Thus, to ensure a maximum position error of 0.1 we can set

$$\varepsilon = 0.1 \qquad (191)$$

The sliding boundary layer is given by

$$|s| \leq \varepsilon \qquad (192)$$

Therefore, once the SPSM has entered this region the error bounds will be satisfied. The SPSM was simulated for the given set of parameters

$$\mu = 0.02 \quad , \quad \varepsilon = 0.1 \quad , \quad k = \alpha_{max} \qquad (193)$$

with initial conditions outside the boundary layer (see Figure 17 to Figure 22). It can be seen from Figure 21 that the trajectories quickly converge inside the boundary layer and remain thereafter. As a result the error bounds are satisfied after a brief transient (see Figure 20). A comparison of the SPSM to the exact solution is shown in Figure 17 to Figure 19. It is apparent that the realization quickly converges to the high index solution until only a small error is involved. Furthermore, the solution will never encounter the singularity at (x=0, y=0) since the error bounds imply that

$$\left| x^2 + y^2 - 1 \right| \leq 0.1 \qquad (194)$$
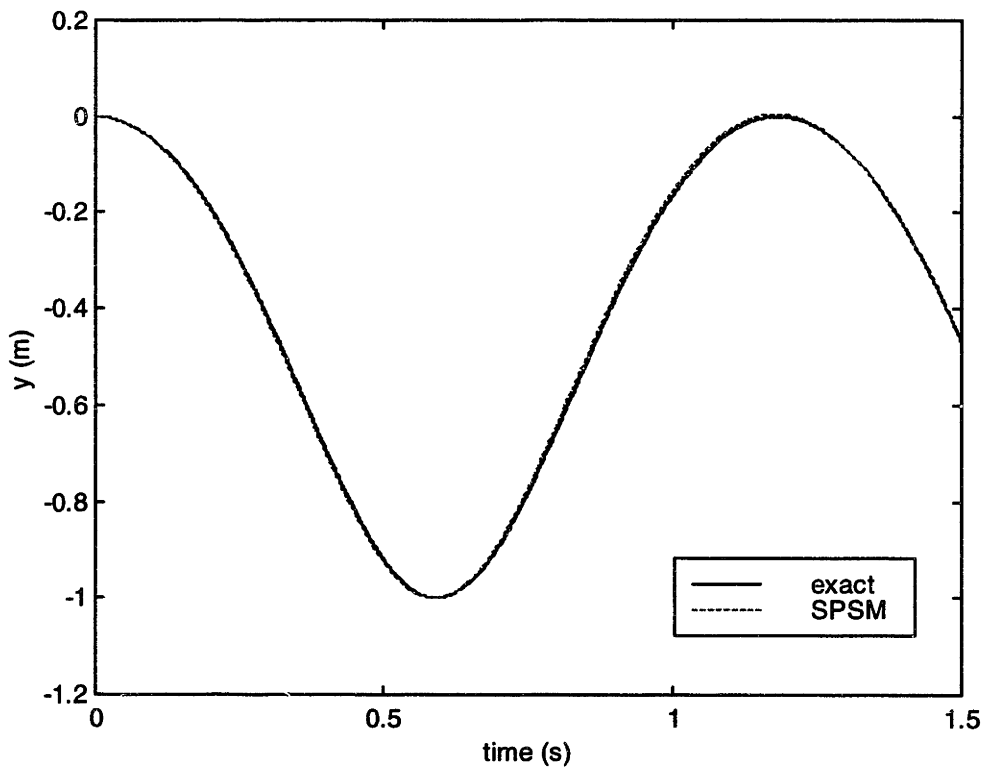
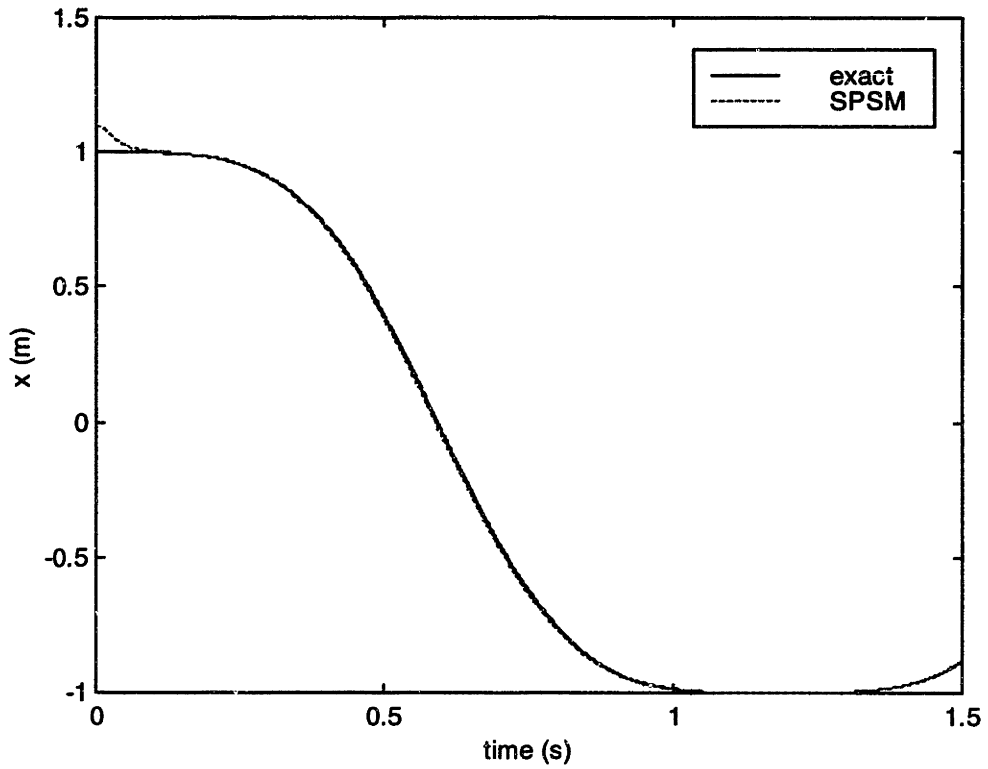$$0.9 \leq x^2 + y^2 \leq 1.1 \qquad (195)$$
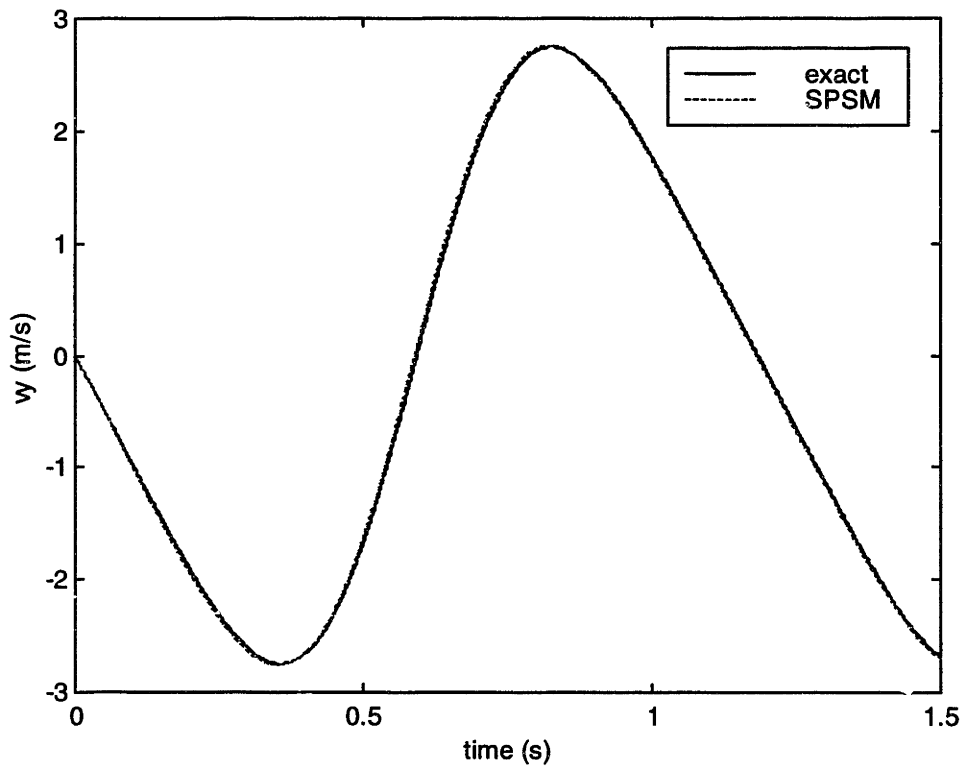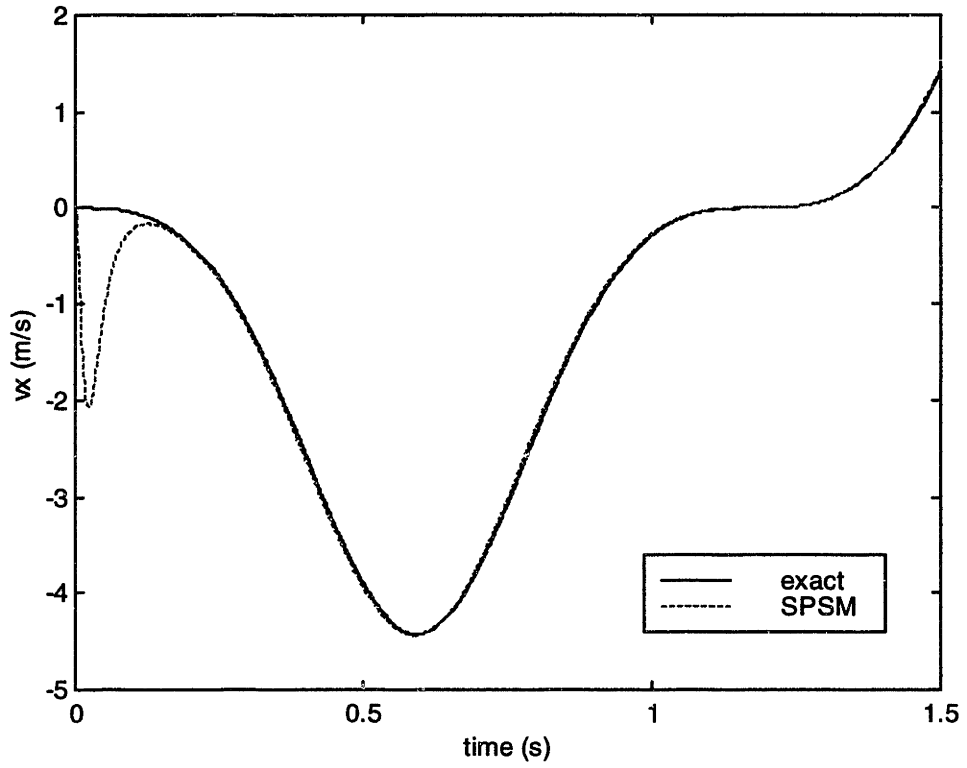
Figure 17. SPSM vs. the exact solution
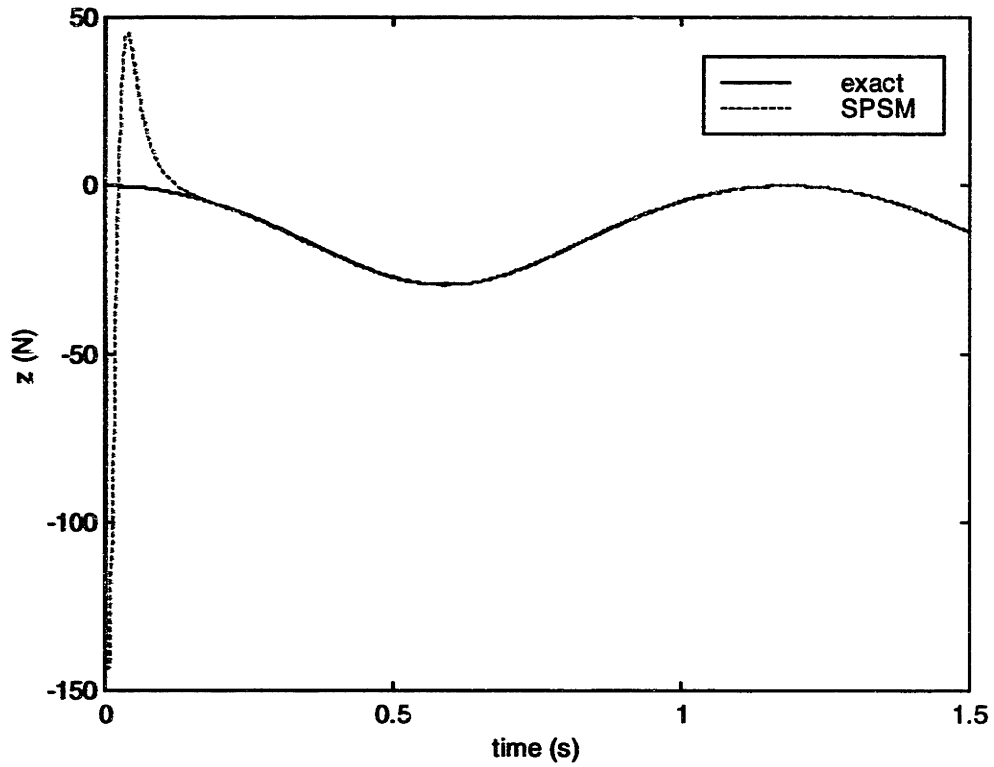
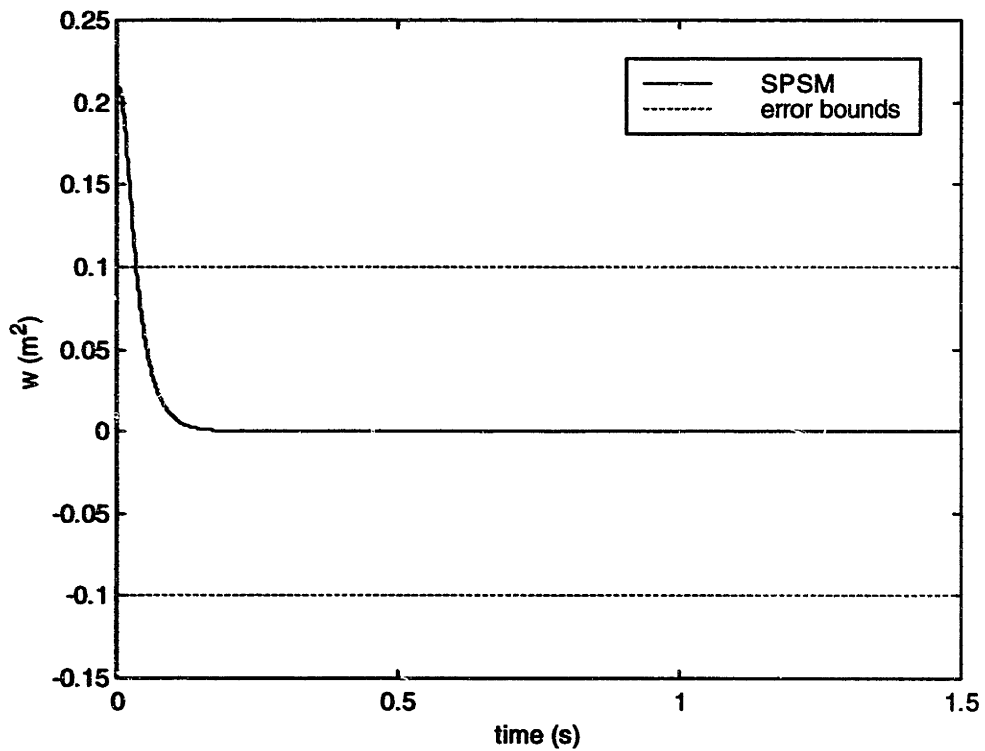Figure 18. SPSM vs. the exact solution

Figure 19. SPSM vs. the exact solution
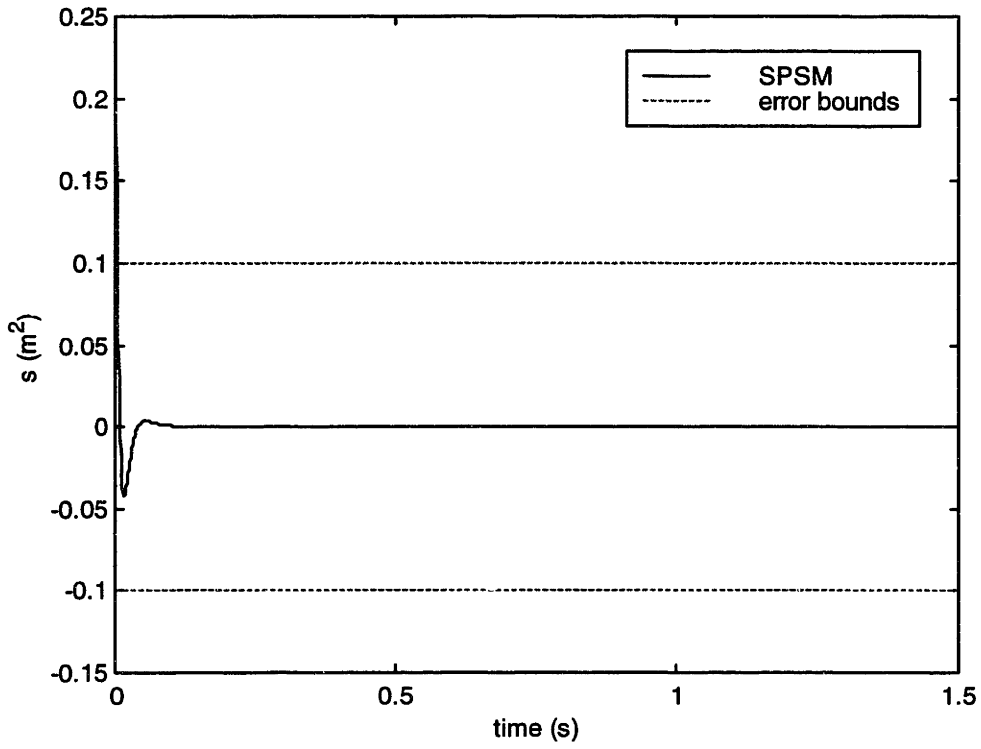

Figure 20. SPSM error bounds
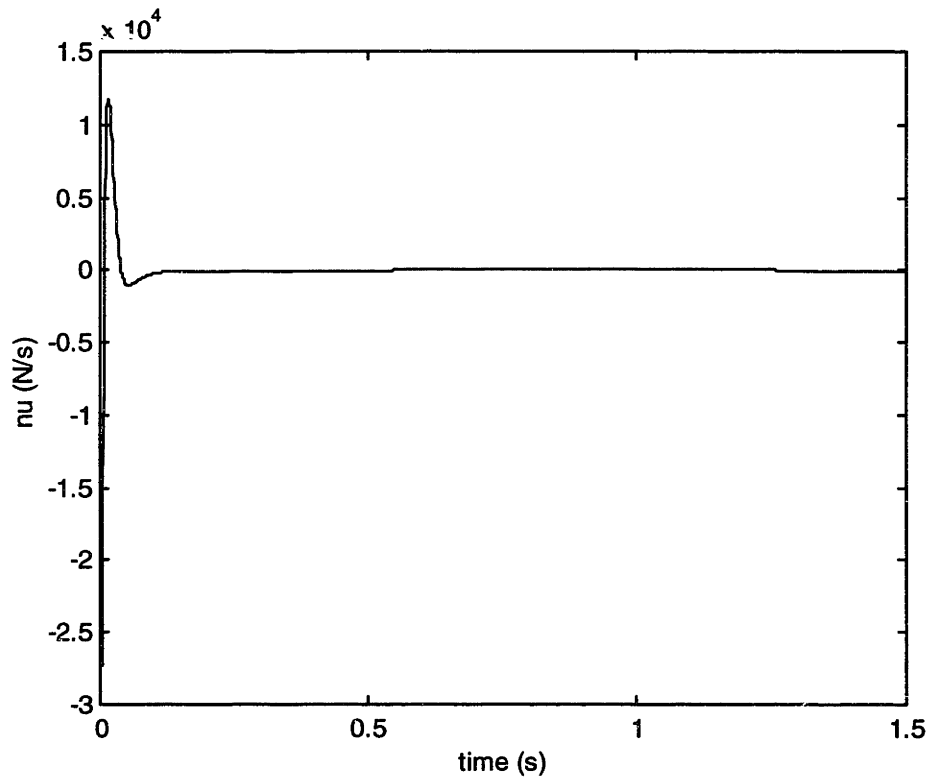
Figure 21. SPSM error bounds

Figure 22. SPSM input

4.5 Control Properties of Singularly Perturbed Sliding Manifolds

For the SPSM realization approach to be an effective tool for control design it is important that control properties such as stability, controllability, and observability are equivalent to the original DAE. These requirements will be affected by the parameters and in turn lead to additional criteria for their selection. This section proves that there always exists values of ε and μ such that the local stability, controllability, and observability are equivalent. The results will be proven for autonomous DAE systems of the form

$$
\begin{array}{cc}
\text{SPSM} & \text{DAE} \\
\dot{x} = f(x,z,u) & \dot{x} = f(x,z,u) \\
\dot{z} = v(x,z,u,\varepsilon,\mu) \quad \Longleftrightarrow \quad & 0 = g(x,z,u) \\
y = h(x,z,u) & y = h(x,z,u)
\end{array}
$$

where u is an external input and y is some defined output.

The stability equivalence of the SPSM to the DAE is proven in the following theorem.

Theorem 5. There exists values of ε and μ such that the SPSM is locally stable iff the DAE is locally stable. $\square$

Proof. It is evident from equation (157) that inside the boundary layer the SPSM realization of an autonomous system with control inputs applied has the form

$$
\begin{aligned}
\dot{x} &= f(x,z) \\
\varepsilon \dot{z} &= R(x,z)s(x,z) + \varepsilon P(x,z)
\end{aligned}
\tag{196}
$$

It will first be shown that the stability of the SPSM is equivalent to the following index one DAE for some value of ε.

$$\dot{x} = f(x, z) \tag{197}$$
$$0 = s(x, z)$$

Then it will be proven that the stability of the index one system is equivalent to the high index system.

$$\dot{x} = f(x, z) \tag{198}$$
$$0 = w(x, z)$$

The system (196) can be linearized at an equilibrium to investigate its local stability properties

$$\dot{x} = A_{11}x + A_{12}z \tag{199}$$
$$\varepsilon\dot{z} = (A_{21} + \varepsilon E_{21})x + (A_{22} + \varepsilon E_{22})z$$

Where the linearized coefficient matrices are defined in the obvious manner, and x, z are offsets from equilibrium values. The reduced model for $\varepsilon = 0$ is given by

$$\dot{x} = A_{11}x + A_{12}z \tag{200}$$
$$0 = A_{21}x + A_{22}z$$

The linear algebraic relation in z can always be inverted since the implicit function theorem guarantees that the associated Jacobian is invertible. Substitution of the second equation into the first equation results in a reduced model in terms of x

$$\dot{x} = [A_{11} - A_{12}A_{22}^{-1}A_{21}]x \tag{201}$$

This equation is equivalent to the linearized index one DAE corresponding to (197) since

$$z = -A_{22}^{-1}A_{21}x = -\left[\frac{\partial Rs}{\partial z}\right]^{-1}\left[\frac{\partial Rs}{\partial x}\right]x = \left[\frac{\partial z}{\partial x}\right]x \qquad (202)$$

From the implicit function theorem this expression is independent of the choice of **R**. Therefore, convergence to the reduced model of (199) is sufficient to imply convergence to the index one DAE.

Following the linear singular perturbation theory derived in [21] it can be concluded that as $\varepsilon \to 0$ the eigenvalues separate into a fast stable region and a slow region (see Figure 23).

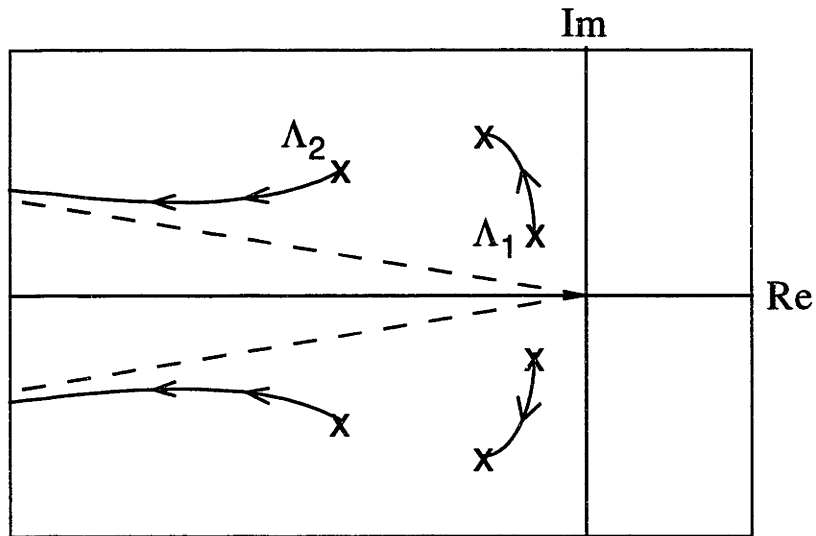Figure 23. Root locus of eigenvalues

The n slow modes converge to the eigenvalues of the index one DAE:

$$\Lambda_1 \to \Lambda(A_0) \quad , \quad \Lambda_1 \in \mathfrak{R}_{nxn} \qquad (203)$$

where

$$A_0 = A_{11} - A_{12}A_{22}^{-1}A_{21} \tag{204}$$

Furthermore, the m fast modes converge to stable asymptotes given by

$$\Lambda_2 \to \Lambda(A_{22})/\varepsilon \quad , \quad \Lambda_2 \in \Re_{mxm} \tag{205}$$

where it can be shown that A_{22} is stable as a result of Tikhonov's stability criterion [11]. By continuity, there exists a value of ε such that the slow eigenvalues of the SPSM are arbitrarily close to the eigenvalues of the index one DAE. Since the other fast eigenvalues are asymptotically stable the stability of the SPSM is equivalent to the index one DAE.

To complete the proof it is necessary to show that the stability of the index one DAE is equivalent to the high index system. This can be accomplished using the singularly perturbed sliding normal form (140). The index one DAE can thus be expressed as

$$\begin{aligned} \dot{\sigma}^i &= A_i\sigma^i \qquad \text{for } 1 \le i \le m \\ s &= 0 \\ \dot{q} &= c(q,0,\sigma) \end{aligned} \tag{206}$$

where A_i is a stable matrix with eigenvalues at $-\mu^{-1}$. This expression represents the internal dynamics of the index one DAE. The local stability of the internal dynamics can be determined by linearizing these equations.

$$\tag{207}$$

$$\begin{bmatrix} \dot{\sigma}^1 \\ \dot{\sigma}^2 \\ \vdots \\ \dot{\sigma}^m \\ \dot{q} \end{bmatrix} = \begin{bmatrix} A_1 & 0 & \cdots & 0 & 0 \\ 0 & A_2 & \cdots & 0 & 0 \\ \vdots & \vdots & & \vdots & \vdots \\ 0 & 0 & \cdots & A_m & 0 \\ B_1 & B_2 & \cdots & B_m & H \end{bmatrix} \begin{bmatrix} \sigma^1 \\ \sigma^2 \\ \vdots \\ \sigma^m \\ q \end{bmatrix}$$

where the linearized coefficient matrices are appropriately defined. Since this matrix is in block triangular form the eigenvalues are determined by the matrices on the diagonal entries. The first m matrices are stable for any value of μ, so the local stability solely depends on H which represents the linearized dynamics of the high index DAE in normal form coordinates. Therefore, the local stability of the index one DAE is equivalent to the stability of the high index system. Combining this with the previous result completes the proof of the theorem. From these results it is apparent that the local stability of the realization doesn't depend on the value of μ given a sufficiently small value of ε. ☐

The stability equivalence property ensures that if a controller is designed that stabilizes the SPSM then the controller will also result in a stable system when applied to the actual DAE. Conversely, if the originally DAE is stable or unstable then this property, which is necessary for control synthesis, will be inherited by the SPSM for some parameter values. The equivalence of controllability is demonstrated by a corollary of the previous theorem.

Corollary 1. There exists values of ε and μ such that the SPSM is locally stabilizable iff the DAE is locally stabilizable. ☐

Proof. If a system is locally stabilizable then, by definition [2], it is possible to find a controller that results in a locally stable system. Therefore, if the original DAE is locally stabilizable a controller can be designed that results in a stable system. The previous theorem then guarantees that there exists a set of parameters such that

the SPSM is also stable. Hence, if the DAE is stabilizable then the SPSM is also stabilizable. It follows in a similar manner that if the SPSM is stabilizable then the DAE is also stabilizable. The existence of linear stabilizing controllers for the two systems is thus equivalent for some value of parameters. In general, it may not be possible to control the stable modes related to the fast dynamics of the SPSM. Therefore, it is only possible to prove that the two systems are stabilizable. ☐

Remark 4. Under some mild smoothness assumptions it can be concluded that if the linearized system can be stabilized then the nonlinear system can also be stabilized. ☐

In general, the fast modes of the SPSM become unobservable as ε and μ approach zero. Therefore, it is only possible to prove detectability.

Theorem 6. There exists values of ε and μ such that the SPSM is locally detectable iff the DAE is locally detectable. ☐

Proof. This proof is beyond the scope of the thesis. ☐

To summarize, it can be concluded that the stability, controllability, and detectability of the SPSM will be equivalent to the original DAE for certain parameter values. These parameters may be determined using a linearization of the SPSM and explicitly checking each criteria. An efficient method for linear parametric analysis of the SPSM is outlined in the following section.

4.6 Selection of Parameters using a Root Locus Technique

The results of the previous sections indicate the existence of parameter values of ε and μ such that the SPSM is a good approximation of the DAE. In this

section a root locus technique is introduced that parameterizes the linear dynamics around an equilibrium point. This allows efficient characterization of the local behavior of the realization over the parameter space to help guide the selection of parameters. To illustrate the technique it will be applied to an index two DAE. It is a straightforward matter to extend the method to more general realizations. The SPSM realization of an autonomous system inside the sliding boundary layer can be written as

$$\dot{\mathbf{x}} = \mathbf{f}(\mathbf{x}, \mathbf{z}) \tag{208}$$

$$\varepsilon \dot{\mathbf{z}} = \mathbf{R}\,\mathbf{s} \tag{209}$$

$$\mathbf{R} = -\hat{\mathbf{J}}_s^{-1}\mathbf{K}\,\mathrm{diag}(\boldsymbol{\rho}) \tag{210}$$

where $\hat{a}$ is set equal to zero. Substituting the expression for s gives

$$\varepsilon \dot{\mathbf{z}} = \mathbf{R}(\mu \dot{\mathbf{w}} + \mathbf{w}) = \mu \mathbf{R}\dot{\mathbf{w}} + \mathbf{R}\mathbf{w} \tag{211}$$

The realization can now be linearized as follows

$$\dot{\mathbf{x}} = \mathbf{A}_{11}\mathbf{x} + \mathbf{A}_{12}\mathbf{z} \tag{212}$$
$$\dot{\mathbf{z}} = \mathbf{A}_{21}\mathbf{x} + \mathbf{A}_{22}\mathbf{z}$$

where

$$\mathbf{A}_{11} = \frac{\partial \mathbf{f}}{\partial \mathbf{x}} \quad , \quad \mathbf{A}_{12} = \frac{\partial \mathbf{f}}{\partial \mathbf{z}} \tag{213}$$

$$\mathbf{A}_{21} = \varepsilon^{-1}\mu\frac{\partial(\mathbf{R\dot{w}})}{\partial\mathbf{x}} + \varepsilon^{-1}\frac{\partial(\mathbf{Rw})}{\partial\mathbf{x}} \quad , \quad \mathbf{A}_{22} = \varepsilon^{-1}\mu\frac{\partial(\mathbf{R\dot{w}})}{\partial\mathbf{z}} + \varepsilon^{-1}\frac{\partial(\mathbf{Rw})}{\partial\mathbf{z}} \tag{214}$$

It is now evident that the SPSM parameter dependencies can be separated from the linearized terms. Note that the parameter dependency in $\mathbf{R}$ may also have to be separated. For instance, if

$$\mathbf{R} = -\mathbf{J}_s^{-1} \tag{215}$$

then using theorem 2 we have

$$\frac{\partial(\mathbf{R\dot{w}})}{\partial\mathbf{x}} = -\mu^{-1}\frac{\partial[\mathbf{J}_\Omega^{-1}(\mathbf{x},\mathbf{z})\dot{\mathbf{w}}(\mathbf{x},\mathbf{z})]}{\partial\mathbf{x}}$$

$$\frac{\partial(\mathbf{Rw})}{\partial\mathbf{x}} = -\mu^{-1}\frac{\partial[\mathbf{J}_\Omega^{-1}(\mathbf{x},\mathbf{z})\mathbf{w}(\mathbf{x},\mathbf{z})]}{\partial\mathbf{x}}$$

$$\frac{\partial(\mathbf{R\dot{w}})}{\partial\mathbf{z}} = -\mu^{-1}\frac{\partial[\mathbf{J}_\Omega^{-1}(\mathbf{x},\mathbf{z})\dot{\mathbf{w}}(\mathbf{x},\mathbf{z})]}{\partial\mathbf{z}} \tag{216}$$

$$\frac{\partial(\mathbf{Rw})}{\partial\mathbf{z}} = -\mu^{-1}\frac{\partial[\mathbf{J}_\Omega^{-1}(\mathbf{x},\mathbf{z})\mathbf{w}(\mathbf{x},\mathbf{z})]}{\partial\mathbf{z}}$$

$$\mathbf{J}_\Omega = \frac{\partial\dot{\mathbf{w}}}{\partial\mathbf{z}}$$

Therefore, the Jacobian matrices need to be evaluated only once at an equilibrium point. Hence, for any set of parameters the linearized dynamics can be calculated by performing simple matrix additions. This result is a very useful tool for parameter selection since the linear parameterization can easily be used in efficient optimization and search algorithms. One important use is to test for local stability, controllability, and detectability equivalence. It can also be used to study the effect of interactions between the sliding manifold (μ) and singular perturbation dynamics (ε) by drawing a root locus of the eigenvalue locations.

5. A DAE Modeling Approach for Vapor Compression Cycles

5.1 Introduction

In recent years, dynamic modeling, control, and diagnostics of vapor compression cycles have become active areas of research to improve the performance of air conditioning and heat pump systems. Most research efforts have been concerned with increasing steady state efficiency despite the fact that steady conditions are rarely achieved. Dynamic behavior, such start-up and shut-down transients, can substantially degrade performance and reduce system reliability. Systematic modeling and control methods are therefore needed to improve dynamic behavior of vapor compression cycles. This is especially true for new vapor compression cycle designs that employ multiple indoor heat exchangers for HVAC systems used in large buildings (see Figure 24). The dynamic behavior of multiple-zone vapor compression cycles are highly nonlinear with substantial processes uncertainties which make modeling and control design difficult problems. In this chapter, a new DAE based modeling approach is developed for describing the dynamics of multiple-zone vapor compression cycles. Since this formulation results in a nonlinear high index DAE system it provides motivation and a realistic application for the SPSM realization method. The SPSM method is applied to this new problem in chapter 6.
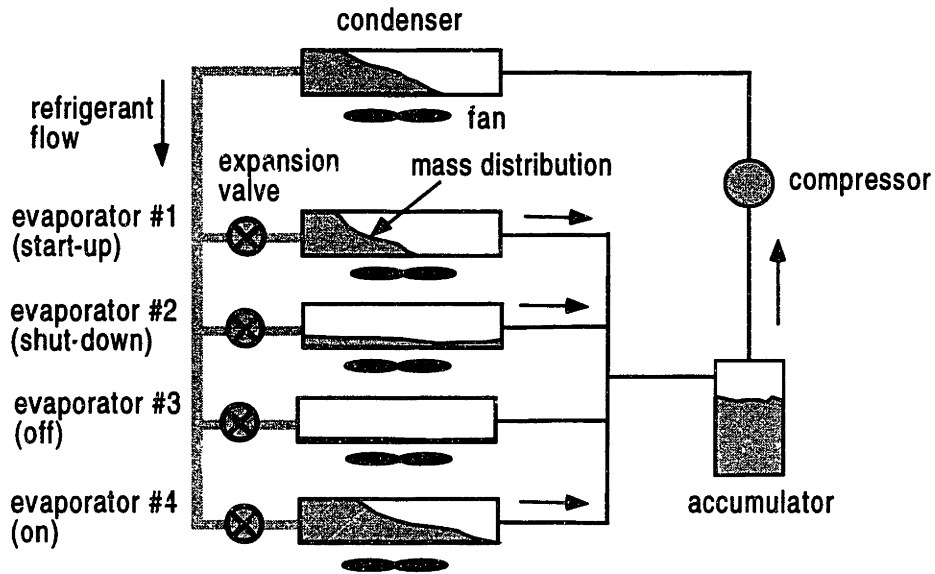
Figure 24. A Multiple-zone Vapor Compression Cycle

5.2 Evaporator Subsystems

The dynamic behavior of the evaporator heat exchanger is governed by complex interactions between refrigerant flowing in single phase or two phase states and fin arrays that thermally communicate with ambient environments. These coupled fluid mechanics and heat transfer processes are inherently distributed in nature. They can be formulated as a set of coupled one dimensional partial differential equations (PDEs) by applying the principles of mass, momentum and energy conservation [20]. The equations can be expressed as

mass balance

$$\frac{\partial \rho}{\partial t} + \frac{\partial(\rho u)}{\partial z} = 0 \tag{217}$$

95

momentum balance

$$\frac{\partial(\rho u)}{\partial t} + \frac{\partial(\rho u^2)}{\partial z} = -\frac{\partial P}{\partial z} + F_{wall} \tag{218}$$

energy balance

$$\frac{\partial(\rho h - P)}{\partial t} + \frac{\partial(\rho u h)}{\partial z} = \frac{4}{D_i}\alpha_i (T - T_w) \tag{219}$$

thermodynamic state equations

$$h = h(\rho, P) \qquad T = T(\rho, P) \tag{220}$$

where the dependant field variables ρ, u, P, h, and T are density, flow velocity, pressure, specific enthalpy, and temperature respectively. The independent variables are time and length along the heat exchanger. In the formulation of the energy equation viscous dissipation, axial conduction, pressure drop, and gravity terms were neglected. The gravity term was also neglected in the momentum equation. These equations assume a homogeneous flow pattern and a one dimensional cylindrical geometry.

The three coupled nonlinear PDEs along with the two thermodynamic state equations can be solved for the five field variables using numerical techniques. However, low order ODE approximations of these equations are required for control system design. The main objective of the modeling approach is to capture the basic mechanisms governing the dynamic interactions in the system and their impact on energy efficiency. With this goal, the mass and energy equations were integrated assuming a moving boundary flow pattern [15]. Figure 25 illustrates the concept. The heat exchanger flow field is divided into a two phase region with a liquid film on the inside of the tube wall (annular flow) and a gas phase section (superheated)

with the variable $l_e(t)$ describing the position of the liquid-vapor transition point. In the two phase region the volume ratio of gas $\bar{\gamma}$ (mean void fraction) is assumed to be approximately constant. It is important to model the dynamics of the liquid-vapor transition point because a small superheat section is required for efficiency, but it must not be too small otherwise liquid will enter and damage the compressor. Therefore, the length of the superheat section must be accurately controlled. The moving boundary method has been shown to be effective for capturing the dynamics of the liquid-vapor transition point in vapor compression cycles with one indoor heat exchanger [8]. This investigation generalizes the method to multi-zone systems (see Figure 26). Integration of the mass and energy equations (217,219) was performed from $z = 0$ to $z = l_e(t)$ using the moving boundary method (see Appendix B). This yields the following set of low order ordinary differential equations for each indoor evaporator k:

$$A_{ck}(1-\bar{\gamma}_k)(\rho_{lk} - \rho_{gk})\frac{dl_k}{dt} + A_{ck}l_k\left[\bar{\gamma}_k\frac{d\rho_{gk}}{dP_k} + (1-\bar{\gamma}_k)\frac{d\rho_{lk}}{dP_k}\right]\frac{dP_k}{dt} = \dot{m}_{vk} - \dot{m}_{ok} \qquad (221)$$

$$A_{ck}(1-\bar{\gamma}_k)(\rho_{lk}h_{lk} - \rho_{gk}h_{gk})\frac{dl_k}{dt} + A_{ck}l_k\left[\bar{\gamma}_k\frac{d(\rho_{gk}h_{gk})}{dP_k} + (1-\bar{\gamma}_k)\frac{d(\rho_{lk}h_{lk})}{dP_k} - 1\right]\frac{dP_k}{dt} \qquad (222)$$
$$= \dot{m}_{vk}h_{oc} - \dot{m}_{ok}h_{gk} + \pi D_{ik}\bar{\alpha}_{ik}l_k[T_{wk} - T_{sat}(P_k)]$$

$$(\rho A_c c_p)_{wk}\frac{dT_{wk}}{dt} = \pi D_{ok}\bar{\alpha}_{ok}[T_{ak} - T_{wk}] - \pi D_{ik}\bar{\alpha}_{ik}[T_{wk} - T_{sat}(P_k)] \qquad (223)$$

See appendix C for relevant variable definitions. The superheat section of the evaporator was modeled using steady state equations since the time scale of its dynamics are much faster than the two phase section. The steady state assumption yields algebraic equations for the evaporator outlet enthalpy and superheat as a function of the evaporator state variables and outlet mass flow.
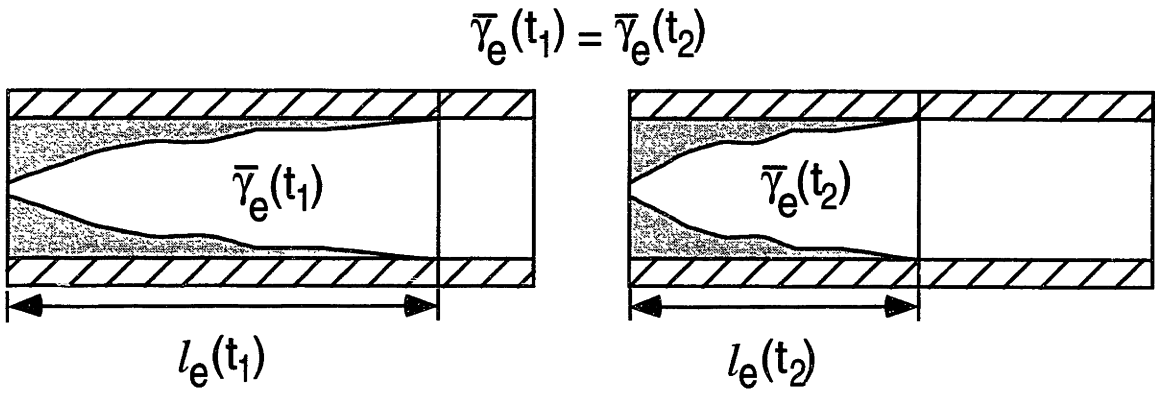
$$\overline{\gamma}_e(t_1) = \overline{\gamma}_e(t_2)$$
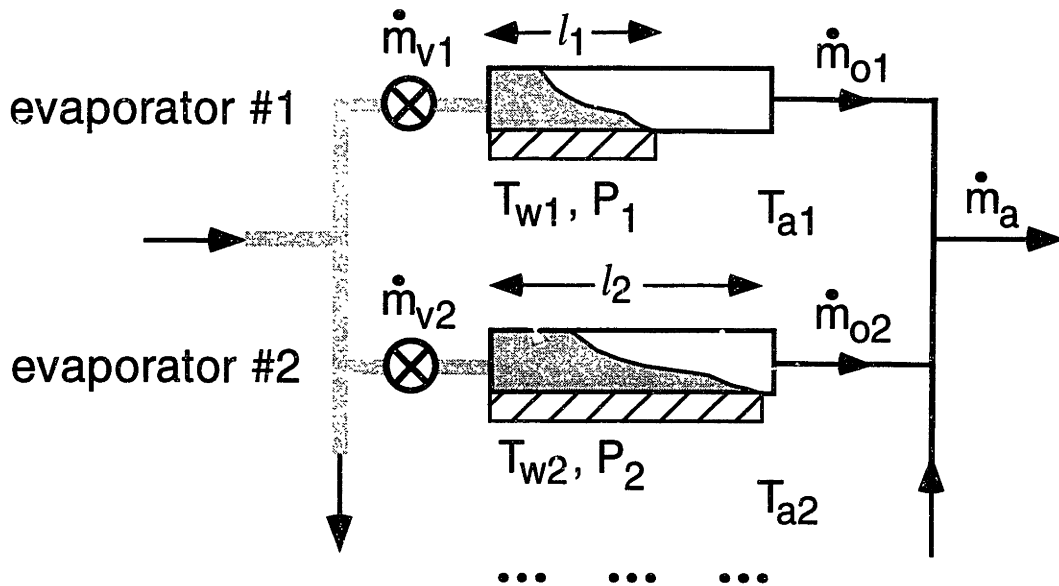
Figure 25. Moving boundary modeling concept

Figure 26. Multiple-zone evaporator model

5.3 Lumped Parameter Subsystems

The other components in the cycle (the condenser and accumulator) were modeled using a standard lumped parameter approach since the accuracy of these models are known to have a much smaller influence on system efficiency [4,8]. The equations for the accumulator are

mass balance

$$\forall_a \frac{d\rho_a}{dt} = \dot{m}_a - \dot{m}_p$$

(224)

energy balance

$$\left[\forall_a \frac{\partial(\rho_a \hat{u}_a)}{\partial P_a} + (mc)_{wa} \frac{\partial T_a}{\partial P_a} \right] \frac{dP_a}{dt} + \left[\forall_a \frac{\partial(\rho_a \hat{u}_a)}{\partial \rho_a} + (mc)_{wa} \frac{\partial T_a}{\partial \rho_a} \right] \frac{d\rho_a}{dt}$$
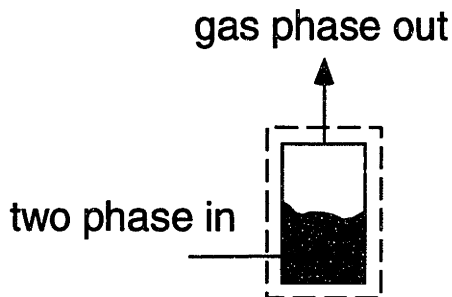$$= \sum_k \dot{m}_{ok} h_{ok} - \dot{m}_p h_{ga}$$

(225)

Figure 27. Accumulator

The equations for the condenser are

mass balance

$$\forall_c \frac{d\rho_c}{dt} = \dot{m}_p - \sum_k \dot{m}_{vk} \qquad (226)$$

energy balance (fluid)

$$\forall_c \frac{\partial(\rho_c \hat{u}_c)}{\partial P_c} \frac{dP_c}{dt} + \forall_c \frac{\partial(\rho_c \hat{u}_c)}{\partial \rho_c} \frac{d\rho_c}{dt} = \dot{m}_p h_{op} - \sum_k \dot{m}_{vk} h_{oc} - (\overline{\alpha}A)_{ic}(T_{sat}(P_c) - T_{wc}) \qquad (227)$$

energy balance (wall and fins)

$$(mc)_{wc} \frac{dT_{wc}}{dt} = (\overline{\alpha}A)_{ic}(T_{sat}(P_c) - T_{wc}) - (\overline{\alpha}A)_{oc}(T_{wc} - T_{ac}) \qquad (228)$$

Figure 28. Condenser

5.4 Actuator Models

The fan, valve, and compressor actuators in the system are known to have much faster time constants than the vapor compression cycle dynamics. Therefore, they were modeled using the following steady state empirical correlations which can be identified through appropriate measurements.

fans (outside heat transfer coefficients)

$$\overline{\alpha}_{ok} = a + bf_k \qquad \overline{\alpha}_{oc} = a + bf_c \tag{229}$$

expansion valve area (mass flow rate)

$$\dot{m}_v = k_v \left(A_{vk} - a\right)^b (P_c - P_k)^c \rho_c^d \tag{230}$$

compressor speed (mass flow rate, power, outlet enthalpy)

$$\dot{m}_p = k_p \rho_{ga} \omega \qquad \dot{W}_p = k_w P_a^e \omega^f \qquad h_{op} = \frac{\dot{m}_p h_{ga} + \dot{W}_p}{\dot{m}_p} \tag{231}$$

5.5 DAE Modeling Approach

The set of differential equations (221-228) and actuator equations (229-231) represent the models of the individual components in the multiple-zone vapor compression cycle. However, the mass flow interactions between the components need to be determined to complete the model. The momentum equation provides the key to determining this information in thermo-fluid systems. Integration of

equation (218) from the accumulator to the center of the indoor unit two phase region gives the following relation:

$$P_k - P_a = (\rho u^2)_{L_k} - (\rho u^2)_{l_k}/2 + \int_{L_k}^{l_k(t)} F_{wall} dz + \int_{l_k(t)}^{l_k(t)/2} F_{wall} dz \qquad (232)$$

where it is assumed that the momentum interactions are much faster than the vapor compression cycle dynamics so that the momentum equation is in a steady state condition. This expression represents the pressure drop from the evaporator heat exchanger to the accumulator entrance. It can be shown to be a nonlinear function of the mass flow and pressure (see Appendix D):

$$P_k - P_a = g(\dot{m}_{ok}, P_k, l_k) \qquad (233)$$

There is also the additional mass flow constraint imposed by the junction to the accumulator:

$$\sum \dot{m}_{ok} - \dot{m}_a = 0 \qquad (234)$$

Together, these algebraic equations give sufficient information to calculate the unknown mass flow rates in the system.

Through suitable manipulations the vapor compression cycle model can be expressed as a collection of DAE subsystems

$$\dot{x}_k = f_k(x, z, u)$$
$$0 = g_k(x, z, u) \qquad (235)$$

$$y_k = y_k(x, z, u) \quad , \quad k = 1..N$$

where:

$$\mathbf{x} = [\mathbf{x}_1{}^T \quad ... \quad \mathbf{x}_N{}^T]^T \quad \mathbf{z} = [z_1 \quad ... \quad z_N]^T \quad \mathbf{u} = [\mathbf{u}_1{}^T \quad ... \quad \mathbf{u}_N{}^T]^T$$

$$\mathbf{x}_k = [l_k \quad P_k \quad T_{wk}]^T, \quad k = 1..N-1 \ , \quad \mathbf{x}_N = [P_a \quad \rho_a \quad P_c \quad \rho_c \quad T_{wc}]^T$$

$$z_k = \dot{m}_{ok} \ , \quad k = 1..N-1 \ , \quad z_N = \dot{m}_a$$

$$\mathbf{u}_k = [A_{vk} \quad f_k]^T , \quad k = 1..N-1 \ , \quad \mathbf{u}_N = [\omega \quad f_c]^T$$

(236)

See appendix E for the subsystem components. This interconnected system is described by a set of differential-algebraic equations. The differential equations are responsible for energy and mass storage in the system, whereas the algebraic constraints are a result of the steady momentum and mass flow constraint equations. In general, the constrained variables $\mathbf{z}$ cannot be eliminated because the constraint equations are nonlinear. Further, if the pressure drops are negligible the constraint equations no longer depend on $\mathbf{z}$ which results in a high index DAE.

The DAE based approach for modeling multi-zone vapor compression cycles simplifies the formulation of the model considerably. The appropriate model can be constructed in a modular fashion by simply combining the DAE subsystems associated with the various components. For instance, a two zone system can be constructed by including the subsystem DAEs for the components shown in Figure 29. A multi-zone system with more than two indoor units can easily be constructed and simulated by adding more subsystems. This procedure can be systematically carried out in an object oriented language such as C++.
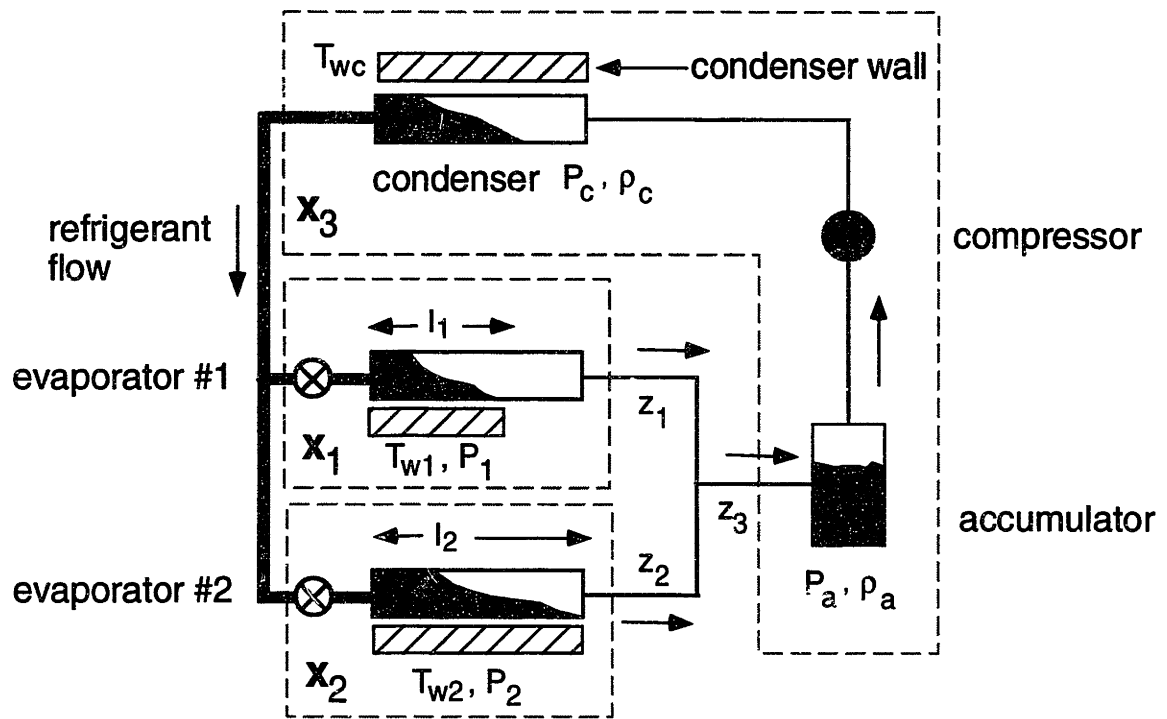
Figure 29. DAE model of a multiple-zone vapor compression cycle

6. Application of the SPSM Method to Vapor Compression Cycles

6.1 Introduction

In the previous chapter it was found that the dynamics of vapor compression cycles could be systematically formulated using a DAE representation. However, in exchange for this modeling simplicity algebraic constraints are introduced that need to be addressed. This chapter uses the SPSM method to construct an explicit state space realization which can be used for simulation or control design. The root locus method introduced earlier is used to select the model parameters and the realization is compared to the exact solution. Furthermore, the SPSM approach is compared to the stiff dynamic element method. The utility of the SPSM approach is demonstrated by simulating a vapor compression cycle over its entire operating envelope. These results verify the method and provide some intuitive understanding of the realization process.

6.2 The Stiff Dynamic Element Method

The stiff dynamic element method is one of the few techniques currently available for realization of nonlinear DAE systems. This section applies the alternative approach to a two evaporator system for comparison to the SPSM method. Following the simple heat exchanger example in section 2.4, the momentum equation was applied to small sections of interconnecting pipe to determine state equations for the unknown mass flow rates in the system (see Figure 30).

$$\varepsilon_1 \frac{dz_1}{dt} = -z_1 + \frac{1}{\varepsilon_2}(P_1 - P_a) \quad , \quad 0 < \varepsilon_1 \ll 1 \qquad (237)$$

$$\varepsilon_1 \frac{dz_2}{dt} = -z_2 + \frac{1}{\varepsilon_2}(P_2 - P_a) \quad , \quad 0 < \varepsilon_1 \ll 1 \qquad (238)$$

Since the evaporators in this example are the same an identical set of parameters are used in the stiff dynamic elements. For general cases, another set of parameters would be necessary. Figure 31 shows the response to a step change in boundary conditions for elements with low damping $\varepsilon_2 \ll 1$. It can be seen that the response is highly oscillatory and the dynamic error is large during the transient. However, when the damping is increased a large steady state error occurs (see Figure 32 to Figure 34). This problem is similar to the simple heat exchanger example presented in section 2.4. To ensure a small steady state error the damping was fixed at a level 20 times greater than the value used in Figure 31. To reduce the approximation error the inertia ε_1 was reduced by a factor of 100 until an acceptable error was achieved. It can be seen from Figure 35 that the error is reduced at the expense of increasing the stiffness of the elements. Figure 36 shows how the eigenvalue locations are varied to improve the approximation error. The four eigenvalues associated with the stiff dynamic elements are off the real axis. It is evident that the natural frequency needs to be increased substantially over the previous case. In both situations the dynamics are very oscillatory. This example clearly shows the tradeoff between element stiffness and approximation error. To achieve a satisfactory error the fast dynamics have to be shifted into the acoustic frequency range (>250 Hz) which is two orders of magnitude greater than the highest frequency in the original DAE (4 Hz). The stiff dynamic element method evidently needs to model the actual acoustic interactions in the system to achieve a good approximation. This is not surprising since the method is based on an approximation of the actual momentum interactions in the system. The severe time scale separation between the stiff dynamics and the DAE will result in stiff

differential equations that are computationally expensive to simulate. Furthermore, this effect can also present numerical problems for many control design methods [18].
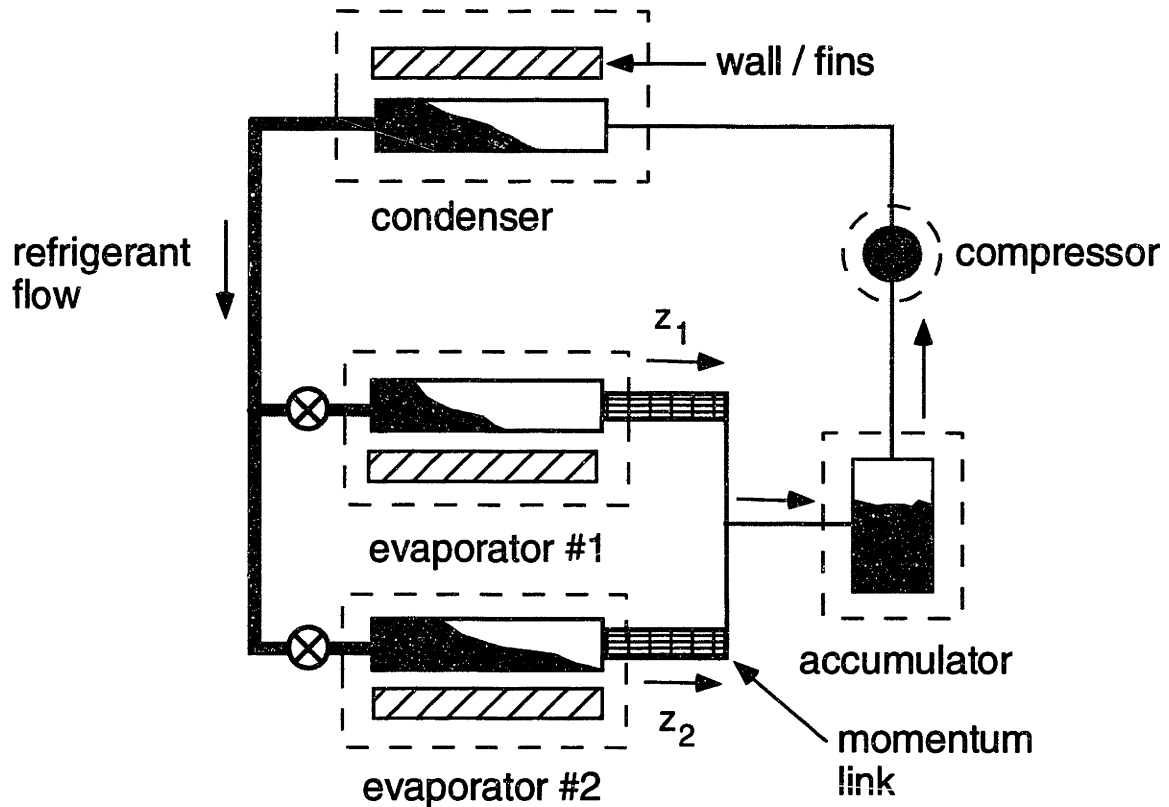

Figure 30. The stiff dynamic element method

6.3 The SPSM Realization Approach

The SPSM approach was applied to develop a state space realization for a vapor compression cycle with two evaporators (see Figure 30). Combining the separate differential-algebraic subsystems in (235) results in the following DAE system:

$$\dot{x} = f(x, z, u) \tag{239}$$

$$0 = g(x, z, u) \tag{240}$$

where

$$\mathbf{x}^T = [P_1 \quad l_1 \quad T_{w1} \quad P_2 \quad l_2 \quad T_{w2} \quad P_a \quad \rho_a \quad P_c \quad \rho_c \quad T_{wc}]^T$$

$$\mathbf{z}^T = [\dot{m}_{o1} \quad \dot{m}_{o2} \quad \dot{m}_a]^T \tag{241}$$

$$\mathbf{u}^T = [A_{v1} \quad A_{v2} \quad \omega]^T$$

$$\mathbf{y}^T = [SH_1 \quad T_{w1} \quad SH_2 \quad T_{w2}]^T$$

The SH output represents the superheat of each indoor unit, and the fans are set constant. It is assumed that the pressure drops in both evaporators are negligible so that the constraints are given by

$$w_1 = P_1 - P_a = x_1 - x_7 \tag{242}$$

$$w_2 = P_2 - P_a = x_4 - x_7 \tag{243}$$

There is also a third constraint given by the mass flow junction into the accumulator

$$w_3 = z_1 + z_2 - z_3 = 0 \tag{244}$$

This equation is trivial to invert so it is used to eliminate one of the constrained states

$$z_3 = z_1 + z_2 \tag{245}$$

Therefore, only two constraints need to be considered for this problem. Since the constraints (242-243) do not depend on z the system is a high index problem. It can be readily shown that the system is an index two problem so that the sliding manifold components are given by

$$s_1 = \left[\mu\frac{d}{dt}+1\right]w_1 = \mu(f_1(t,\mathbf{x},\mathbf{z})-f_7(t,\mathbf{x},\mathbf{z}))+x_1-x_7 \tag{246}$$

$$s_2 = \left[\mu\frac{d}{dt}+1\right]w_2 = \mu(f_4(t,\mathbf{x},\mathbf{z})-f_7(t,\mathbf{x},\mathbf{z}))+x_4-x_7 \tag{247}$$

Applying the generalized singular perturbation form of the SPSM gives the following realization

$$\varepsilon v = - J_s^{-1}s \tag{248}$$

In order to complete the state space model the two parameters ε and μ need to be determined. The root locus technique was used to help select the parameters. Figure 37 presents a root locus as ε is varied for $\mu = 0.1$. The second plot is a zoom in view of the slow DAE eigenvalues. It can be seen that the slow modes of the SPSM converge to the high index DAE when ε is small enough ($\varepsilon=0.07$). At this point the two fastest SPSM modes have only three times the frequency (12 Hz) of the fastest DAE mode. The motivation for the selection of μ can be seen from the first root locus plot. It is evident that as ε approaches zero the two fast modes approach negative infinity and the other two SPSM modes approach the zeros induced by the sliding manifold at $\lambda = -1/\mu$. This pattern follows from the normal

form representation of the SPSM. Therefore, it is always possible to achieve a non oscillatory response. The zero can be placed through appropriate selection of μ to achieve a desired locus shape and SPSM modes that are sufficiently fast. This two stage process of selecting μ and then reducing ϵ until convergence is obtained is more systematic than selecting ϵ and varying μ. Figure 38 illustrates this alternative procedure. It can be seen that if μ is reduced too much then excessive oscillations occur. The shape of the locus is also less intuitive since the eigenvalues approach undesirable locations ($\pm \infty j$).

The system was simulated for a step change in the boundary conditions for parameter values of $\mu = 0.1$ and $\epsilon = 0.07$ (see Figure 40 and Figure 41). Comparing this to the stiff dynamic element method (Figure 35) it is apparent that the response is far less oscillatory. It is also evident from Figure 39 that the frequency needed for the SPSM dynamics to achieve a similar approximation error is more than an order of magnitude less than the stiff dynamic element method ($\omega = 12\,\text{Hz}$ vs. $\omega = 250\,\text{Hz}$). This provides further evidence that the SPSM method requires dynamics that are less stiff to achieve a good approximation. From this example it is evident that the SPSM approach has significant advantages over physically based realization methods.

6.4 Simulation of Multiple-zone Vapor Compression Cycles

The SPSM realization provides a full description of the slow and fast transients in multi-zone systems. Therefore, it can predict long start-up transients from a complete shut down state and short transients that are important for regulator design. Simulations for several types of long and short transients in a two unit system were performed using a standard Runge-Kutta integration routine programmed in C++ (see Figure 42 to Figure 44). A start-up from a complete shut-down state occurs from t=0s to t=500s. Initially, the compressor is running and both expansion valves are fully open. The fast transient is due to the formation of a

pressure distribution between the condenser and the indoor units. The slow transient is the result of changes in the mass distribution (see Figure 44). After the start-up at t=500s a steady state operating condition is predicted. The small transient that occurs at t=700s corresponds to the point when the accumulator dries out (see Figure 44). At t=800s indoor unit #2 is turned off by fully closing the expansion valve. As a result the pressure quickly drops in both evaporators (a short transient). The temperature of the wall in indoor unit #1 decreases and the temperature of indoor unit #2 increases until it becomes room temperature. At t=1200s indoor unit #2 is turned fully on again and a short transient occurs where the superheat rapidly drops and oscillates (see Figure 43). Since the superheat quickly decreases this could potentially violate the superheat reliability requirement. This suggests that the superheat needs to be carefully controlled during start-up and shut-down. At t=1600s the system is completely shut-down by stopping the compressor. It can be seen that the pressures of the indoor units and the condenser quickly reach an equilibrium, and the temperatures of the heat exchanger walls reach an equilibrium with the indoor and outdoor temperatures. From the density states it is apparent that most of the mass moves from the condenser to the accumulator during shut-down. This agrees with published experimental results [4]. At t=2000s the system undergoes a full start-up from a warm shut-down state. It can be seen that the system behavior is essentially the same as the response at t=0s. This provides further evidence of the models ability to simulate start-up and shut-down. From these results it is evident that the SPSM model is capable of predicting the local and global nonlinear behavior of vapor compression cycles. Furthermore, it is evident that the DAE system is highly nonlinear which provides further motivation for the SPSM method.
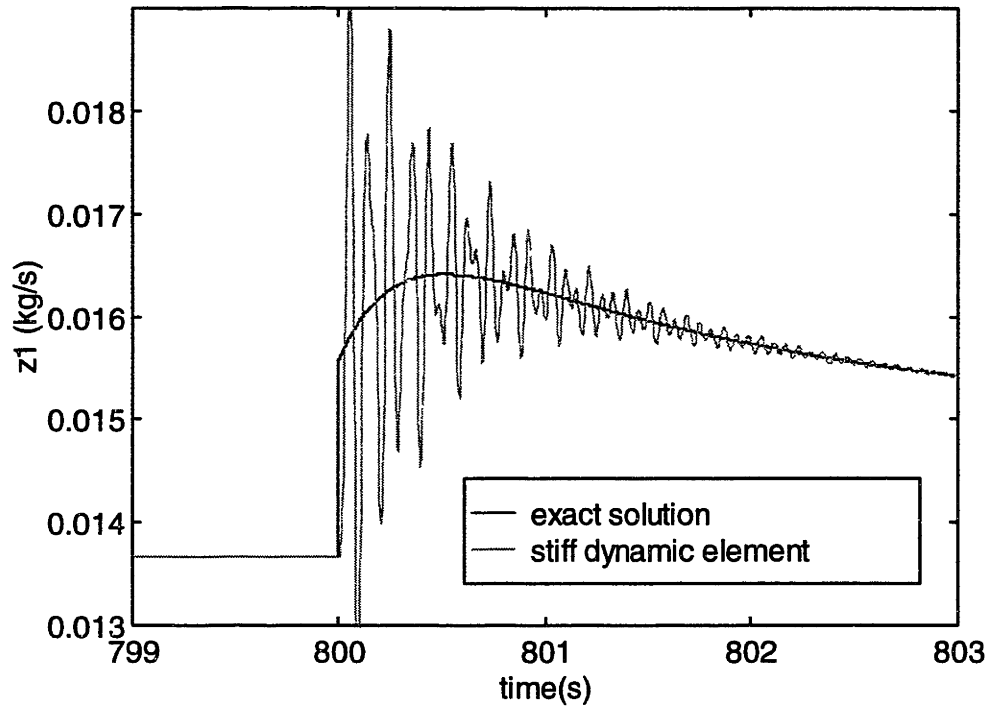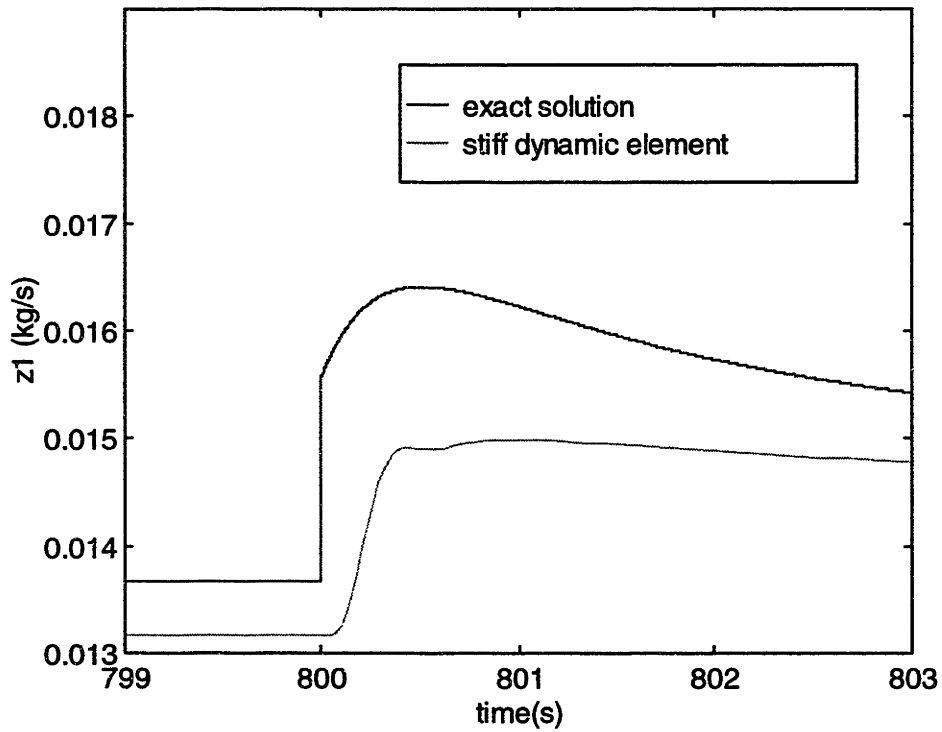
Figure 31. Low damping response
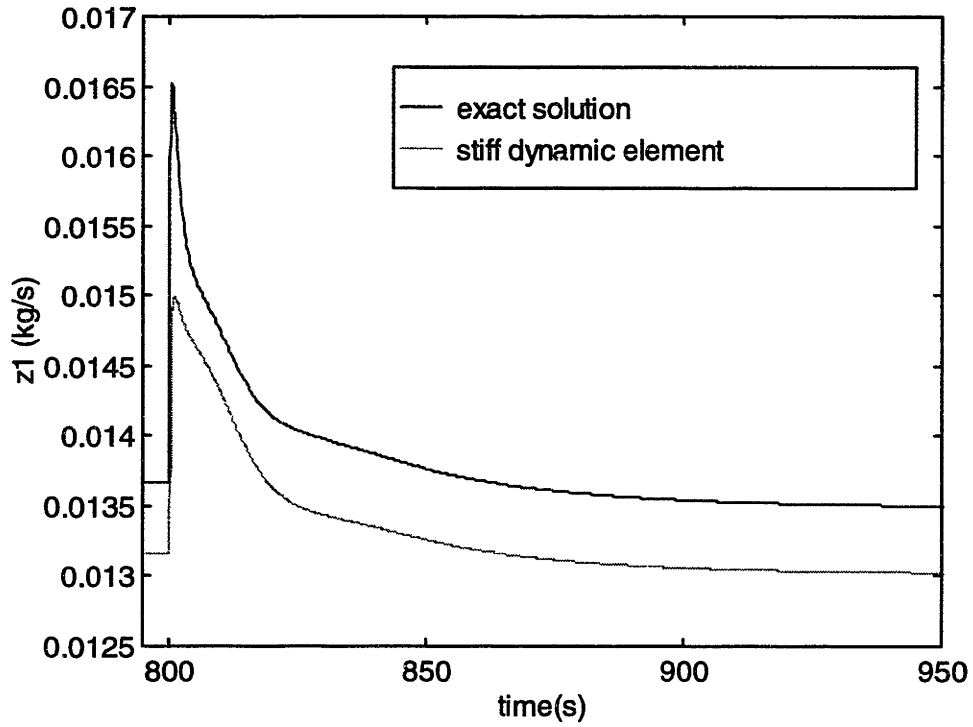

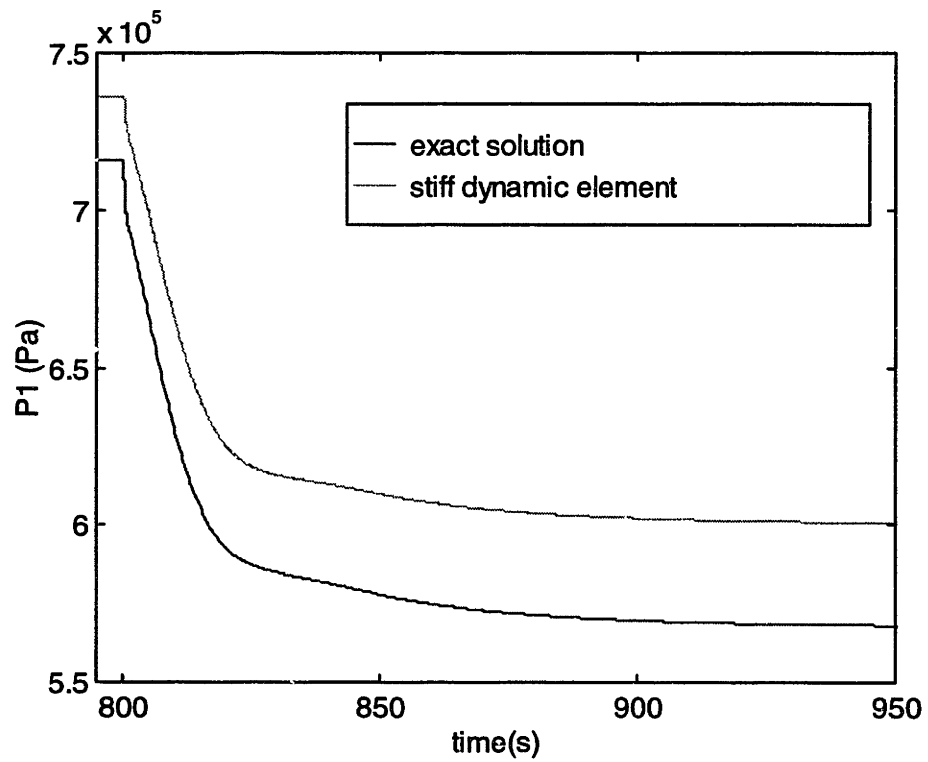Figure 32. High damping response

Figure 33. High damping response

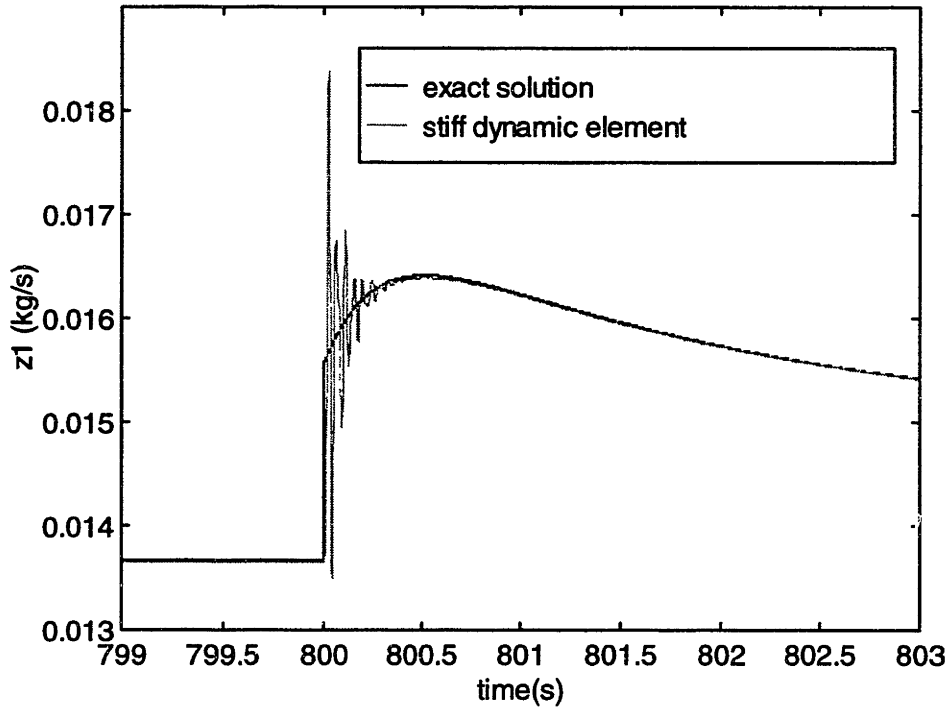Figure 34. High damping response
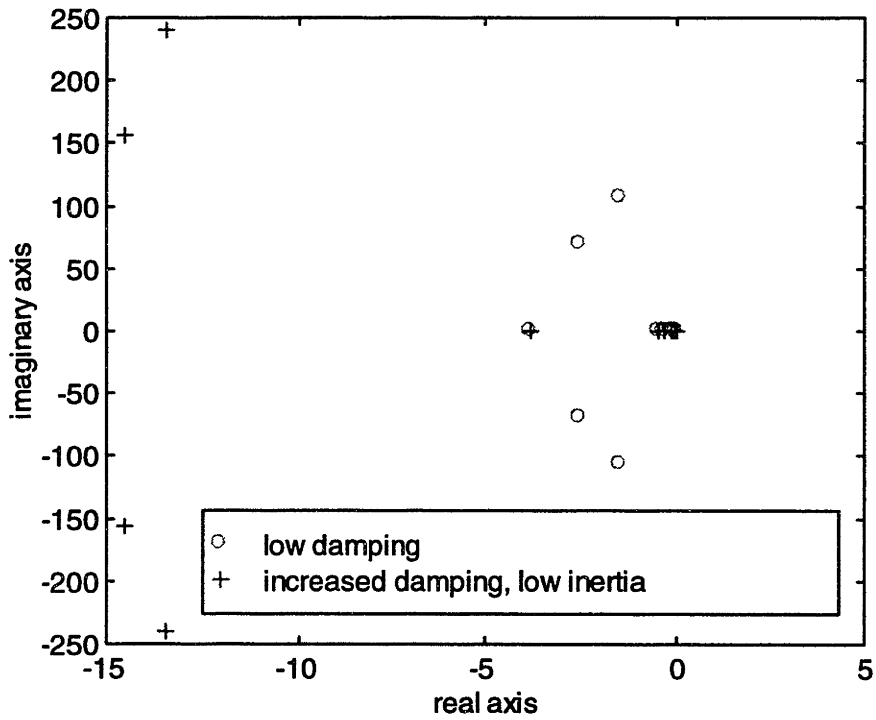
Figure 35. Increased damping, low inertia response

Figure 36. Eigenvalues for stiff dynamic element method
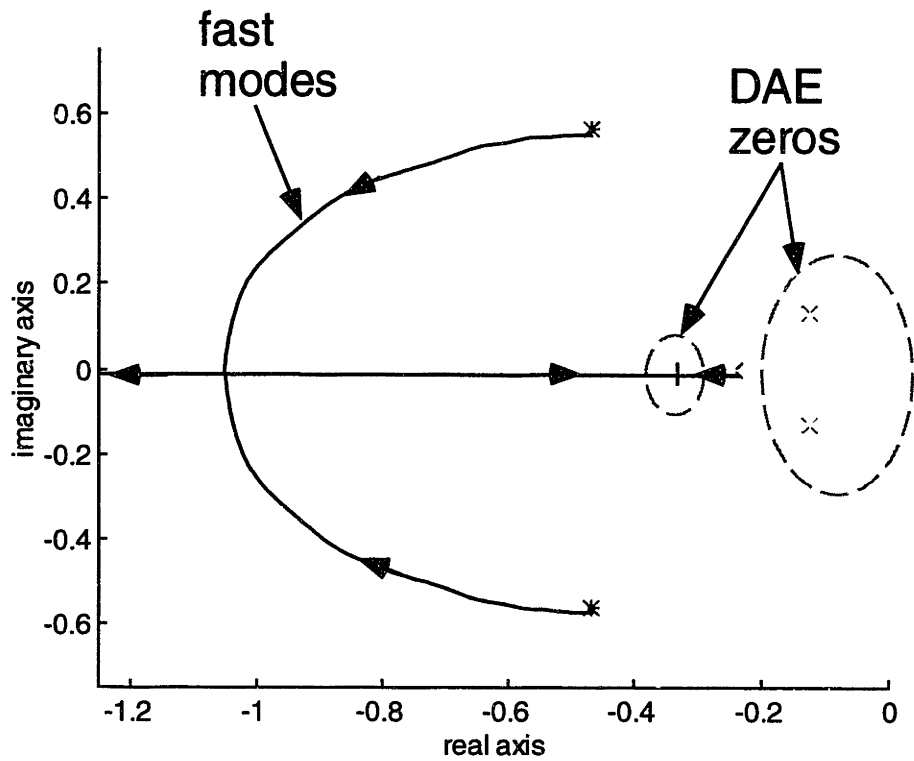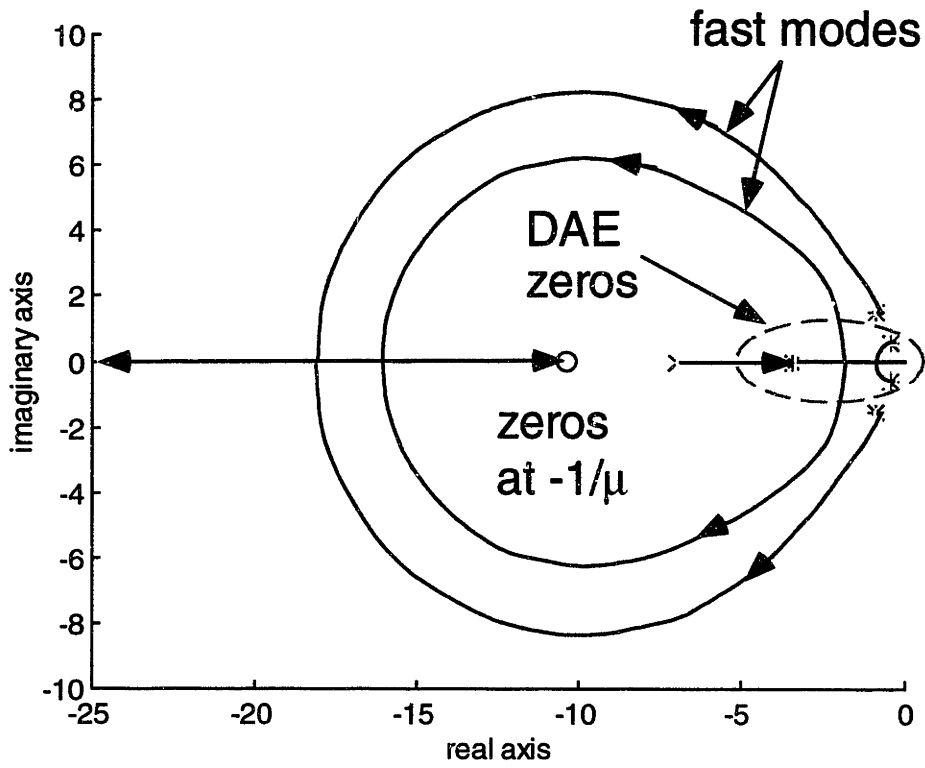
Figure 37. SPSM root locus for μ=0.1 , 0.01 < ε < 2
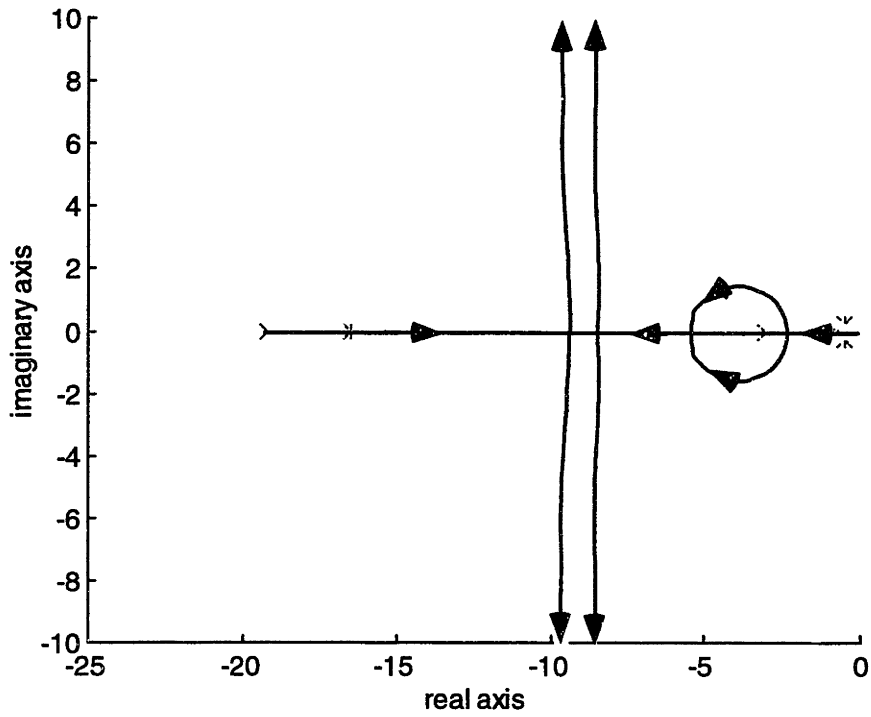
Figure 38. SPSM root locus for ε=0.07 , 0.01 < μ < 2
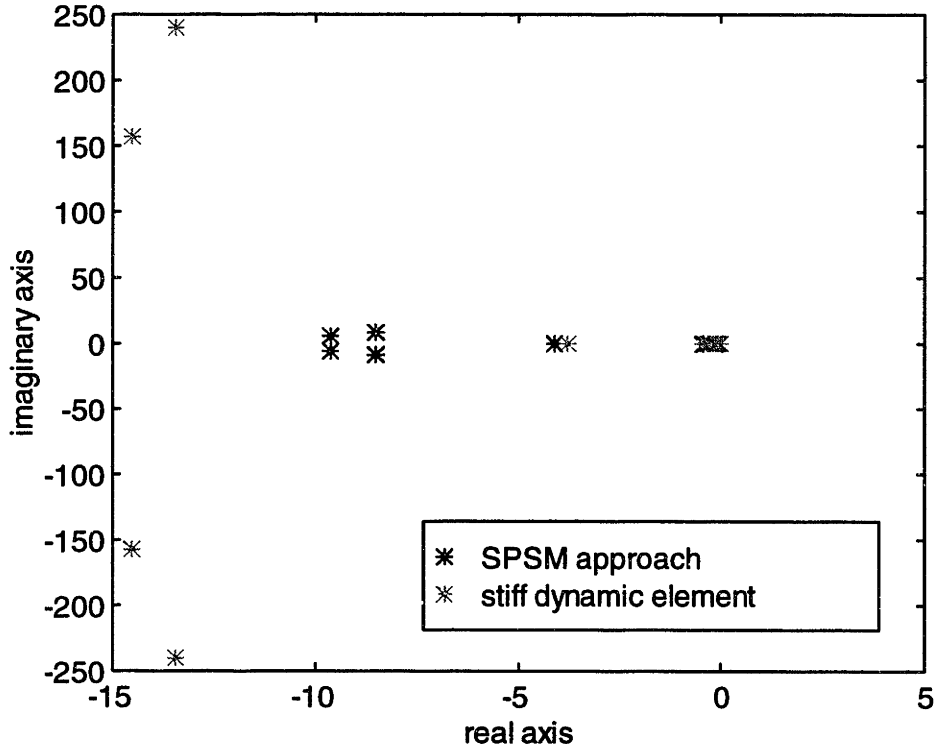

Figure 39. Eigenvalue locations
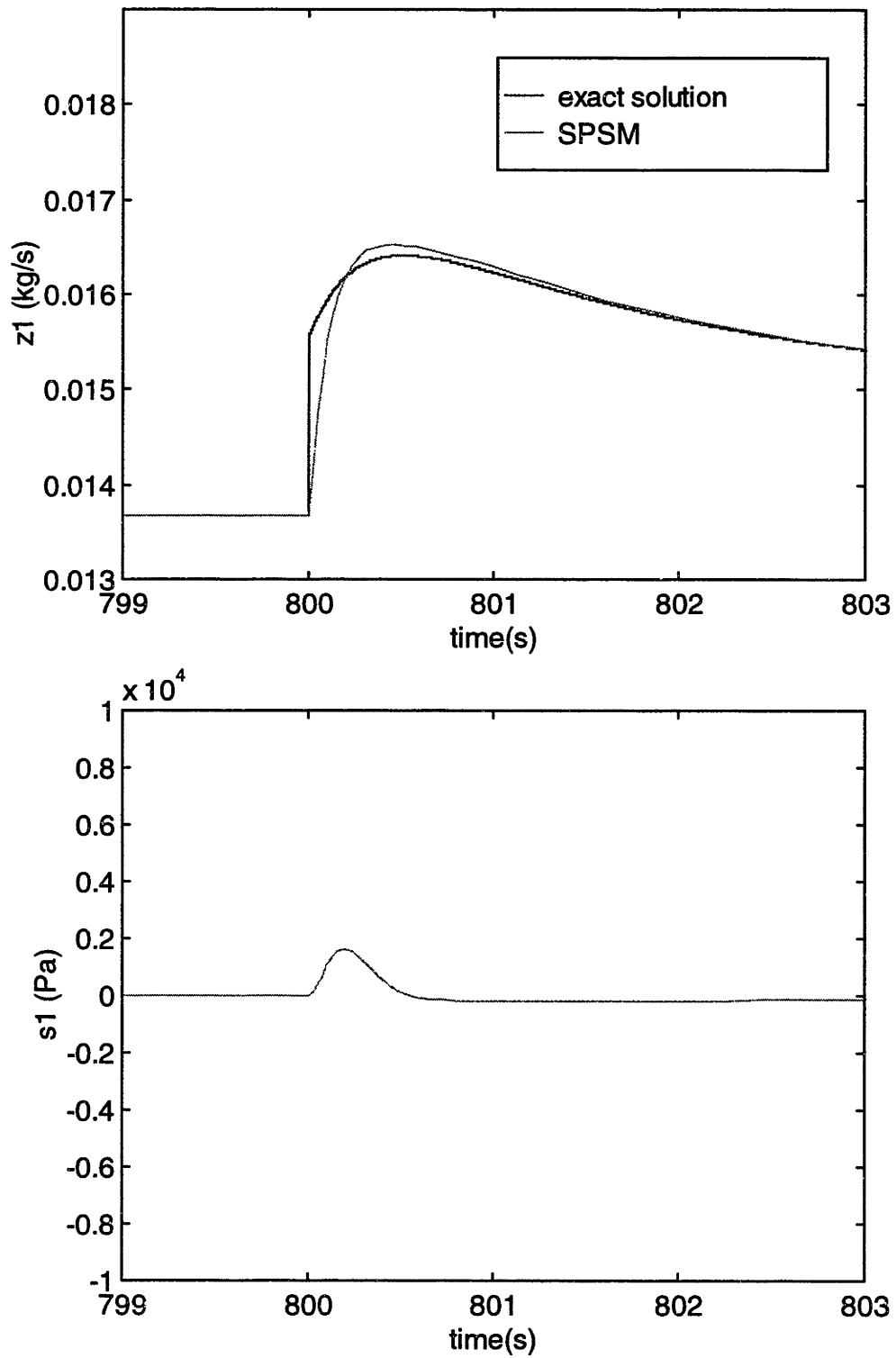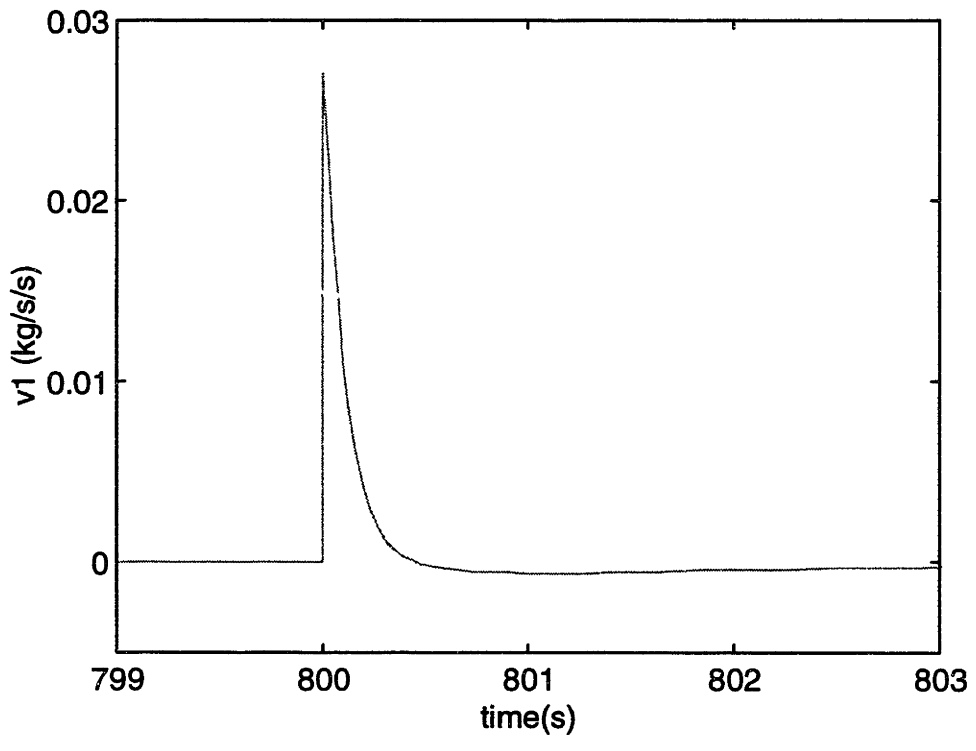
Figure 40. SPSM approach for μ=0.1 , ε=0.07
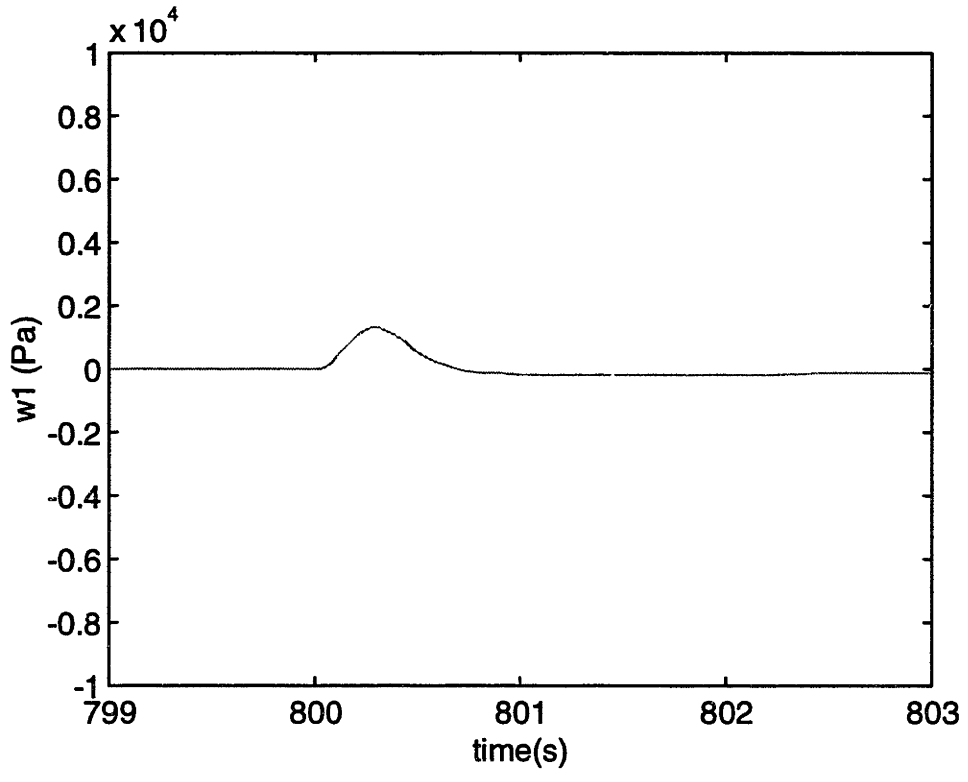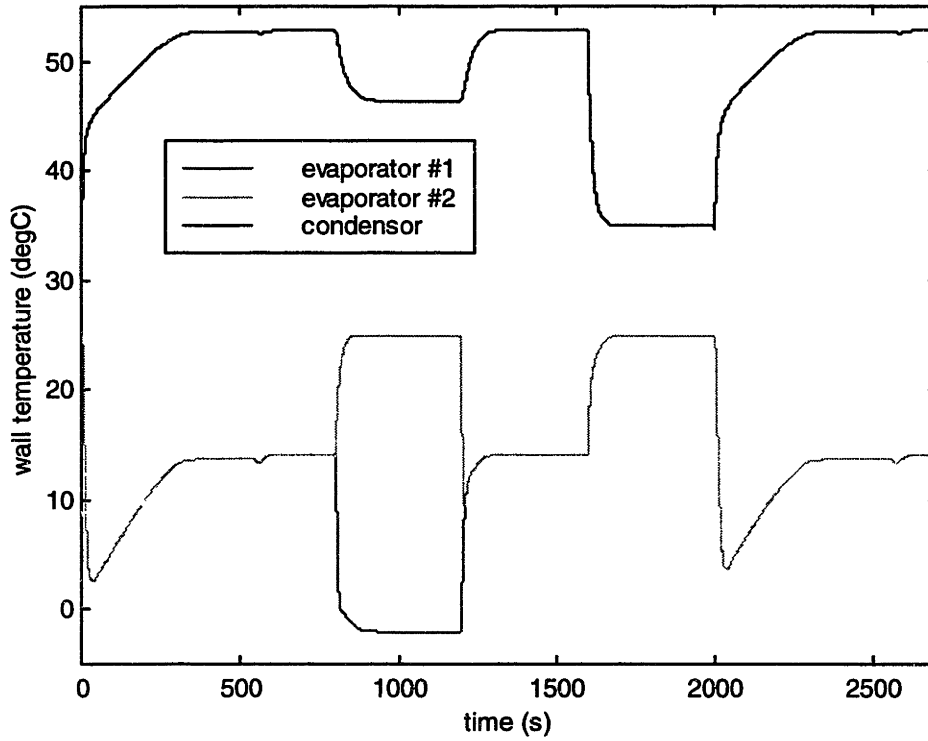
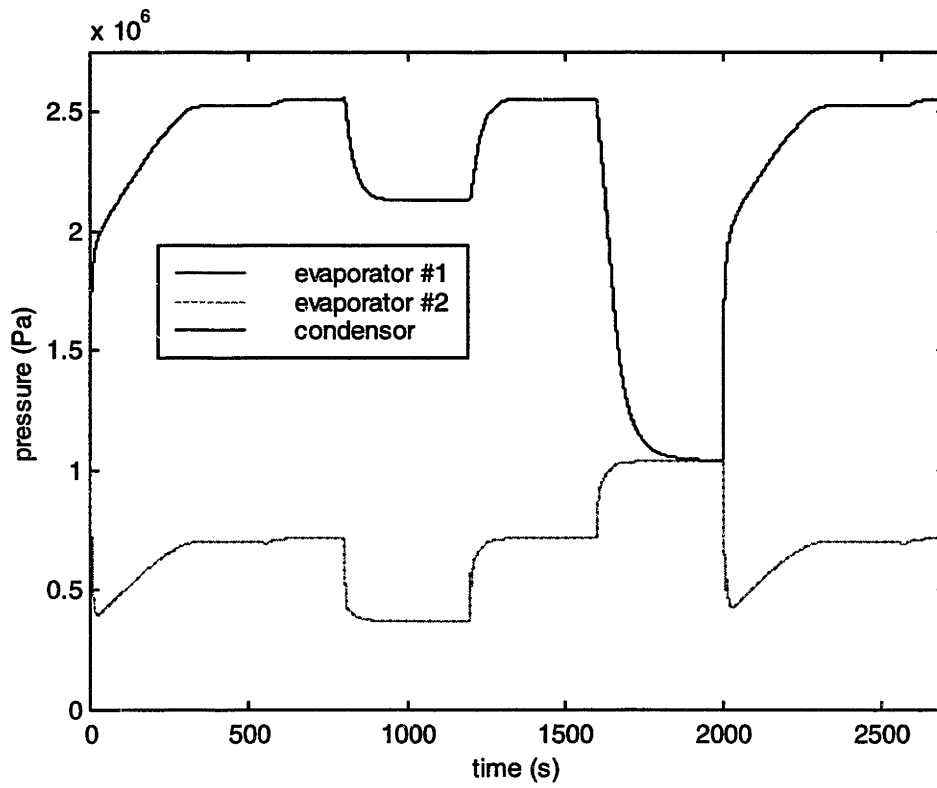Figure 41. SPSM approach for μ=0.1 , ε=0.07

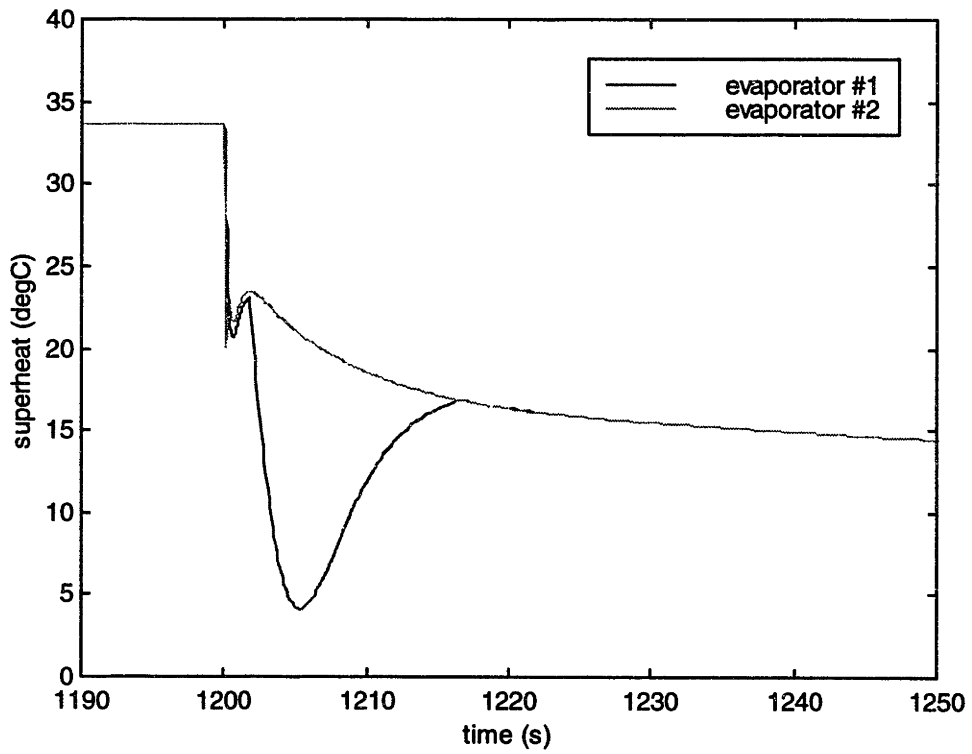Figure 42. Simulation of a two evaporator system
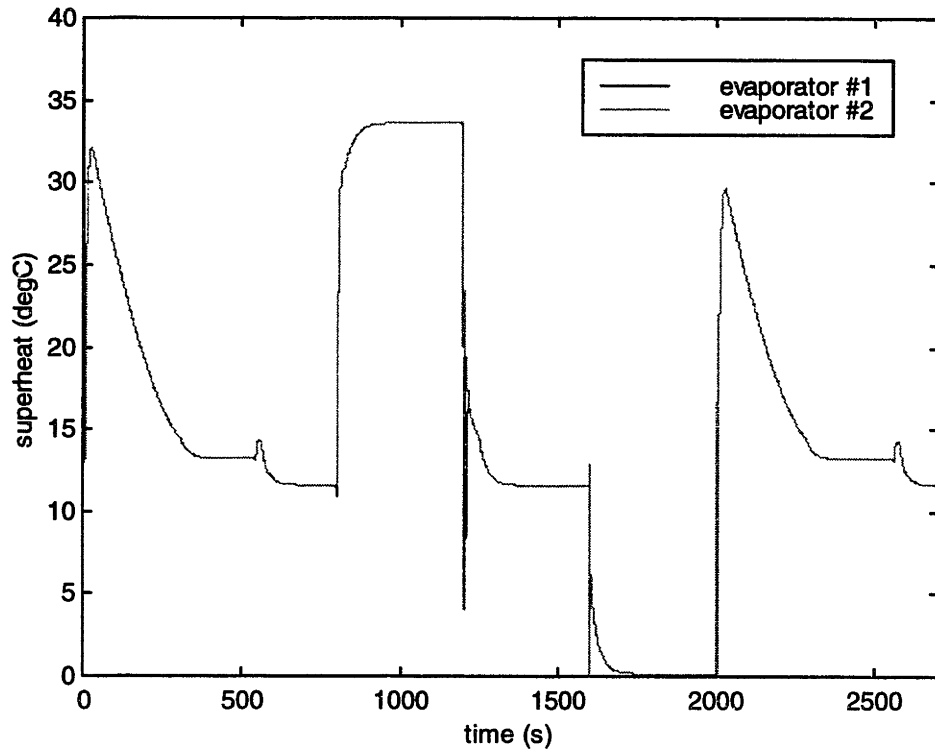
Figure 43. Simulation of a two evaporator system
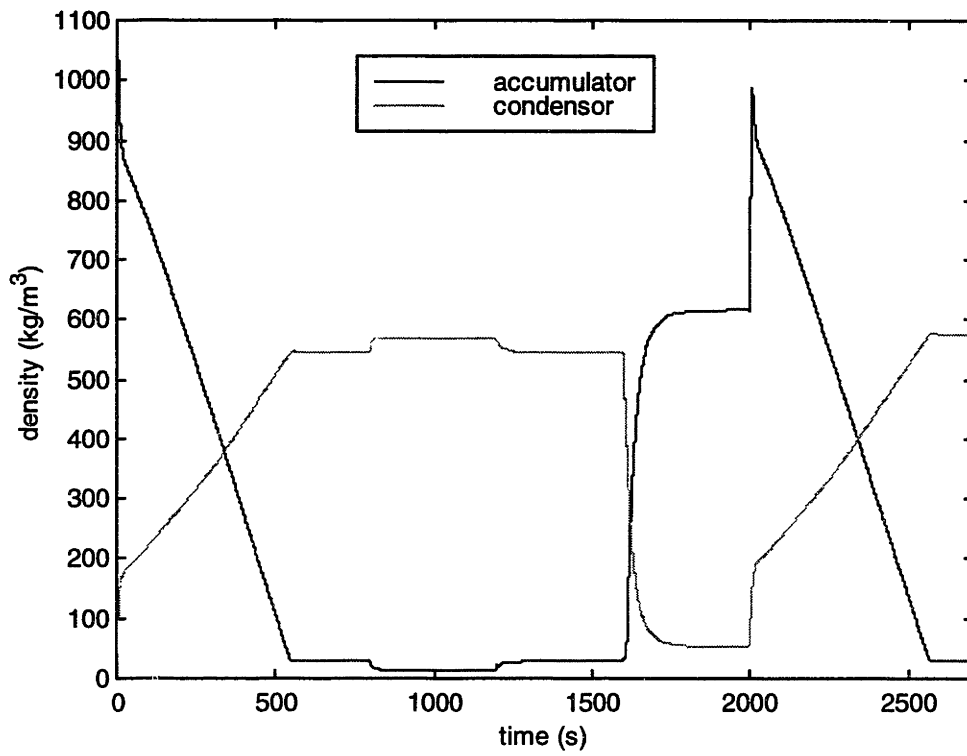
Figure 44. Simulation of a two evaporator system

7. Conclusions

The main results and contributions of this thesis are summarized as follows:

A new approach for realization of DAE systems

One of the key problems associated with simulation and control of DAE systems is the development of an explicit state space realization that allows the application of existing methods. In this thesis, a new approach for realization of DAE systems is developed based on nonlinear control. It is shown that the DAE realization problem can be interpreted as a new type of nonlinear control problem where the violation of the constraints are the outputs and the inputs are the derivatives of the constrained states (see Figure 45):

Figure 45. Block diagram of the new DAE realization approach

With these definitions the relative degree is equal to the index and the zero dynamics are equivalent to the DAE. This allows powerful tools from nonlinear control theory to address the realization problem. New methods were then developed to address a general class of nonlinear high index DAE systems:

1)   That are differentiable a sufficient number of times.

2)   Have an equal number of constraints **w** and constrained states **z** .

3)   Have a constant vector index **r** (definition 2).

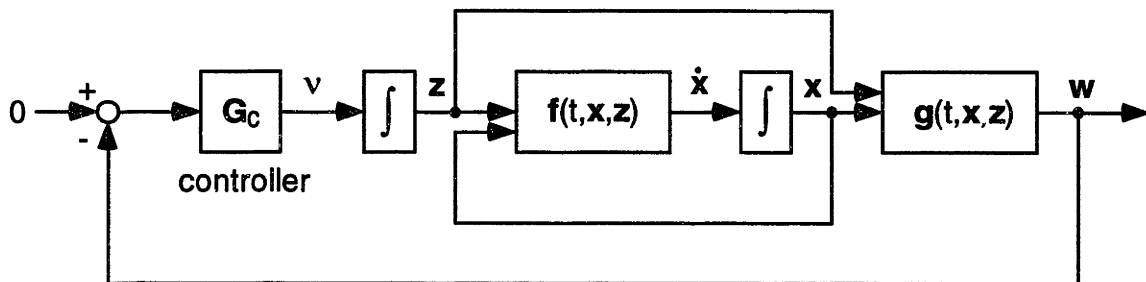Under these mild conditions a sliding manifold can be developed that asymptotically satisfies high index constraints. Boundary layer sliding control can then be used to force the sliding surface to small errors. However, DAE realization presents a number of new problems for the sliding control method. These issues are related to convergence of the approximation error in the presence of state variations. This new problem was investigated using methods from geometrical control and singular perturbation theory. It was found that additional criteria must be satisfied to ensure that the dynamics inside the boundary layer are stable. Together, these new connections lead to the singularly perturbed sliding manifold approach (SPSM) for DAE realization. This represents the first method for realization of DAEs that can systematically reduce computational complexity with guaranteed bounds on the approximation error. Furthermore, results from singular perturbation theory are used to prove that there exists parameter values such that local stability, controllability, observability of the SPSM are equivalent to the high index DAE. This ensures that the SPSM can be used for controller and observer design.

The main original contributions of this work are

1)   The first approach for modeling high index DAEs using nonlinear control

2)   The first method that solves a general class of nonlinear high index DAEs

3) The first work that investigates the connections between the fields of nonlinear control, DAE realization, and modeling (see Figure 46). This is important because it opens a gateway between these fields that results in many new and challenging problems.

4) New concepts such as control property equivalence, vector index, and normal form representation of DAEs are introduced.
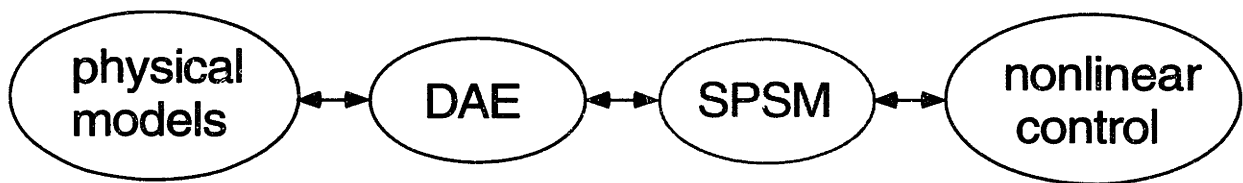
Figure 46. New connections

A new DAE based modeling approach for multiple-zone vapor compression cycles

Application of new methods to specific problems is an important part of control research because it provides valuable insights into their utility, and helps illuminate new ideas and research avenues. With these objectives the SPSM approach was verified on a vapor compression cycle problem. The dynamic behavior of vapor compression cycles are governed by complex interactions between refrigerant flowing in single phase or two phase states and fin arrays that thermally communicate with ambient environments. Low order approximation of these processes results in models described by nonlinear high index DAEs. Application of the SPSM to this problem yields a new control theoretic model of vapor compression cycles that is useful for simulation and multivariable control

design. This can be used to develop multivariable controllers to improve the efficiency and reliability of heat pump and air conditioning systems.

References

[1]   Brenan, K., Campbell, S. and L. Petzold, "Numerical Solution of Initial Value Problems in Differential-Algebraic Equations", North-Holland, Amsterdam, 1989.

[2]   Brogan, W. L., "Modern Control Theory", Prentice Hall, New Jersey, Third Edition, 1991.

[3]   Campbell, S.L., "High-Index Differential Algebraic Equations", Mech. Struct. and Mach., 23(2), pp. 199-222, 1995.

[4]   Goldschmidt, V. W., Murphy, W. E., "Cyclic Characteristics of a Typical Air Conditioner - Modeling of Start-up Transients", ASHRAE Trans., Vol. 91, Part 2., 1985.

[5]   Gordon, B.W., Liu S., and Asada, H., "State Space Modeling of Differential-Algebraic Systems using Singularly Perturbed Sliding Manifolds", Submitted to ASME International Mechanical Engineering Congress and Exposition, 1999.

[6]   Gordon, B.W., and Liu S., "A Singular Perturbation Approach for Modeling Differential-Algebraic Systems", *ASME Journal of Dynamic Systems, Measurement, and Control*, December 1998.

[7]   Gordon, B.W., Liu S., and Asada, H., "Dynamic Modeling of Multiple-zone Vapor Compression Cycles using Variable Order Representations", Proc. of 1999 Amer. Contr. Conf., FM11-2.

[8]   He, X., Liu, S., and Asada, H., "Modeling of Vapor Compression Cycles for Multivariable Feedback Control of HVAC Systems", *ASME Journal of Dynamic Systems, Measurement, and Control*, Vol. 119, pp. 183-191, 1997.

[9]   Isidori, A. "Nonlinear Control Systems", 2nd ed., Springer-Verlag, 1989.

[10]   Karnopp, D. and D. Margolis, "Analysis and Simulation of Planar Mechanism Systems Using Bond Graphs", *ASME Journal of Mechanical Design*, Vol. 101, Apr., 1979.

[11]   Khalil, H.K., "Nonlinear Systems", Macmillian, 1992.

[12]   Kokotovic, P., Khalil, H.K. and J. O' Reilly, "Singular Perturbation Methods in Control: Analysis and Design", Academic Press, 1986.

[13]   Kumar, A. and P. Daoutidis, "Regularization and Control of Nonlinear Differential Algebraic Process Systems", Proc. Of 1995 Amer. Contr. Conf., 2215, 1995.

[14]   Luenberger, D.G., "Dynamic Equations in Descriptor Form", IEEE Transactions on Automatic Control, vol. ac-22, no. 3, June 1977.

[15]   MacArthur, J.W., Grald, E.W., "A moving-boundary formulation for modeling time-dependant two-phase flows", Int. J. Heat and Fluid Flow, Vol. 13, No. 3, September, 1992.

[16]   McClamroch, N. H., "Feedback Stabilization of Control Systems Described by A Class of Nonlinear Differential Algebraic Equations", Syst. and Contr. Lett., 15, 53, 1990.

[17] Rosenberg, R. C., "Exploiting bond graph causality in physical system models", *ASME Journal of Dynamic Systems, Measurement, and Control*, Vol. 109, pp. 378-383, 1987.

[18] Shouse, K.R., and Taylor D.G., "Discrete-Time Observers for Singularly Perturbed Continuous-Time Systems: Part I, Autonomous Systems", Proc. Of 1993 Amer. Contr. Conf., 2616, 1993.

[19] Slotine, J.E. and W. Li, "Applied Nonlinear Control", Prentice Hall, 1991.

[20] Tong, L. S., and Tang Y. S., "Boiling Heat Transfer and Two-Phase Flow", Taylor and Francis, London, Second Edition, 1997.

[21] Vidyasagar, M., "Nonlinear Systems Analysis", Prentice Hall, 1978.

[22] Zeid, A.A. and J.L. Overholt, "Singularly Perturbed Bond Graph Models for Simulation of Multibody Systems", *ASME Journal of Dynamic Systems, Measurement and Control*, Vol. 117, pp. 401-410, 1995.

Appendix A: State Equations for Heat Exchanger Example

Energy balance equation for node 1.

$$V_1 \frac{\partial(\rho_1 u_1)}{\partial \rho_1} \frac{d\rho_1}{dt} + V_1 \frac{\partial(\rho_1 u_1)}{\partial P_1} \frac{dP_1}{dt} = \dot{m}_i h_i - \dot{m}_1 h_1 - A_1 \overline{\alpha}_1 (T_1 - T_3) \tag{249}$$

Mass balance equation for node 1.

$$V_1 \frac{d\rho_1}{dt} = \dot{m}_i - \dot{m}_1 \tag{250}$$

Energy balance equation for node 2.

$$V_2 \frac{\partial(\rho_2 u_2)}{\partial \rho_2} \frac{d\rho_2}{dt} + V_2 \frac{\partial(\rho_2 u_2)}{\partial P_2} \frac{dP_2}{dt} = \dot{m}_1 h_1 - \dot{m}_2 h_2 \tag{251}$$

Mass balance equation for node 2.

$$V_2 \frac{d\rho_2}{dt} = \dot{m}_1 - \dot{m}_2 \tag{252}$$

Energy balance equation for node 3.

$$C_{p3} \frac{dT_3}{dt} = A_1 \overline{\alpha}_1 (T_1 - T_3) - A_3 \overline{\alpha}_3 (T_3 - T_a) \tag{253}$$

The state equations (249) to (253) have the form

$$\mathbf{f}_l(t, x, z)\dot{x} = \mathbf{f}_r(t, x, z) \tag{254}$$

It can be shown that the coefficient matrix $\mathbf{f}_l$ is always invertible so that

$$\dot{x} = \mathbf{f}(t, x, z) \tag{255}$$

Appendix B: Derivation of Evaporator State Equations

Integration of the energy balance equation (219) from $z = 0$ to $z = l_e(t)$ gives:

$$\int_0^{l_e(t)} \frac{\partial (\rho h)}{\partial t} dz - l_e \frac{dP_e}{dt} = (\rho u h)\big|_0 - (\rho u h)\big|_{le} + l_e \frac{4}{D_i} \alpha_i (T - T_w) \tag{256}$$

Then use the following integral identity:

$$\int_{z1(t)}^{z2(t)} \frac{\partial f(z,t)}{\partial t} dz = \frac{d}{dt} \int_{z1(t)}^{z2(t)} f(z,t) dz - f(z_2(t),t) \frac{dz_2(t)}{dt} + f(z_1(t),t) \frac{dz_1(t)}{dt} \tag{257}$$

This gives:

$$\int_0^{l_e(t)} \frac{\partial (\rho h)}{\partial t} dz = \frac{d}{dt} \int_0^{l_e(t)} (\rho h) dz - \rho_{eg} h_{eg} \frac{dl_e(t)}{dt} \tag{258}$$

Now use the moving boundary principle of invariant mean void fraction:

$$\frac{d}{dt} \int_0^{l_e(t)} (\rho h) dz = \frac{1}{A} \frac{d}{dt} \int_0^{l_e(t)} h(\rho A dz) = \frac{1}{A} \frac{d}{dt} \int_0^{l_e(t)} h \delta m = \frac{1}{A} \frac{d}{dt} \left[(\rho_{el} h_{el} (1 - \bar{\gamma}_e) + \rho_{eg} h_{eg} \bar{\gamma}_e) A l_e \right] \tag{259}$$

Back substitution and multiplication by A yields the desired result (222). The mass balance equation (221) and energy balance equation for the tube wall (223) can be obtained in a similar fashion.

Appendix C: Variable Glossary

V = volume

D = diameter

L = length of heat exchanger

N = total number of subsystems

u = flow velocity

z = length along heat exchanger

$\overline{\alpha}$ = heat transfer coefficient

ρ = density

h = specific enthalpy

$\hat{u}$ = specific internal energy

P = pressure

T = temperature

$\dot{m}$ = mass flow rate

A_c = inside cross section area of evaporator

A_v = expansion valve area

h_o = outlet specific enthalpy

$\dot{m}_o$ = outlet mass flow rate

T_a = ambient temperature

$(mc)_w$ = heat capacity of wall section

$(\rho A_c c_p)_w$ = heat capacity per unit length of heat exchanger wall

$\dot{W}_p$ = power input to compressor

ω = compressor speed

f = fan speed

$\overline{\gamma}$ = mean void fraction

l = length of two phase region

F_{wall} = wall friction force per unit volume

Subscripts:

a   = accumulator

c   = condenser

e   = evaporator

g   = gas phase

l   = liquid phase

i   = inside heat exchanger

k   = number of indoor heat exchanger

o   = outside heat exchanger

p   = compressor

sat   = saturated state

v   = expansion valve

w   = heat exchanger wall

Appendix D: Evaporator Pressure Drop Correlation

Assuming that the mass flow in the heat exchanger is equal to the outlet mass flow rate the pressure drop can be estimated as:

$$P_k - P_a = \frac{\dot{m}_{ok}^2}{\rho_o A_c^2} - \frac{\dot{m}_{ok}^2}{\rho_g A_c^2} - a(L_k - l_k)\dot{m}_{ok}^b P_k^c - d\frac{l_k}{2}\dot{m}_{ok}^e P_k^f \tag{260}$$

where a, b, c, d, e, f are empirical constants.

Appendix E: Subsystem Components

The state equations can be obtained after some algebra from

$$\mathbf{f}_k = (221\text{-}223) \quad , \ 1 \le k \le (N-1)$$
$$\mathbf{f}_N = (224\text{-}228) \tag{261}$$

The constraint equations are given by

$$\mathbf{g}_k = P_k - P_a - g(\dot{m}_{ok}, P_k, l_k) \ , \ 1 \le k \le (N-1)$$
$$\mathbf{g}_N = \sum_{k=1}^{N-1} \dot{m}_{ok} - \dot{m}_a \tag{262}$$

The outputs are defined to be

$$\mathbf{y}_k = [SH_k \quad T_{wk}]^T, \ 1 \le k \le (N-1) \tag{263}$$

THESIS PROCESSING SLIP

FIXED FIELD: ill. _____ name _____

index _____ biblio _____

► **COPIES:** (Archives)   Aero   Dewey   (Eng)   Hum

Lindgren   Music   Rotch   Science

TITLE VARIES: ► ☐ _____

_____

_____

NAME VARIES: ► ☑ william _____

_____

IMPRINT: (COPYRIGHT) _____

► **COLLATION:** _____ 134 p. _____

► **ADD: DEGREE:** _____ ► **DEPT.:** _____

SUPERVISORS: _____

_____

— — _____

— — _____

— — _____

— — _____

— — _____

— — _____

— — _____

NOTES:

cat'r: _____ date: _____

	page:
► **DEPT:** M.E.	► S39

► **YEAR:** 1999   ► **DEGREE:** Ph.D.

► **NAME:** GORDON, Brandon W.